University of Genoa

Doctorate in Chemical and Materials Sciences and Technologies

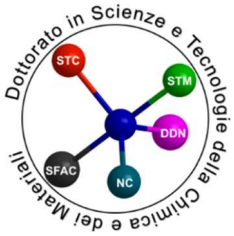

Curriculum Chemical Sciences and Technologies

XXXIII Cycle

New membranes for membrane distillation process

Candidate: Marcello Pagliero

Supervisor: Prof. Antonio Comite

Index

List of abbreviations

AGMD	Air gap membrane distillation
DCMD	Direct contact membrane distillation
DMF	N,N Dimethylformamide
FAS	Fluoroalkylsilanes
GLDP	Gas-liquid displacement porometry
GP	Gas permeation
HSP	Hansen solubility parameters
LEP_w	Liquid entry pressure (water)
LGMD	Liquid gap membrane distillation
LLDP	Liquid-liquid displacement porometry
MD	Membrane distillation
MF	Microfiltration
MTS	Methyltrichlorosilane
NIPS	Nonsolvent induced phase separation
NW	Nonwoven
PE	Polyethylene
PEG	Polyethylene glycol
PET	Polyethylene terephthalate
PGMD	Permeate gap membrane distillation
PP	Polypropylene
PTFE	Polytetrafluoroethylene
PVDF	Polyvinylidene fluoride
PVDF-HFP	Polyvinylidene fluoride-hexafluoropropylene
PVP	Polyvinyl pyrrolidone
RO	Reverse osmosis
SGMD	Sweeping gas membrane distillation
TIPS	Thermally induced phase separation
VMD	Vacuum membrane distillation
ZLD	Zero liquid discharge

List of symbols

a_w	Water activity
C_b	Bulk concentration
C_m	Concentration on the membrane
D	Diffusion coefficient
d_p	Particle size
h_g	Gas thermal conductivity
h_m	Membrane thermal conductivity
h_s	Solid thermal conductivity
J	Distillate flux
K	Gas permeability
k_b	Boltzmann constant
k_m	Membrane mass transfer coefficient
Kn	Knudsen number
k_m^V	Poiseuille mass transfer coefficient
k_m^D	Molecular diffusion mass transfer coefficient
k_m^K	Knudsen mass transfer coefficient
m_d	Dry membrane mass
m_s	Dry support mass
m_w	Wet membrane mass
M_w	Water molecular weight
N	Molar flux
P	Total pressure
p_w°	Vapour pressure
P_a	Air pressure
p_{av}	Mean pressure
p_f	Solution vapour pressure
Q_C	Conductive heat loss
Q_L	Latent heat
R	Universal gas constant
r	Pore radius
$R\%$	Salt rejection
r_{max}	Largest pore size
T	Temperature
T_m	Temperature on the membrane
$v_{ns(in)}$	Nonolvent in-flux rate
$v_{s(out)}$	Solvent out-flux rate
x_w	Water molar fraction

Greek symbols

ϕ_ι	Surface fraction occupied by phase i
ϕ_σ	Surface fraction occupied by the solid
γ_ω	Water activity coefficient
ρ_{oc}	1-octanol density
ρ_{pol}	PVDF density
ρ_s	Support material density
γ_l	Liquid surface tension
ΔP	Pressure drop
δ	Thickness
δ_d	Dispersive component of HSP
δ_h	Hydrogen bonding component of HSP
δ_L	Laminar boundary layer
δ_p	Polar component of HSP
δ_T	Turbulent boundary layer
ε	Porosity
θ	Contact angle
θ_C	Concentration polarization coefficient
θ_T	Temperature polarization coefficient
λ	Mean free path
μ	Dynamic viscosity
v_M	Mean molecular speed
σ	Collision diameter
σ_d	Distillate electrical conductivity
σ_f	Feed electrical conductivity
τ	Tortuosity

Summary

The PhD research program was focused of the development of new hydrophobic membranes suitable for membrane distillation (MD) operation. In particular, the preparation of polymeric flat sheet membranes via nonsolvent induced phase separation (NIPS) technique was investigated. This method allows to fine-tune a large number of variables in order to obtain membranes with an ample variety of different morphologies and properties. Therefore, a systematic study on the important factors affecting the membrane structure, which in turn determines the distillation performance, was carried out. The selected polymer was polyvinylidene fluoride (PVDF), the solvent was dimethylformamide (DMF).

First, the effect of the dope solution composition was evaluated. The polymer amount was found to be a key element in defining the porosity and the pore size of the final membrane. Moreover, a minimum critical concentration required to obtain a proper structure was identified on the basis of the dope solution viscosity. In fact, at lower concentrations brittle or defective films were produced.

Another important preparation parameter thoroughly investigated was the coagulation bath strength. Harsh nonsolvents induce fast precipitation creating a dense skin above a macrovoid-dominated layer, while weak coagulation media promote a delayed demixing and generate uniform and symmetric structures. Using a semi crystalline polymer such as PVDF, the precipitation rate becomes even more important because it also influences the crystallization of the polymer. The strength of the coagulation bath was regulated by adding different amounts of ethanol to the water bath, from 0% up to 96% v/v. Optimization of this parameter allowed to prepare almost superhydrophobic membranes that were able to withstand the pressure and temperature conditions during vacuum membrane distillation (VMD) tests and to deliver high distillate fluxes and total salt rejection when treating a concentrated NaCl solution.

A different approach to improve the membrane performance was exploited in further phase of activity. Different kinds of pore forming agents – such as polyethylene glycols and lithium chloride – were added to the dope solution in order to enhance the porosity and control the pore size. Since the support material can act as an added mass transfer resistance, it was decided to cast these membranes without any reinforcement. However, the absence of any rigid support caused severe shrinkage phenomena during the drying of the membranes leading to an almost complete collapse of the porous structure. It was found that the structure could be preserved by simply clamping the wet membrane on a stiff planar surface and leaving it to dry at room temperature.

The amount and type of the additive had impacts on both kinetic and thermodynamic factors governing the phase separation process. By adjusting the dope solution composition, it was possible to favour one or the other to obtain membranes with the desired structure and performance. These unsupported membranes were not able to bear the pressure difference normally applied during VMD, therefore they were tested using a direct contact membrane distillation (DCMD) setup.

Since the presence of the support material is mandatory for VMD application, the effect of different kinds of supports was investigated. In particular, several commercial nonwovens were used to prepare PVDF membranes based on the knowledge acquired during the first phase of the PhD activity. Moreover, along with the nonwovens, three polymeric nets, characterized by different structure and made with different polymers, were tested as possible supports. While the commercial nonwovens did not alter too much the performance and morphology of the PVDF membranes, using the nets some remarkable effects were registered. The alternation between holes and crests of the nets caused the formation of membranes with zones having different porosities. The VMD tests highlighted the better performance of the nonwoven casted membranes. However, the patterned surface of the net supported membranes resulted in lower flux decline when a concentrated NaCl solution was used as feed.

Polymeric membranes are the most studied type for MD application both for the easy processability and the low production costs. Moreover, the commonly used polymers can withstand the normal operation conditions for desalination or wastewater treatment applications. However, the possibility of producing membranes able to resist higher temperatures and pressures would open the way to new MD applications. One of the possible paths to reach this goal is the exploitation of ceramic membranes. Ceramic material are nevertheless naturally hydrophilic and surface modification procedures must be carried out in order to turn such membranes hydrophobic. Therefore, the reaction between the surface hydroxyl groups of alumina commercial membranes and a silanizing agent was exploited. By changing the reaction conditions, it was possible to obtain highly hydrophobic membranes without affecting the initial pore size and porosity. This functionalizing surface layer proved to be stable up to 400°C which would allow to cover any possible MD operation condition.

Chapter 1

1 Introduction to membrane distillation

1.1 Basic principles

Water is considered a resource under growing risk of pollution while the worldwide demand is increasing. In principle efficient policies for effective water distribution and consumption should be adopted in order to minimize wastewater generation but the paradigm according to which wastewater can be considered as a valuable resource to generate again safe water seems to be necessarily implemented to achieve a water sustainability. To effectively implement policies for water and wastewater management, the exploitation of effective technological processes enabling to achieve a full clean water recovery is becoming mandatory and membrane technology is recognized as one of the prominent key technologies for advanced water and wastewater treatment. Some membrane processes as microfiltration (MF) and reverse osmosis (RO) are already widely applied on a commercial scale for water depuration, desalination and wastewater treatments. Nonetheless emerging membrane processes are attracting growing attention, and among them membrane distillation, while it is still at the beginning of its commercialization stage in the desalination field. MD is accounted among the membrane processes which should facilitate the achievement of zero liquid discharge (ZLD) solutions aimed at maximizing water recycle and minimizing wastewater volumes [1].

The first patent on MD has been filed by Bodell in 1963 [2] when suitable membranes where not available. When hydrophobic polymer membranes appeared on the market the first studies on MD were devoted to desalination and then to food processing. The application of MD to wastewater treatment and for desalination purposes has been studied during the last two decades by several researchers, but MD can be still considered at an infant stage and some challenges need to be faced in order to see this technology at a commercial level for wastewater treatment.

The distillation process is known to allow the components of a liquid solution to be separated on the basis of their different volatilities. The vapor pressure of a pure liquid can be empirically estimated by using the Antoine equation.

$$log_{10}(p_w^\circ) = A - \frac{B}{T + C} \qquad 1.1$$

where p_w° is the vapor pressure (Pa or bar), T the temperature (K or °C) and A, B and C the constants specific for each substance. For the vapor pressure of pure water expressed in Pa with

the temperature in K the values of the Antoine's constant are A=23.1964, B=3816.44, C=46.13 [3,4]. By increasing the temperature, the vapor pressure increases. When non-volatile solutes are diluted in a water solution the Raoult equation can account for the change in the vapor pressure p_f

$$p_f = x_w p_w^o \qquad 1.2$$

where x_w is the molar fraction of water. For more concentrated solution where solute-water interactions become more important x_w needs to be replaced by the water activity

$$p_f = a_w p_w^o = \gamma_w x_w p_w^o \qquad 1.3$$

where a_w is the water activity and γ_w is the activity coefficient for water. Therefore, when a solute is present usually the vapor pressure is lower than for pure water. The evaporation takes place at the interface between the liquid and the vapor phases and therefore the molar flow rate of evaporation depends on the evaporation surface area and on the water flux. When the distillation process is mediated at the evaporation interface by a porous membrane which is not filled by the liquid phase but only by the vapor phase it is referred to as MD. Considering an aqueous feed, a hydrophobic porous membrane can create a controlled and known (from geometrical considerations) evaporation surface. Then only the vapours of the volatile components, solvent and/or other volatile species, in the feed will diffuse through the porous structure of the membrane to the other side where they can be drained out by vacuum, by a sweep gas, or condensed in a liquid phase which can have or not a direct contact with the membrane surface. In this chapter we will not consider the osmotic distillation which is an isothermal process based on the presence of a high salinity draw aqueous solution on the condensing side of the membrane in order to create a vapor pressure gradient [5].

The MD is essentially a thermally driven separation process in which a hydrophobic porous membrane in contact with a hotter liquid solution (usually an aqueous one) works as an artificial evaporation interface. By exploiting simultaneously a gradient of temperature between the feed phase and the collecting phase on the permeate side and a sufficiently high contact area, high evaporation flow rates are possible even with temperatures of the feed lower than its boiling point. Since in MD the flow rate can be easily raised by increasing the membrane contact area, the feed does not need to be heated up to the solvent boiling point and low-grade thermal sources, such as

solar or geothermal, can be conveniently exploited. Furthermore, since the driving force of the process is a difference of partial pressure of water at the two sides of the membrane, the operating pressures of MD are well below the ones used for pressure driven membrane processes such as RO and this fact results in less severe fouling phenomena and operating costs for the same concentration factor. Moreover, unlike RO the osmotic pressure is not a limiting factor for achieving both very high concentration factor and water recovery. Since only water vapor can pass through the membrane, theoretically MD can provide a complete rejection of all non-volatile compounds.

All these features mean that MD can be really considered a competitive process for water treatment. Nevertheless, MD application nowadays has been hindered by some limiting factors. The thermal conductivity of the membrane as well as the evaporation and condensation processes lead to high heat losses. Moreover, the permeate flux is lower compared to RO performance and heavily affected by the feed fluid dynamics and by temperature and concentration polarization effects.

Although in most of the MD applications the feed temperature can be lower compared to traditional distillation processes, in some processes it might be required a temperature of the feed close to its boiling point at ambient pressure or even higher for pressurized feeds. Indeed, it is well known that usually an higher feed temperature allow to reach a higher vapour flux through the membrane and a higher thermal efficiency of the process [6,7].

Four main MD configurations have been developed:

- vacuum membrane distillation (VMD),
- sweeping gas membrane distillation (SGMD),
- direct contact membrane distillation (DCMD),
- air gap membrane distillation (AGMD).

In Figure 1.1 the different MD configurations are schematized.

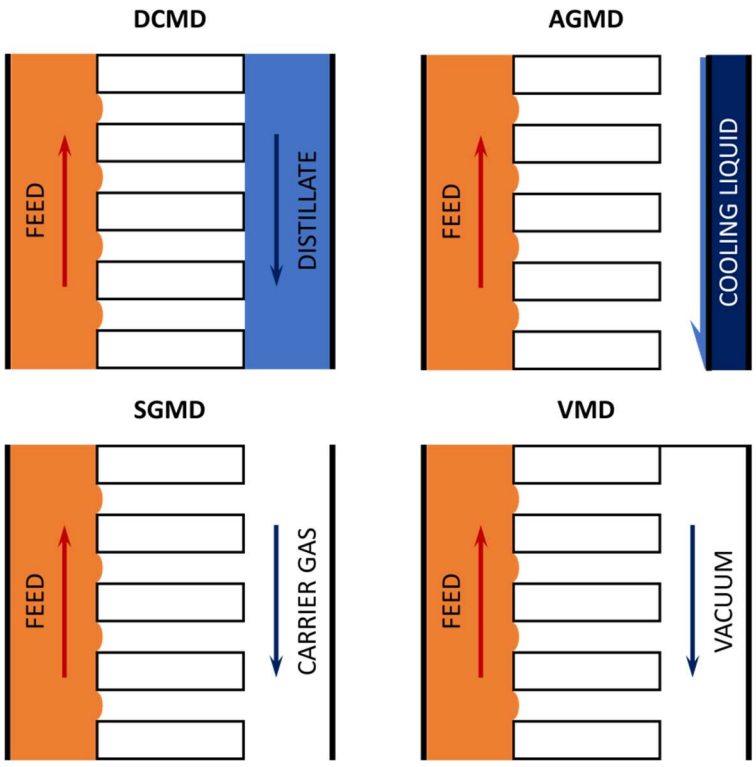

Figure 1.1: Simplified membrane distillation configurations: DCMD = direct contact membrane distillation, AGMD = air-gap membrane distillation, SGMD = sweep gas membrane distillation and VMD = vacuum membrane distillation.

In DCMD configuration the hot feed and the cold distillate are directly in contact through the membrane; since it is the simplest configuration and provides a stable flux of distillate, DCMD is already employed for desalination process. However, DCMD is also characterized by a low energy efficiency and a high pore wetting tendency because of the direct contact between hot and cold liquids. DCMD is probably the simplest configuration but it has the highest heat loss by conduction and it is not suitable to recover other volatile compounds or dissolved gases.

In order to limit the disadvantages of DCMD, in the AGMD configuration a space filled with stagnant air separates the permeate side of the membrane from a cooled plate where the distillate condenses. This reduces the wetting at the permeate side and the thermal loss for conduction through the membrane but also the flux is lowered. AGMD has less conductive heat loss, low tendency to fouling, high flux but there is an additional mass transfer resistance and module design is more difficult. Variants of AGMD are the liquid gap membrane distillation (LGMD) or permeate gap membrane distillation (PGMD) where a liquid, usually the permeate fills the gap between the membrane and the condenser surface [8].

In the VMD configuration vacuum is applied on the permeate side of the membrane and the vapour is condensed in an external cooler. The heat loss is lower than the one of the other MD configurations but the pore wetting on the feed side and fouling phenomena can be more relevant

due to the presence of a pressure gradient [9–11]. In VMD the conductive heat loss is negligible due the lower heat transfer conductivity of vapours at low pressure, the permeate flux is high and the recovery of the most volatile compound occurs. In VMD due to the establishment of a pressure gradient between the two membrane sides, the risk of pore wetting is higher as well as the possibility of fouling the membrane. In VMD an external vacuum pump and an external condenser need to be included in the process layout.

In the SGMD configuration a carrier gas flows in the distillate channel of the membrane module and carries the vapour to an external cooler. The permeate flux is lower than in VMD and in addition large condensers are necessary due to the low vapor concentration in the sweep gas.

SGMD is less affected by thermal polarization than the following DCMD and it is suitable to remove volatile compounds and dissolved gases like as VMD.

1.2 Mass transport

The driving force of membrane distillation is a difference in water vapour pressure across the porous membrane and the flux can be described as follows [12]:

$$J = k_m(p_f - p_d) \qquad 1.4$$

where k_m is the membrane mass transfer coefficient, p_f and p_d are the water vapour pressure at the feed side and at the distillate side, respectively.

The mass transport through the membrane pores can be modelled following three possible mechanisms: molecular diffusion, Knudsen diffusion and Poiseuille flow [12–14]. The relative contribution to the overall transmembrane flux is governed by the membrane pore size and by the pressure of the system.

In order to determine which transfer mechanism is predominant in a determined case, it is useful to evaluate the Knudsen number (*Kn*) defined as the ratio between the mean free path of water molecules (λ) and the membrane pore diameter (*2r*), $Kn = \lambda/2r$. It is worth quoting that the mean free path can be expressed as follows [15]:

$$\lambda = \frac{k_b T}{\sqrt{2} p_{av} \sigma^2} \qquad 1.5$$

where σ is the collision diameter, k_b is the Boltzmann constant, p_{av} is the mean pressure inside the pores and T is the absolute temperature.

When the pores are filled with air, such as the case of AGMD, SGMD and normal DCMD, the molecular diffusion model is adequate when $Kn < 0.01$, while with $Kn > 1$ pure Knudsen diffusion model must be used to calculate the mass transfer coefficient. Instead, when $0.01 < Kn < 1$, the mass transfer through the membrane happens following a combined mechanism, in which one of the two processes can be predominant [9].

For what concerns deaerated systems (such as VMD and deaerated DCMD), Knudsen numbers lower than 0.01 are related to pure Poiseuille flow while Knudsen numbers higher than 1 indicate a state of pure Knudsen diffusion [5,9].

Since the majority of the membranes has various families of pore sizes, the different mass transfer mechanisms can coexist during the distillation process [15,16].

1.2.1 Molecular diffusion.

Molecular diffusion occurs in aerated systems when $Kn < 0.01$. In these conditions, the interactions between every water molecule passing through the membrane and the pore walls are negligible in comparison with the collisions between the water molecule and the air components.

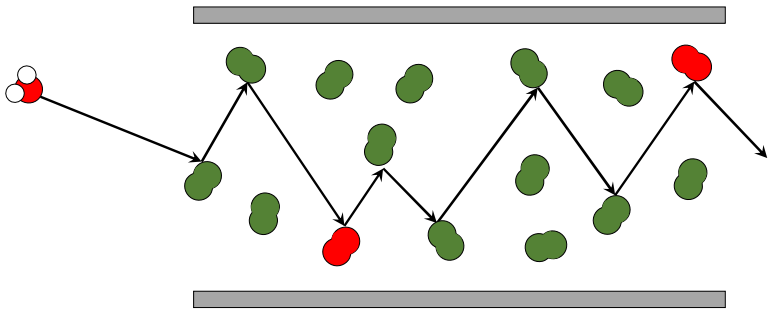

Figure 1.2: Molecular diffusion mechanism.

The path followed by a water molecule through a pore in pure molecular diffusion conditions is schematized in Figure 1.2. The mass transfer resistance is generated by the loss of momentum after each collision between the water molecule and the air in the pores. Therefore, the mass transfer coefficient for this mechanism (k_m^D) can be evaluated as follows [5]:

$$k_m^D = \frac{DP}{RTP_a} \cdot \frac{\varepsilon}{\delta\tau} \qquad 1.6$$

where D is the diffusion coefficient of water molecules in air, P is the total pressure inside the membrane pores, R is the universal gas constant, T is the absolute temperature, P_a is the air pressure in the pores, ε is the membrane porosity, τ is the pore tortuosity and δ is the membrane thickness. The porosity, as well as the membrane thickness, can be easily measured while the tortuosity is usually unknown. However, some empirical relationships, like Equation 1.7 [17], have been developed to correlate the tortuosity value to the porosity grade:

$$\tau \approx \frac{1}{\varepsilon} \qquad 1.7$$

A similar concept can be exploited to evaluate the diffusion coefficient (D). For water/air systems, the term DP in Equation 1.6, can be calculated using the following equation [16]:

$$DP = 1.895 \cdot 10^{-5} \cdot T^{2.072} \qquad 1.8$$

On the basis of Equation 1.8, the molecular diffusion mass transfer coefficient is almost proportional to the temperature increase.

1.2.2 Knudsen diffusion

As reported in Paragraph 1.2, pure Knudsen diffusion takes place when $Kn > 1$. This condition happens when the pore size is small enough for the water molecule to collide more frequently with the pore walls than with the trapped air constituents, as schematized in Figure 1.3.

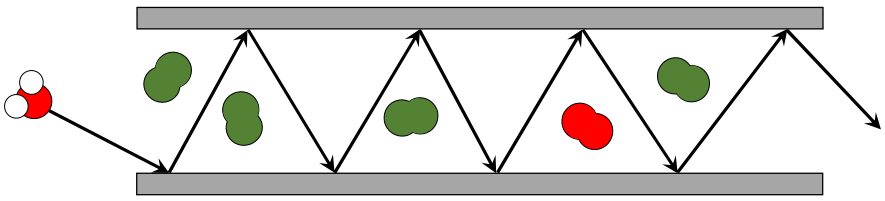

Figure 1.3: Knudsen diffusion mechanism.

Therefore, mass transfer resistance is generated by the transfer of momentum to the pore walls and the mass transfer coefficient can be estimated using the following equation [18]:

$$k_m^K = \frac{2}{3RT} \cdot \sqrt{\frac{8RT}{\pi M_w}} \cdot \frac{\varepsilon r}{\delta \tau} \qquad 1.9$$

where r is the pore radius and M_w is the water molecular weight.

The raise of the temperature results in an increase of the frequency of the water molecule – pore walls collision, causing consequently a reduction of the mass transfer coefficient [5].

1.2.3 Poiseuille flow

Poiseuille – or viscous – flow takes place in deaerated systems under a pressure gradient when the pores are large enough (e.g. $d_p > 100\lambda$) [15].

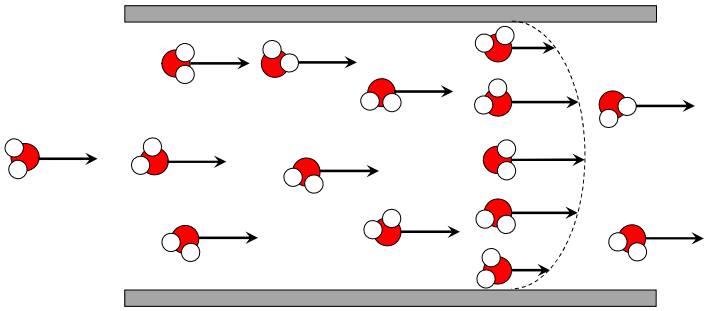

Figure 1.4: Poiseuille flow mechanism.

In this state, the mass transfer resistance is generated by the transfer of momentum from the water molecules to the pore walls because of viscous drag. Since Poiseuille flow takes place only in deaerated systems, in MD applications it is limited to deaerated DCMD and VMD configurations [5].

The mass transfer coefficient for this mechanism can be estimated as follows [12]

$$k_m^V = \frac{M_w P_a}{8\mu RT} \cdot \frac{\varepsilon r^2}{\delta\tau} \qquad 1.10$$

where μ is the dynamic viscosity of water vapor at the temperature of operation.

1.2.4 Concentration polarization

The concentration polarization effect is the increase of the solute concentration in the boundary layer close to membrane surface in the feed channel as schematized in Figure 1.5.

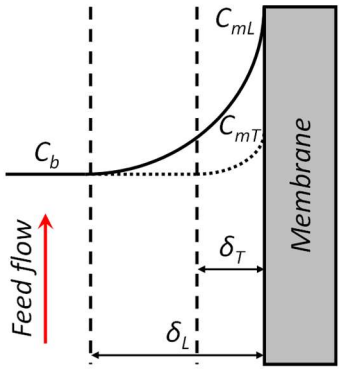

Figure 1.5: Concentration profiles in the feed channel under laminar and turbulent regime.

This phenomenon, common to all membrane separation processes, is induced by the removal of water from the feed by the membrane and can generate various undesired effects. First, the boundary layer increases the overall mass transfer resistance [19]; secondly the increase of the concentration on the membrane surface can lead to pore wetting or even to scaling and fouling formation [20].

Concentration polarization is an equilibrium process and steady-state solute concentration profiles are established when the rate of back diffusion induced by the concentration difference between the membrane surface and the feed bulk becomes equal to the rate at which new solutes are transported to the interface by convective flow [5]. In order to reduce the boundary layer thickness, and the concentration polarization effect, high feed velocities and turbulence promoters can be applied [21]. The concentration polarization coefficient (θ_C) can be used as an indicator of the mass transfer resistance provided by the boundary layer and can be evaluated as [5]:

$$\theta_C = \frac{C_m}{C_b} \qquad 1.11$$

1.3 Heat transport

During MD operation, mainly two heat transfer phenomena occur. Firstly, the heat loss due to conduction through the membrane (Q_C), and secondly the latent heat transfer (Q_L) correlated with the mass transfer, easily calculated as the product of the transmembrane water flux and the latent

heat of evaporation of water. Instead, the heat transfer due to conduction can be evaluated with the following equation [12]:

$$Q_c = \frac{h_m}{\delta}(T_{fm} - T_{dm}) \qquad 1.12$$

where T_{fm} and T_{dm} are the temperatures on the membrane surface at the feed and distillate side, respectively, while h_m is the effective thermal conductivity of the membrane. Since the membrane is porous, h_m can be calculated considering the porosity and the thermal conductivities of the solid material (h_s) and of the gas trapped within the pores (h_g), as follows [22].

$$h_m = \varepsilon h_g + (1 - \varepsilon)h_s \qquad 1.13$$

The two mechanisms happen in different extent in every MD configuration; however, heat loss due to conduction through the membrane can be neglected in the VMD configuration thanks to low gas pressure on the distillate side of the membrane [23].

1.3.1 Temperature polarization

The temperature polarization phenomenon is the change of the temperature on the membrane surface in respect to the bulk value. This effect can occur on both sides of the membrane, as schematized in Figure 1.6.

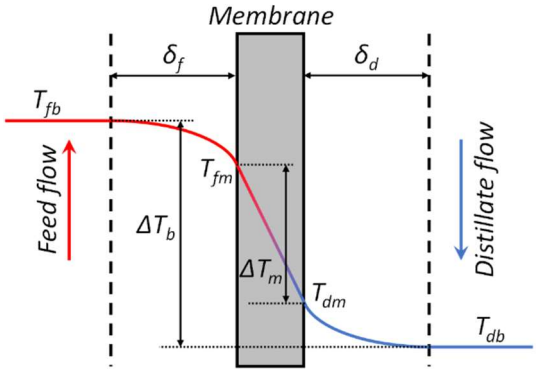

Figure 1.6: Temperature polarization profiles.

On the feed side, the temperature on the membrane surface is lower than in the bulk while on the distillate side the membrane surface is hotter than the bulk distillate. This phenomenon is generated by the heat transfer through the membrane and by the presence of a boundary layer on each membrane side. This effect results in a decrease of the effective driving force for MD process. The

temperature polarization coefficient (θ_T) quantifies the fraction of the total thermal driving force (ΔT_b between feed and distillate bulk) that contributes to the mass transfer driving force (ΔT_m between the membrane sides) and referring to Figure 1.6 it is expressed as [24]:

$$\theta_T = \frac{\Delta T_m}{\Delta T_b} = \frac{T_{fm} - T_{dm}}{T_{fb} - T_{db}} \qquad 1.14$$

Temperature polarization is an unavoidable effect during MD, but its intensity can be moderated operating in turbulent conditions [25].

1.4 Membranes and modules for MD

Like in other membrane processes the membrane itself is one of the most important factors contributing to the MD performance. The hydrophobic character is essential since it prevents pore wetting but other important requirements are a high porosity to extend as much as possible the effective liquid-gas interface and a narrow pore size distribution [26]. In fact, the largest pores are flooded more easily and can let the feed solution pass through the membrane compromising the separation properties of the whole process [10,27].

Since during the distillation operation the membrane porosity should remain only filled by the vapours generated on the feed side, one of the most important parameters is the liquid entry pressure (LEP_w) which is defined as the lowest feed pressure that allows the passage of liquid through the membrane. From this value, the largest pore size can be estimated using the Cantor-Laplace equation:

$$LEP_w = \frac{2B\gamma_l cos\theta}{r_{max}} \qquad 1.15$$

Where B is a geometric factor accounting for the pore shape ($0<B<1$ for non-cylindrical shapes; $B=1$ for cylindrical pores), γ_l is the liquid surface tension, r_{max} is the largest pore size and θ is the contact angle between the membrane and the liquid feed.

The liquid entry pressure usually decreases by increasing the temperature due to decreasing contact angle and surface tension. LEP_w is of particular significance in VMD which works under a pressure gradient. Therefore, for VMD the requirement of a very narrow pore size is more important that with the other configurations.

Usually in MD polymeric membranes originally designed for microfiltration are still widely used, and therefore the optimization of the structure/material and a proper membrane functionalization can still strongly improve the performance of the MD process [10,26]. It is suggested that the maximum pore size to prevent wetting remains between 0.1 and 0.6 microns [9]. An example of study on the effect of process variables on the membrane wettability was recently reported by Jacob et al. [28].

As seen LEP_w depends on the liquid surface tension and the contact angle. For the application of MD to the treatment of wastewater, in addition to the influence on the wettability of dissolved inorganic compounds, also the presence of organic molecules, and in particular of oils and surfactants, can strongly affect the surface tension and the contact angle determining the pore wetting and in turn the liquid intrusion in the membrane porosity. An example of how the presence of a surfactant can affect the membrane wettability is given by Eykens et al. [29]. Then we should warn that a partial membrane flooding might occur even at pressures lower than LEP_w determined with pure or saline water. Moreover, pore wetting can take place slowly, then the long-term stability assessment at specific operating conditions becomes a necessary step before any evaluation of application on an industrial scale.

The main polymers used because of their lower surface energy are polytetrafluoroethylene (PTFE), polyvinylidene fluoride (PVDF) and polypropylene (PP). Commercial membranes made of those polymers are easily available. In Figure 1.7 the surface morphologies of some commercial PP and PTFE membranes are shown.

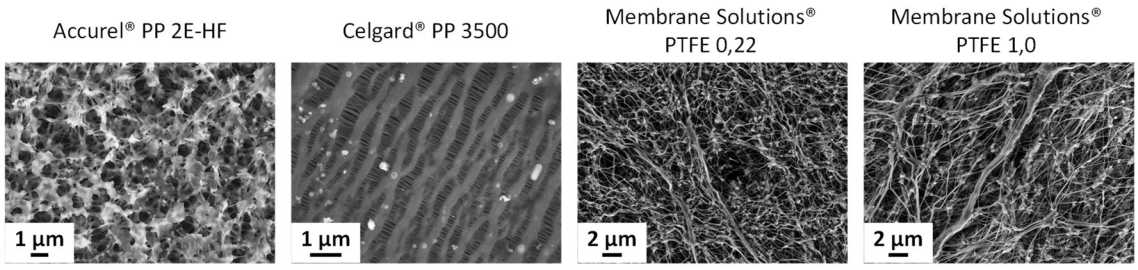

Figure 1.7: Examples of surface morphology of four commercial membranes.

Researchers are also developing membranes based on polyvinylidene fluoride-hexafluoropropylene (PVDF-HFP) [30,31] or poly(tetrafluoroethylene-co-hexafluoropropylene-co-vinylidene fluoride) prepared by electrospinning [32].

Some efforts in developing novel MD membranes are aimed to create membrane surfaces less prone to pore wetting by introducing omniphobic character [33,34]. As reported in the review of Lu et al. [34] one of the approaches to obtain an omniphobic character is to improve the roughness

of the membrane surface for example by addition of hydrophobic nanoparticles. Therefore, omniphobic membranes are of high interest for MD application in wastewater with low surface tension. Another approach to mitigate wetting and reduce the fouling impact consists in creating layered hydrophobic-hydrophilic membranes. The presence of an hydrophilic surface layer hosts an hydration layer which prevents the oil wetting [35,36].

However, with polymeric membranes the maximum temperature of the feed stream is limited by the physical properties of the material itself. On the other hand, ceramic membranes are made of metal oxides (e.g. alumina, silica) and have better mechanical properties and a higher thermal resistance but, because of the hydroxyl groups on their surface, they have a hydrophilic behaviour [37–41].

Various techniques to change the hydrophilicity of the membrane, such as plasma modification, microwave plasma-enhanced chemical vapour deposition and reaction with low surface energy compounds, have been investigated [39]. As a matter of fact, the development of hydrophobic ceramic membranes can extend the possible applications of MD processes to cases in which the operating conditions (e.g. temperature, pressure) prevent the use of polymeric membranes [42].

1.5 Membrane preparation techniques

The manufacturing of the membranes follows different techniques depending on the polymer such as nonsolvent or thermally induced phase separation (NIPS or TIPS), melt extrusion stretching, sintering and electrospinning [11]. PTFE is characterized by an excellent thermal and chemical stability as well as a low surface energy that allow to prepare membranes with great hydrophobicity and good wetting resistance. The melting point of PTFE is very high (327°C) and since it does not dissolve in any solvent at room temperature the preparation of the PTFE membranes is quite complicated. PTFE membranes are prepared by extrusion, rolling, stretching, sintering or only in particular conditions by melt processing techniques [10,11,26].

PP membranes can be prepared both with a stretching method and by the TIPS process. In this latter case a PP polymer is mixed with adequate diluents and heated up to its melting point: a homogeneous solution is formed and cast. The phase separation is then obtained by cooling [43].

PVDF is a soluble polymer, therefore TIPS and NIPS process are used. Differently from the thermal process, in the non-solvent induced phase separation the casted solution is submerged in an adequate liquid that extracts the solvent from the solution. Thus, the polymer precipitates forming a porous matrix; the morphology of the membrane is controlled by the composition of the solution and by the interaction between the non-solvent and the solvent.

1.5.1 Sintering

The sintering technique is used to prepare mainly ceramic membranes. A powder of the starting material is first put in a mould of a proper shape and is subsequently pressed and heated up to a temperature similar to the material melting point. This technique produces symmetric membranes and the pore sized is determined by the powder size and the sintering protocol, namely the applied temperature and pressure [44,45].
In order to tune the pore size to the most appropriate value for each application, multiple layers can be produced. Each subsequent layer is produced using smaller particles and the membrane is sintered at lower temperatures [46].
The sintering technique has also been proposed for the preparation of polymeric membranes made of fluoropolymers, such as polytetrafluoroethylene [47,48]

1.5.2 Stretching

The stretching method is widely used to produce membranes starting from semi-crystalline polymers, such as PTFE [49], PP and PE [50].
First, a dense polymeric layer is produced by means of extrusion and is then thinned using rolling systems until it reaches the needed thickness. The dense layer is the stretched two times, the first at room temperature to create initial micropores, and a second time at higher temperature in order to increase the pore size and the overall porosity [51]. Moreover, the stretching process can be applied on one direction (creating the structure reported in Figure 1.7B) or to perpendicular axis, generating the morphology showed in Figure 1.7C and D [44].

1.5.3 Electrospinning

Electrospinning is a new technique to prepare porous membranes that is still at a developing stage. A polymeric solution – or a melted polymer – is put in a pump syringe and a high electrical potential is applied between the syringe needle and a collector plate. Under the electric field, the polymer solution forms a Taylor cone at the needle exit. As the jet becomes thinner, the solvent evaporates and the polymer creates fibres that are collected on the plate [52].
The membrane morphology can be tuned by modifying the spinning conditions and the solution characteristics [51].

1.5.4 Thermally induced phase separation (TIPS)

During the TIPS process, the phase separation is obtained lowering the temperature of a homogeneous solution. The polymer - diluent system must be chosen considering some requirements:

- It must create a homogeneous solution at high temperature;
- It must present a miscibility gap at lower temperature;
- The polymer and the diluent must be stable at high temperatures.

Figure 1.8 schematize the phase diagram for a semicrystalline polymer – diluent system. Once the hot dope solution is obtained (A_1, B_1, C_1), it is extruded in the required form (flat sheet, tube of hollow fibre) and is then cooled under the critical temperature (T_c) at a controlled cooling rate, inducing the phase separation (A_2, B_2, C_2). The residual diluent trapped in the porous structure is then removed using an extractant that is subsequently evaporated to obtain the final dry membrane [15,44,53].

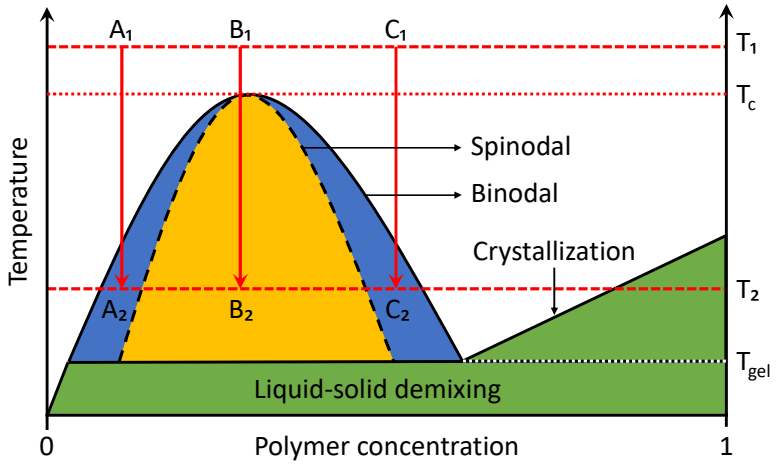

Figure 1.8: Schematic phase diagram of a binary polymer/diluent system.

The phase separation can proceed following two different paths, on the basis of the dope solution composition: nucleation and growth or spinodal composition. When the starting solution, prepared at a temperature higher than the critical temperature (T_c), is cooled, it can reach two different zones in the phase diagram (Figure 1.8): a metastable zone (blue) where phase separation proceeds via nucleation and growth, and a unstable zone (yellow) where spinodal decomposition takes place [15,44]. In the case of semicrystalline polymers, at certain preparation conditions – such as high polymer concentrations – polymer crystallization can take place [54].

1.5.5 Non-solvent induced phase separation (NIPS)

In the nonsolvent induced phase separation process, a polymer solution is casted onto a flat surface and then immersed in an adequate nonsolvent bath. A solvent/nonsolvent exchange takes place and, once passed a critical composition, the polymer solution becomes thermodynamically unstable and faces a liquid-liquid phase separation into a polymer-rich and a polymer-poor solution [55–57]. Figure 1.9 schematize a phase diagram for a crystallizable polymer – solvent – nonsolvent system.

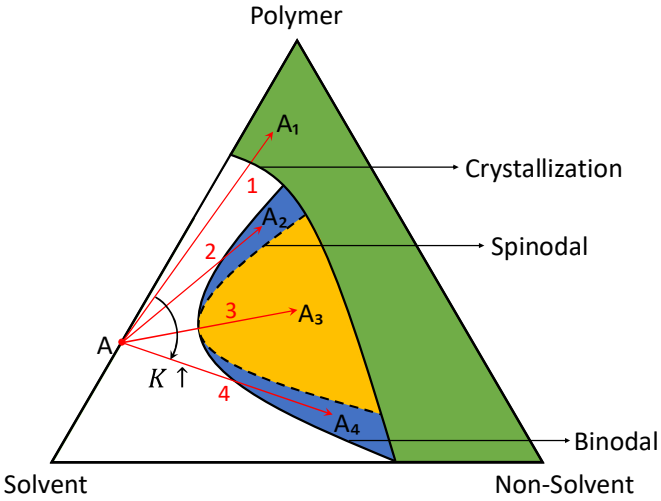

Figure 1.9: Schematic phase diagram of a ternary polymer/solvent/nonsolvent system.

Starting from a homogeneous solution (A) the phase separation can proceed following four different paths, reaching the points A1, A2, A3 or A4 depending on the solvent-nonsolvent exchange rates. As the parameter K – defined as the ratio between the solvent outflux rate and the nonsolvent influx rate ($K = v_{s(out)}/v_{ns(in)}$) – decreases, the system moves from path 1 to path 4 leading to different structures [15].

Following path 1, the system crosses the crystallization/vitrification line without entering the metastable or the unstable regions and a homogeneous dense film is created.

Paths 2 and 4 bring the system in the metastable region after crossing the binodal line. The phase separation takes place via a nucleation and growth mechanism of the polymer-poor (path 2), or of the polymer rich phase (path 4). In the first case, dispersed pores in the polymer matrix are created while in the latter a brittle film constituted by polymer globes is formed [53].

Finally, if the system follows path 3, it crosses the binodal and spinodal lines in a zone close to the critical point reaching the unstable zone. The membrane is formed by a spinodal decomposition process and is characterized by a bicontinuous structure [58].

When the polymer can crystallize, the phase diagram becomes more complicated and it present zones where a crystalline and a liquid phase are in equilibrium and other zones where two liquid phases coexist. Therefore, polymer crystallization and liquid-liquid demixing take place simultaneously [54].

The phase demixing kinetics is highly influenced by the system components and their concentrations. In particular the nonsolvent is defined strong when its affinity with the polymer is low and the solvent nonsolvent exchange rate is fast [59–61]; in this case instantaneous demixing of the polymer solution takes place and the membrane is characterized by a denser top layer onto a substrate presenting finger-like or pear-shaped macrovoids [62]. Instead, when the nonsolvent affinity with the polymer is higher, the precipitation is slower and delayed demixing (liquid-liquid phase separation) occurs [60,61,63–66]. In this conditions, being PVDF a semi-crystalline polymer, its phase separation behaviour is more complicated, i.e. a solid-liquid phase separation via the nucleation-growth mechanism of polymer crystals becomes also possible [63,67,68]. The precipitation rate is related to the affinity of the polymer with both the nonsolvent and the solvent. Both the polymer-nonsolvent and polymer-solvent interactions can be estimated in terms of solubility parameters difference. Large differences between the polymer and the nonsolvent solubility parameters result in lower compatibility of the two substances and fast precipitation rates. On the other hand, small disparity between the polymer and the solvent parameters are related to greater affinity. In this condition, the removal of the solvent is hindered and the phase separation process is slower [69].

The different combinations of liquid-liquid and solid liquid demixing in the formation process can yield to very dissimilar and sophisticated morphologies [63,67,68], determining the overall membrane structure and its mechanical properties. Moreover, using weak nonsolvents, the membrane tends to have a more symmetric structure.

1.6 Membrane modules

One of the reasons for popularity of membrane technology is certainly due to its easier scalability being modular. Membranes assembled in adequate modules should exploit their productivity by optimizing all the operational variables. Indeed, module design has the main objective of realizing very high specific membrane area per volume ratios, allowing high flow rates in a small footprint. Moreover, the fluid dynamics are highly affected by the module geometry and as mentioned above play a key role in the membrane performance, controlling temperature and concentration polarization phenomena along the membrane.

In conclusion the optimal design approaches able to provide the highest heat and mass transfer in a MD module should:

- minimize the concentration polarization effects
- minimize the temperature polarization effects
- ensure low fouling tendency

To minimize the polarization phenomena the module should allow high feed velocity in order to be as much as possible in a turbulent regime near the membrane surface. Most of the studies carried out on MD pilot units used modules developed for other membrane processes and therefore not optimized for the distillation purposes.

Many membrane modules have been proposed in order to satisfy different process requirements [70]. In general three main module schemas are categorized:

- shell and tube modules for hollow fibre or tubular membranes
- spiral wound for flat sheet membranes
- plate and frame modules for flat sheet membranes

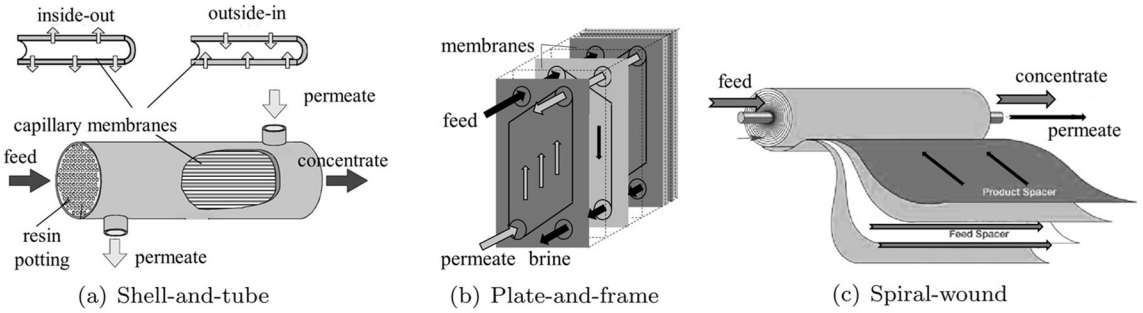

Figure 1.10: Membrane modules. a) Shell-and tube, b) plate and frame, c) spiral wound (adapted from [70]).

The shell-and-tube module is widely studied and used for all the MD configurations (DCMD, AGMD, SGMD and VMD) because it allows to reach high surface area/module volume ratios and it is also easy to produce. The tubular or the hollow fibre membranes can operate in outside-in configuration, where the feed is flowing on the external side of the tubes or in the inside-out configuration where the feed is sent in the membrane lumen. The wide availability of membranes with different pore size and channel diameter makes it possible to treat many different feeds, even with suspended solids (if the outside-in configuration is used). However, low flux and weakness of the fibres are the main disadvantages of this scheme [71].

Instead, flat sheet membranes can be assembled in plate and frame or spiral wound modules. Since this kind of membranes is thinner than hollow fibres, they can provide higher permeability but also

need a porous support that provides the mechanical strength. The two module types have different strengths and weaknesses: the plate and frame modules allow higher tangential flow rates, diminishing concentration polarization and fouling effects and, moreover, the membranes can be easily replaced. However the plate and frame modules provide a low packing density (100–400 m^2/m^3) and a poor energy efficiency [26,72].

The choice of the appropriate module configuration as well as the MD process mode relies on the feed characteristics and the needed recovery. Thus, various companies provide plants with different configurations and scales [73]. Some examples are reported in Table 1.1:

Table 1.1: Some commercial membrane desalination technologies and their characteristics.

Company	Technology	Module Geometry	Productivity	Reference
Memsys	V-MEMD	Plate and frames	3-1000 m^3/day	[74]
Aquastill	DCMD AGMD LGMD	Spiral wound	4800-24000+ m^3/day	[75]
Thermosift	Joule Tompson effect	Hollow fibre	1- 50 m^3/day	[76]
Petrosep	VMD	Hollow fibre	50-1000 m^3/day	[77]
KMX	VMD	Hollow fibre	10-1000 m^3/day	[78,79]
Econity	VMD	Hollow fibre	400 m^3/day	[79]
Solar Spring	PGMD	Spiral wound	0.6 m^3/day	[79]
Scarab AB	AGMD	Plate and frames	2 m^3/day	[79]

The development of MD modules requires practical and engineering skills to properly configure an effective exploitation of the membrane area during the distillation process. Modelling becomes an essential tool to design and foresee the module behaviour during the distillation process since both mass and heat transfer dynamics in the module itself need to be understood and controlled. The theoretical description of MD in the different configurations has been well discussed by some authors elsewhere [80] and it is not included in the aim of this chapter. Examples of theoretical analysis and simulation of MD modules can be found in [81,82].

1.7 Aim of PhD work

The aim of the PhD research activity was the development of new and efficient membranes for distillation applications. Indeed, the membrane performance is still one of the limiting factors that hinder the development of the MD process up to an industrial level.

As explained, membranes for application in MD should possess as minimum requirements high hydrophobicity, small pore size, high porosity to display a satisfactory and stable MD performance (permeability and selectivity). Hydrophobic polymers are the most studied materials to this end, and in particular PVDF owing its optimal characteristics, especially its solubility in many solvents. This allows to use the NIPS technique, a simple and flexible method to prepare porous membranes. This choice was considered a good starting point to continue development and improvement of the membrane characteristics, as a great deal of research is still to be done on this polymeric material. A vast variety of final structures can be expected in the case of polymers, as PVDF, that can crystallize extensively, because membrane formation involves a complex interplay of different phenomena. Employing semicrystalline polymers, the sequence and the extent of the phase separation steps (liquid-liquid or solid-liquid demixing, crystallization) directs the ultimate porous structure of the membrane. The phase demixing kinetics is highly influenced by the system components and their concentrations.

Therefore, the main parameters influencing morphology and performance of the formed membrane were extensively investigated, including polymer concentration in the dope solution, casting thickness of the initial solution, harshness of the precipitation bath (Chapter 2), addition of pore formers (Chapter 3), use of different types of supports (or casting without a support) (Chapter 4). The focus was on developing PVDF membranes with narrow pore size distribution and high porosity and LEP, suitable for MD and in particular for VMD applications.

In most of the MD applications the feed temperature is quite low, but in principle MD could be extended to processes in which the operating temperature and pressure are more severe. These conditions prevent the use of polymeric membranes, whereas hydrophobic ceramic membranes could be excellent candidates. Ceramic membranes are however intrinsically hydrophilic and for this reason appropriate surface treatments are necessary to switch the membrane behaviour towards hydrophobicity. Part of the research program was devoted to this interesting subject (Chapter 5). In particular ceramic membranes alumina-based were treated by grafting methyltrichlorosilane at different functionalization degrees, with the objective of getting hydrophobic membranes with high thermal stability and satisfying MD performance.

References

[1] M. Yaqub, W. Lee, Zero-liquid discharge (ZLD) technology for resource recovery from wastewater, Sci. Total Environ. 681 (2019) 551–563.

[2] B.R. Bodell, Silicone rubber vapor diffusion in saline water distillation, U.S. Patent 285 032, 1963.

[3] K. W. Lawson, D. R. Lloyd, Membrane Distillation - Review, J. Memb. Sci. (1997).

[4] J.I. Mengual, M. Khayet, M.P. Godino, Heat and mass transfer in vacuum membrane distillation, Int. J. Heat Mass Transf. 47 (2004) 865–875. doi:10.1016/j.ijheatmasstransfer.2002.09.001.

[5] R.A. Johnson, M.H. Nguyen, Understanding Membrane Distillation and Osmotic Distillation, John Wiley & Sons, Inc., Hoboken, New Jersey, 2017. doi:10.1002/9781118880319.

[6] A.M. Alklaibi, N. Lior, Membrane-distillation desalination: Status and potential, Desalination. 171 (2004) 111–131. doi:10.1016/j.desal.2004.03.024.

[7] A. Luo, N. Lior, Study of advancement to higher temperature membrane distillation, Desalination. 419 (2017) 88–100. doi:10.1016/j.desal.2017.05.020.

[8] L. Cheng, Y. Zhao, P. Li, W. Li, F. Wang, Comparative study of air gap and permeate gap membrane distillation using internal heat recovery hollow fiber membrane module, Desalination. 426 (2018) 42–49. doi:10.1016/j.desal.2017.10.039.

[9] A. Alkhudhiri, N. Darwish, N. Hilal, Membrane distillation: A comprehensive review, Desalination. 287 (2012) 2–18. doi:10.1016/j.desal.2011.08.027.

[10] E. Drioli, A. Ali, F. Macedonio, Membrane distillation: Recent developments and perspectives, Desalination. 356 (2015) 56–84. doi:10.1016/j.desal.2014.10.028.

[11] P. Wang, T.S. Chung, Recent advances in membrane distillation processes: Membrane development, configuration design and application exploring, J. Memb. Sci. 474 (2015) 39–56. doi:10.1016/j.memsci.2014.09.016.

[12] R.W.W. Schofield, A.G.G. Fane, C.J.D.J.D. Fell, Heat and mass transfer in membrane distillation, J. Memb. Sci. 33 (1987) 299–313. doi:10.1016/S0376-7388(00)80287-2.

[13] R.W. Schofield, A.G. Fane, C.J.D. Fell, Gas and vapour transport through microporous membranes. I. Knudsen-Poiseuille transition, J. Memb. Sci. 53 (1990) 159–171. doi:10.1016/0376-7388(90)80011-A.

[14] R.W. Schofield, A.G. Fane, C.J.D. Fell, Gas and vapour transport through microporous membranes. II. Membrane distillation, J. Memb. Sci. 53 (1990) 173–185.

doi:10.1016/0376-7388(90)80012-B.

[15] M. Khayet, T. Matsuura, Membrane Distillation: Principles and Applications, Elsevier, 2011. doi:10.1016/C2009-0-17487-1.

[16] J. Phattaranawik, R. Jiraratananon, A.G. Fane, Effect of pore size distribution and air flux on mass transport in direct contact membrane distillation, J. Memb. Sci. 215 (2003) 75–85. doi:10.1016/S0376-7388(02)00603-8.

[17] L. Li, K.K. Sirkar, Influence of microporous membrane properties on the desalination performance in direct contact membrane distillation, J. Memb. Sci. 513 (2016) 280–293. doi:10.1016/j.memsci.2016.04.015.

[18] T. Matsuura, Synthetic Membranes and Membrane Separation Processes, CRC Press, 1993. doi:10.1201/9781003068037.

[19] K.W. Lawson, D.R. Lloyd, Membrane distillation, J. Memb. Sci. 124 (1997) 1–25. doi:10.1016/S0376-7388(96)00236-0.

[20] M. Rezaei, D.M. Warsinger, J.H. Lienhard V, M.C. Duke, T. Matsuura, W.M. Samhaber, Wetting phenomena in membrane distillation: Mechanisms, reversal, and prevention, Water Res. 139 (2018) 329–352. doi:10.1016/j.watres.2018.03.058.

[21] S. Armbruster, O. Cheong, J. Lölsberg, S. Popovic, S. Yüce, M. Wessling, Fouling mitigation in tubular membranes by 3D-printed turbulence promoters, J. Memb. Sci. 554 (2018) 156–163. doi:10.1016/j.memsci.2018.02.015.

[22] G.C. Sarti, C. Gostoli, S. Matulli, Low energy cost desalination processes using hydrophobic membranes, Desalination. 56 (1985) 277–286. doi:10.1016/0011-9164(85)85031-1.

[23] K.W. Lawson, D.R. Lloyd, Membrane distillation. I. Module design and performance evaluation using vacuum membrane distillation, J. Memb. Sci. 120 (1996) 111–121. doi:10.1016/0376-7388(96)00140-8.

[24] A.G. Fane, R.W. Schofield, C.J.D. Fell, The efficient use of energy in membrane distillation, Desalination. 64 (1987) 231–243. doi:10.1016/0011-9164(87)90099-3.

[25] N.N. Li, A.G. Fane, W.S.W. Ho, T. Matsuura, eds., Advanced Membrane Technology and Applications, John Wiley & Sons, Inc., Hoboken, NJ, USA, 2008. doi:10.1002/9780470276280.

[26] L. Eykens, K. De Sitter, C. Dotremont, L. Pinoy, B. Van der Bruggen, Membrane synthesis for membrane distillation: A review, Sep. Purif. Technol. 182 (2017) 36–51. doi:10.1016/j.seppur.2017.03.035.

[27] K.Y. Wang, T.S. Chung, M. Gryta, Hydrophobic PVDF hollow fiber membranes with narrow pore size distribution and ultra-thin skin for the fresh water production through membrane distillation, Chem. Eng. Sci. 63 (2008) 2587–2594. doi:10.1016/j.ces.2008.02.020.

[28] P. Jacob, S. Laborie, C. Cabassud, Influence of operating conditions on wetting and wettability in membrane distillation using Detection of Dissolved Tracer Intrusion (DDTI), Desalination. 468 (2019) 114086. doi:10.1016/j.desal.2018.06.006.

[29] L. Eykens, K. De Sitter, C. Dotremont, W. De Schepper, L. Pinoy, B. Van Der Bruggen, Wetting Resistance of Commercial Membrane Distillation Membranes in Waste Streams Containing Surfactants and Oil, Appl. Sci. 7 (2017) 118–130.

[30] M.C. García-Payo, M. Essalhi, M. Khayet, Preparation and characterization of PVDF-HFP copolymer hollow fiber membranes for membrane distillation, Desalination. 245 (2009) 469–473. doi:10.1016/j.desal.2009.02.010.

[31] M.C. García-Payo, M. Essalhi, M. Khayet, Effects of PVDF-HFP concentration on membrane distillation performance and structural morphology of hollow fiber membranes, J. Memb. Sci. 347 (2010) 209–219. doi:10.1016/j.memsci.2009.10.026.

[32] Y. Zhang, B. Yang, K. Li, D. Hou, C. Zhao, J. Wang, Electrospun porous poly(tetrafluoroethylene-: Co -hexafluoropropylene- co -vinylidene fluoride) membranes for membrane distillation, RSC Adv. 7 (2017) 56183–56193. doi:10.1039/c7ra09932k.

[33] S. Lin, S. Nejati, C. Boo, Y. Hu, C.O. Osuji, M. Elimelech, Omniphobic Membrane for Robust Membrane Distillation, Environ. Sci. Technol. Lett. 1 (2014) 443–447. doi:10.1021/ez500267p.

[34] K.J. Lu, Y. Chen, T.S. Chung, Design of omniphobic interfaces for membrane distillation – A review, Water Res. 162 (2019) 64–77. doi:10.1016/j.watres.2019.06.056.

[35] K. Wang, D. Hou, J. Wang, Z. Wang, B. Tian, P. Liang, Hydrophilic surface coating on hydrophobic PTFE membrane for robust anti-oil-fouling membrane distillation, Appl. Surf. Sci. (2018). doi:10.1016/j.apsusc.2018.04.180.

[36] Y.X. Huang, Z. Wang, J. Jin, S. Lin, Novel Janus Membrane for Membrane Distillation with Simultaneous Fouling and Wetting Resistance, Environ. Sci. Technol. (2017). doi:10.1021/acs.est.7b02848.

[37] A. Larbot, L. Gazagnes, S. Krajewski, M. Bukowska, W. Kujawski, Water desalination using ceramic membrane distillation, Desalination. 168 (2004) 367–372. doi:10.1016/j.desal.2004.07.021.

[38] C.-Y. Huang, C. Ko, L. Chen, C. Huang, Y. Liao, A simple coating method to prepare superhydrophobic layers on ceramic alumina for vacuum membrane distillation, Sep. Purif. Technol. 198 (2018) 79–86. doi:10.1016/J.SEPPUR.2016.12.037.

[39] W. Kujawski, J. Kujawa, E. Wierzbowska, S. Cerneaux, M. Bryjak, J. Kujawski, Influence of hydrophobization conditions and ceramic membranes pore size on their properties in vacuum membrane distillation of water-organic solvent mixtures, J. Memb. Sci. 499 (2016) 442–451. doi:10.1016/j.memsci.2015.10.067.

[40] X. Chen, X. Gao, K. Fu, M. Qiu, F. Xiong, D. Ding, Z. Cui, Z. Wang, Y. Fan, E. Drioli, Tubular hydrophobic ceramic membrane with asymmetric structure for water desalination via vacuum membrane distillation process, Desalination. 443 (2018) 212–220. doi:10.1016/j.desal.2018.05.027.

[41] J. Kujawa, S. Cerneaux, W. Kujawski, K. Knozowska, Hydrophobic Ceramic Membranes for Water Desalination, Appl. Sci. 7 (2017) 402. doi:10.3390/app7040402.

[42] Y. Yang, Q. Liu, H. Wang, F. Ding, G. Jin, C. Li, H. Meng, Superhydrophobic modification of ceramic membranes for vacuum membrane distillation, Chinese J. Chem. Eng. 25 (2017) 1395–1401. doi:10.1016/j.cjche.2017.05.003.

[43] J.-H. Zuo, Z.-K. Li, C. Wei, X. Yan, Y. Chen, W.-Z. Lang, Fine tuning the pore size and permeation performances of thermally induced phase separation (TIPS) -prepared PVDF membranes with saline water as quenching bath, J. Memb. Sci. 577 (2019) 79–90. doi:10.1016/J.MEMSCI.2019.02.005.

[44] N. Hilal, A.F. Ismail, C. Wright, eds., Membrane Fabrication, CRC Press, 2015. doi:10.1201/b18149.

[45] P. Wang, P. Huang, N. Xu, J. Shi, Y.S. Lin, Effects of sintering on properties of alumina microfiltration membranes, J. Memb. Sci. 155 (1999) 309–314. doi:10.1016/S0376-7388(98)00297-X.

[46] E. Levänen, T. Mäntylä, Effect of sintering temperature on functional properties of alumina membranes, J. Eur. Ceram. Soc. 22 (2002) 613–623. doi:10.1016/S0955-2219(01)00334-X.

[47] F.A. Ghani, K. Hamzah, W. Norharyati, W. Salleh, H. Mohamed, Preparation and characterization of PTFE flat sheet membrane: Effect of sodium benzoate content, 2017.

[48] K.C. Chao, M.C. Porter, Method for forming microporous fluorocarbon polymer sheet and product, US4196070A, 1980.

[49] R.W. Gore, Process for producing porous products, US3953566A, 1971.

[50] X. Wei, C. Haire, Biaxially oriented microporous membrane, US8795565B2, 2007.

[51] B.S. Lalia, V. Kochkodan, R. Hashaikeh, N. Hilal, A review on membrane fabrication: Structure, properties and performance relationship, Desalination. 326 (2013) 77–95. doi:10.1016/j.desal.2013.06.016.

[52] F.E. Ahmed, B.S. Lalia, R. Hashaikeh, A review on electrospinning for membrane fabrication: Challenges and applications, Desalination. 356 (2015) 15–30. doi:10.1016/j.desal.2014.09.033.

[53] A.G. Fane, C.Y. Tang, R. Wang, Membrane Technology for Water: Microfiltration, Ultrafiltration, Nanofiltration, and Reverse Osmosis, Treatise Water Sci. 4 (2011) 301–335. doi:10.1016/B978-0-444-53199-5.00091-9.

[54] P. Van De Witte, P.J. Dijkstra, J.W.A. Van Den Berg, J. Feijen, Phase separation processes in polymer solutions in relation to membrane formation, J. Memb. Sci. 117 (1996) 1–31. doi:10.1016/0376-7388(96)00088-9.

[55] Y. Li, C. Jin, Y. Peng, Q. An, Z. Chen, J. Zhang, L. Ge, S. Wang, Fabrication of PVDF hollow fiber membranes via integrated phase separation for membrane distillation, J. Taiwan Inst. Chem. Eng. 95 (2019) 487–494. doi:10.1016/j.jtice.2018.08.036.

[56] J.T. Jung, J.F. Kim, H.H. Wang, E. di Nicolo, E. Drioli, Y.M. Lee, Understanding the non-solvent induced phase separation (NIPS) effect during the fabrication of microporous PVDF membranes via thermally induced phase separation (TIPS), J. Memb. Sci. 514 (2016) 250–263. doi:10.1016/j.memsci.2016.04.069.

[57] F. Abdulla AlMarzooqi, M. Roil Bilad, H. Ali Arafat, Improving Liquid Entry Pressure of Polyvinylidene Fluoride (PVDF) Membranes by Exploiting the Role of Fabrication Parameters in Vapor-Induced Phase Separation VIPS and Non-Solvent-Induced Phase Separation (NIPS) Processes, Appl. Sci. 7 (2017) 181. doi:10.3390/app7020181.

[58] L.K. Wang, J.P. Chen, Y.-T. Hung, N.K. Shammas, eds., Membrane and Desalination Technologies, Humana Press, Totowa, NJ, 2011. doi:10.1007/978-1-59745-278-6.

[59] M.G. Buonomenna, P. Macchi, M. Davoli, E. Drioli, Poly(vinylidene fluoride) membranes by phase inversion: the role the casting and coagulation conditions play in their morphology, crystalline structure and properties, Eur. Polym. J. 43 (2007) 1557–1572. doi:10.1016/j.eurpolymj.2006.12.033.

[60] P. Sukitpaneenit, T.S. Chung, Molecular elucidation of morphology and mechanical properties of PVDF hollow fiber membranes from aspects of phase inversion, crystallization and rheology, J. Memb. Sci. 340 (2009) 192–205. doi:10.1016/j.memsci.2009.05.029.

[61] T. Marino, F. Russo, A. Figoli, The Formation of Polyvinylidene Fluoride Membranes with Tailored Properties via Vapour/Non-Solvent Induced Phase Separation, Membranes (Basel). 8 (2018) 71. doi:10.3390/membranes8030071.

[62] A. Bottino, G. Capannelli, A. Comite, Novel porous poly (vinylidene fluoride) membranes for membrane distillation, Desalination. 183 (2005) 375–382. doi:10.1016/j.desal.2005.03.040.

[63] D. Zuo, B. Zhu, C. Jian-hua, Y. Xu, Influence of alcohol-based nonsolvents on the formation and morphology of PVDF membranes in phase inversion process, Chinese J. Polym. Sci. 24 (2006) 281–289.

[64] A. Bottino, G. Camera-Roda, G. Capannelli, S. Munari, The formation of microporous polyvinylidene difluoride membranes by phase separation, J. Memb. Sci. 57 (1991) 1–20. doi:10.1016/S0376-7388(00)81159-X.

[65] H. Strathmann, K. Kock, The formation mechanism of phase inversion membranes, Desalination. (1977). doi:10.1016/S0011-9164(00)88244-2.

[66] C.A. Smolders, A.J. Reuvers, R.M. Boom, I.M. Wienk, Microstructures in phase-inversion membranes. Part 1. Formation of macrovoids, J. Memb. Sci. 73 (1992) 259–275. doi:10.1016/0376-7388(92)80134-6.

[67] M. Tao, F. Liu, B. Ma, L. Xue, Effect of solvent power on PVDF membrane polymorphism during phase inversion, Desalination. 316 (2013) 137–145. doi:10.1016/j.desal.2013.02.005.

[68] L.P. Cheng, T.H. Young, L. Fang, J.J. Gau, Formation of particulate microporous poly(vinylidene fluoride) membranes by isothermal immersion precipitation from the 1-octanol/dimethylformamide/poly(vinylidene fluoride) system, Polymer (Guildf). 40 (1999) 2395–2403. doi:10.1016/S0032-3861(98)00462-5.

[69] H. Strathmann, Synthetic Membranes and Their Preparation, in: Synth. Membr. Sci. Eng. Appl., Springer Netherlands, Dordrecht, 1986: pp. 1–37. doi:10.1007/978-94-009-4712-2_1.

[70] D. Winter, J. Koschikowski, F. Gross, D. Maucher, D. Düver, M. Jositz, T. Mann, A. Hagedorn, Comparative analysis of full-scale membrane distillation contactors - methods and modules, J. Memb. Sci. 524 (2017) 758–771. doi:10.1016/j.memsci.2016.11.080.

[71] M.M. Teoh, N. Peng, T.S. Chung, L.L. Koo, Development of novel multichannel rectangular membranes with grooved outer selective surface for membrane distillation, Ind. Eng. Chem. Res. 50 (2011) 14046–14054. doi:10.1021/ie201292j.

[72] E. Guillén-Burrieza, D.-C. Alarcón-Padilla, P. Palenzuela, G. Zaragoza, Techno-economic assessment of a pilot-scale plant for solar desalination based on existing plate and frame MD technology, Desalination. 374 (2015) 70–80. doi:10.1016/J.DESAL.2015.07.014.

[73] L.M. Camacho, L. Dumée, J. Zhang, J. de Li, M. Duke, J. Gomez, S. Gray, Advances in membrane distillation for water desalination and purification applications, Water (Switzerland). 5 (2013) 94–196. doi:10.3390/w5010094.

[74] Memsys, Products, (2017). https://www.memsys.eu/products.html.

[75] Aquastill, Technology, (2015). http://aquastill.nl/technology/aquapilots/.

[76] Thermosift, Products, (2019). https://www.thermosift.com/products/.

[77] Petrosep, Our products, (2015). http://petrosep.com/our-products/aqua-sep-membrane-distillation-2/.

[78] KMX, Membrane Distillation for Brine Management, 2019.

[79] G. Zaragoza, J.A. Andrés-Mañas, A. Ruiz-Aguirre, Commercial scale membrane distillation for solar desalination, Npj Clean Water. 1 (2018) 1–6. doi:10.1038/s41545-018-0020-z.

[80] B. Bin Ashoor, A. Giwa, S.W. Hasan, Full-Scale Membrane Distillation Systems and Performance Improvement Through Modeling, in: Curr. Trends Futur. Dev. Membr., Elsevier, 2019: pp. 105–140. doi:10.1016/b978-0-12-813551-8.00005-x.

[81] G. Dong, W. Cha-Umpong, J. Hou, C. Ji, V. Chen, Open-source industrial-scale module simulation: Paving the way towards the right configuration choice for membrane distillation, Desalination. (2019). doi:10.1016/j.desal.2019.04.018.

[82] J. Koo, S. Lee, J.S. Choi, T.M. Hwang, Theoretical analysis of different membrane distillation modules, Desalin. Water Treat. (2015). doi:10.1080/19443994.2014.927801.

Chapter 2

2 Effects of polymer concentration and nonsolvent strength

Several studies were performed in order to select good nonsolvents. It was demonstrated by several authors [1–5] that using weaker non solvents the phase separation process follows a different path in which liquid-liquid demixing is delayed and polymer gelation/crystallization can take place before reaching the binodal curve. For example, the phase diagrams of water-DMF-PVDF and 1-octanol/DMF/PVDF systems have been investigated in the past and reported by Young and co-workers [4]. These authors found that there is a wider gap between the crystallization line and the binodal curve for the 1-octanol/DMF/PVD system than for the water/DMF/PVDF system. This indicates the possibility of a crystallization-dominated membrane structure.

On the other hand, Sukitpaneenit et al. [6] ascertain that using increasingly weak alcohols the membrane structure is gradually transformed from an interconnected-cellular type (when water is used as nonsolvent) to an interconnected-globular type morphology consisting of spherical globules made of semi-crystalline PVDF (when the nonsolvent is an alcohol). However, the membrane feature changes in the same order from tight to loose globule-packing while mechanical properties deteriorate and fragility increases. The harshness of the nonsolvent can be estimated on the basis of the difference of Hansen Solubility Parameters (HSP) between the polymer and the nonsolvent. Polyvinylidene fluoride HSP is 23.2 $MPa^{½}$ [7] while water – which acts as strong nonsolvent – has a HSP of 47.9 $MPa^{½}$ [8].

In light of these and many other evidences, ethanol (HSP = 26 $MPa^{½}$ [9]) was selected for our purposes because of its weakness. The reason of this choice was the chance of obtaining membrane structures with well-interlinked semi-crystalline particles. This constitutes an important novelty in the current scenery about the structure-properties relationships of the membranes designed for MD processes.

Therefore, in this work, PVDF solutions in dimethylformamide at different concentrations were used to prepare porous hydrophobic membranes for distillation of saline water. Mixtures of water and ethanol were selected as nonsolvent. The membranes were obtained by means of the isothermal immersion-precipitation technique. The effects of two important factors, i.e. polymer concentration and coagulation bath composition, were extensively investigated. Several characterization assessments were performed on the samples produced, as well as performance tests, in order to understand and govern the membrane formation process. The aim was to obtain highly hydrophobic and porous membranes with high flux and maximized solute rejection, optimal for MD applications.

2.1 Material and Methods

2.1.1 Membrane preparation

The polymer selected for membrane preparation was high molecular weight PVDF (Solvay Speciality Polymers SOLEF® 6020 – Italy; Mw: 670-700 KDa [10]). N,N-dimethylformamide, DMF, (Carlo Erba – Italy) was used as solvent in order to obtain dope solutions at different polymer concentrations. Mixture stirring was carried out at 50°C for 6 h to ensure the complete dissolution of PVDF in DMF. The nonsolvent baths were prepared by mixing ethanol 96% (Carlo Erba – Italy) and deionized water in different proportions.

A 100 μm thick non-woven support (PET Viledon FO-2401, Freudenberg, Germany), characterized by an elastic modulus (E) of 1200 N/mm^2, was fixed on a flat glass plate with adhesive tape on one of the edges and then it was impregnated with DMF to enhance the membrane adhesion on the support itself. The PVDF solution was cast, at 20°C, using a doctor blade with a gap of 350 μm. Finally, the glass plate was immersed in the nonsolvent bath at 5 cm/s and left to coagulate for few hours; then the membranes were detached from the glass, washed with deionized water and left to dry overnight. Table 2.1 reports the preparation conditions of all the tested membranes.

Table 2.1: Membrane preparation conditions

Polymer concentration [w/w]	8 - 15%
Coagulating bath composition [v/v]	pure H_2O EtOH 25 - 96%
Casting and nonsolvent bath temperature	20°C

2.1.2 Characterization

Several techniques were used to investigate the morphology and properties of the membranes.

The hydrophobic character was evaluated using a digital optical tensiometer (Biolin Scientific Attension Theta). A 3 μL drop was automatically created using a syringe and dropped onto the active surface of the membrane. For every sample, 3 drops in different spots were analysed for 10 seconds at 15 counts per second.

The pore size and pore distribution were measured by Liquid-Liquid Displacement Porometry (LLDP) using a porometer built in the laboratory [11]. The system used a couple of immiscible liquids with low interfacial tension: water/1-octanol were chosen as displacing and wetting liquid

respectively (interfacial tension of 1-octanol/water = 8.5 mN/m, at 20°C [12]). The membranes were immersed in the organic phase overnight and put in a 76 mm^2 test cell. The wetting liquid was then displaced from the membrane using the water phase flux provided by a HPLC-pump (ISCO 260D). For every membrane, three different samples were tested.

Liquid entry pressure of water was evaluated putting the membrane in a suitable cell, pressurizing water on the feed size using compressed air and measuring the pressure at which the first drop of water was formed at the permeate side of the membrane.

The total porosity of the membrane ($\varepsilon\%$) was measured gravimetrically, weighing a portion of the membrane, previously detached from the non-woven support, before and after the impregnation with 1-octanol. The values were calculated using the following equation:

$$\varepsilon\% = \frac{V_{empty}}{V_{tot}} \cdot 100 = \frac{\frac{(m_w - m_d)}{\rho_{oc}}}{\frac{m_d}{\rho_{pol}} + \frac{(m_w - m_d)}{\rho_{oc}}} \cdot 100 \qquad 2.1$$

Where m_w and m_d are the masses (g) of impregnated and dry membrane, respectively, ρ_{oc} is the 1-octanol density (0.83 g/cm^3) and ρ_{pol} is the density of PVDF (1.8 g/cm^3) at 25°C.

The solution viscosity was measured using a Brookfield DV II viscometer at 25°C adjusting the shear rate for every sample in order to obtain data with torque values between 20 and 90%. The viscosity data were collected after 60 seconds at a constant shear rate.

Field emission scanning electron microscopy (FESEM) analysis of the membranes was carried out with a Carl Zeiss AG - SUPRA 40VP FE-SEM. A piece of membrane sample was mounted on an aluminium stub and sputter coated with a carbon nanofilm before FESEM observation. The accelerating voltage was fixed at 5kV and the images were collected using a conventional secondary electron detector or the in-lens detector. The cross sections of the membranes were obtained by fracturing the membrane in liquid nitrogen. Finally, to evaluate the mechanical properties of the prepared membranes, rectangular samples (3 X 1 cm) were tested using an Instron 5565 tensometer and the elastic modulus was determined.

2.1.3 Membrane distillation tests

The membranes with adequate characteristics (high LEP_w and contact angles over 90°) were tested in a lab-scale Vacuum Membrane Distillation plant (Figure 2.1).

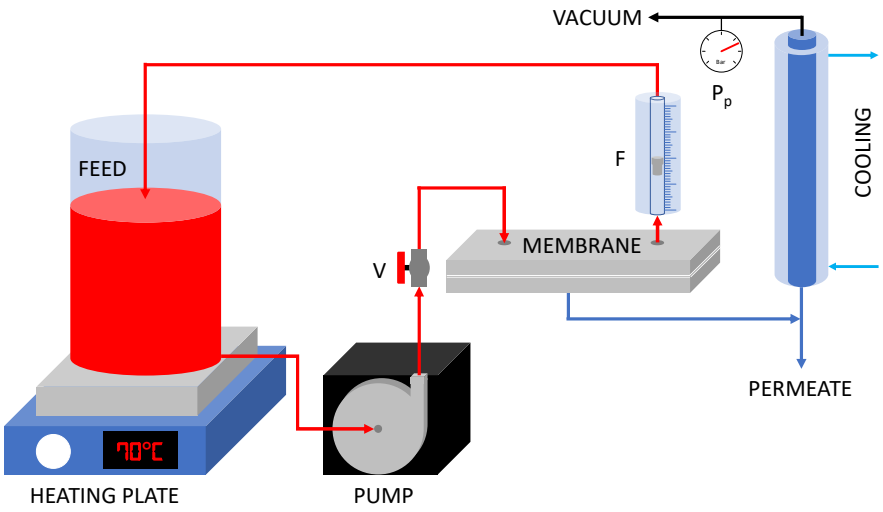

Figure 2.1: Vacuum Membrane Distillation (VMD) plant.

The feed (2 L) was heated with an external heating plate to the target temperature and sent to the membrane module with a centrifugal pump. The feed flow was controlled by a valve to keep the feed velocity in the membrane cell constant (7.5 cm/s) for all the experiments and measured with a flow meter installed on the concentrate stream. The membrane cell had a 25 cm^2 area. Vacuum was applied with a water pump and measured with a digital vacuum-meter (LLG – DVR 2pro). The stream of vapour extracted from the module was then condensed with glass condensers connected to a circulating cooling bath set at 0.1 °C. The distillate flow rate was evaluated by measuring the volume of condensed water at fix time intervals (10 minutes), while the salt rejection was calculated on the basis of the electrical conductivity of the feed and the permeate samples. The test conditions are reported in Table 2.2

Table 2.2: VMD tests conditions.

Tested Feeds	Deionized water NaCl solution 90 g/L
Feed temperatures	30°C 50°C 70°C
Feed flowrate	200 L/h
Feed velocity	7 cm/s
Membrane area	25 cm^2
Vacuum grade	20 mbar

2.2 Results

2.2.1 Effect of polymer solution concentration

Initial polymer solution concentration is one of the key factors determining the membrane characteristics and properties. In this work PVDF concentrations between 8% and 14% were first investigated following the suggestion of AlMarzooqi et al. [13].

In order to find the ideal polymer concentration leading to a defect-free active surface other authors [6,14] suggested to carry out a screening on the viscosity of the dope solutions. This should allow to identify the so-called "critical concentration". Below this value, the macromolecules can flow easier because a low number of entanglements exists between different chains. At higher concentrations the interactions between different polymer molecules are more relevant and limit their mobility [14]. As a rule of thumb, the optimal polymer concentration may be located at the critical concentration or 1–2 wt% above. Figure 2.2 illustrates the procedure. At low and high concentrations, the viscosity dependence is nearly linear, and extrapolating the intersection point of the two linear trends the critical concentration can be roughly identified.

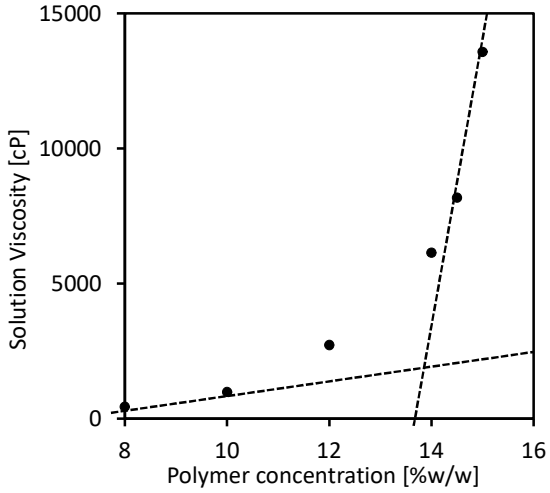

Figure 2.2: PVDF/DMF solution viscosities measured at 25°C.

The viscosity of our polymer solution changed its behaviour at PVDF concentration around 14%. Increasing the polymer content from 14 to 14.5% leads to a moderate increase in the viscosity (about 2000 cP) while the viscosity enhancement moving from 14.5 to 15% is higher (more than 5500 cP). Noticeably these findings are fully congruent with the results displayed in the following of this section.

While the effect of the nonsolvent on the membrane structure will be discussed in a subsequent section, in order to explore the influence of the polymer concentration, initially the extreme compositions of the coagulating bath were selected, i.e. pure water or ethanol 96%. The membranes prepared with water as nonsolvent presented an asymmetric structure, typical of an instantaneous liquid‑liquid demixing, with a flat skin layer. A representative FESEM micrograph of the cross section for the membrane PVDF 14% is showed in Figure 2.3, where the unwanted formation of macrovoids under the skin layer can be observed [15]. In place of the common bicontinuous structure, a globular morphology is observed in the sublayer. This structure is discussed in detail in Section 2.2.2 (Figure 2.6F and Figure 2.7A).

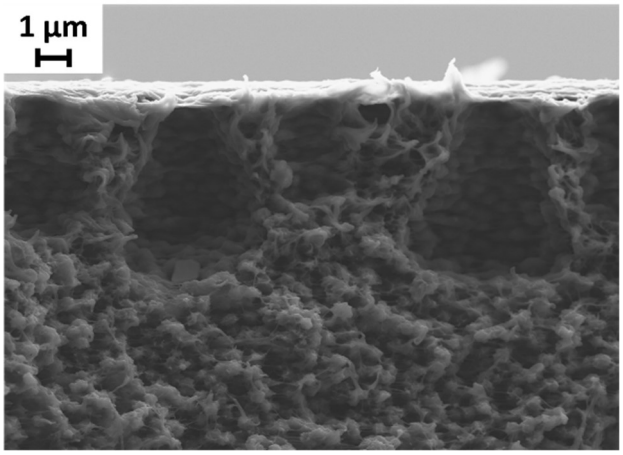

Figure 2.3: FESEM image of the cross section of the membrane PVDF 14% coagulated with water.

Measured water contact angles on the surfaces of all the membranes prepared from water bath were invariably lower than 90°. These values prevent the use in MD processes since severe membrane wetting phenomena could arise.

Instead, by using ethanol 96% as nonsolvent membranes with more interesting properties were obtained. However, in this second set of assessments, starting from the 8% PVDF solution the polymer coagulated in a powdery not bound sheet with no mechanical properties and low integrity [16]. This fact can be explained as follows. For glassy polymers, precipitation in NIPS is mainly governed by liquid‑liquid demixing, whereas for semi-crystalline polymers, like PVDF, both liquid‑liquid demixing and solid‑liquid demixing, associated with crystallization, control the precipitation [17]. Solid‑liquid demixing leads to more or less interlinked semi-crystalline structures where, in the case of PVDF, spherulites are clearly observable [6]. For the PVDF 8% solution the low polymer concentration clearly reduces the mutual interactions among the spherulitic globules, which grow independently from each other. Using higher polymer

concentrations, (in particular higher than the critical concentration defined above) firm membranes were successfully prepared. In Figure 2.4 the top surface images of the membranes prepared from the 10%, 12% and 14% PVDF solutions are reported.

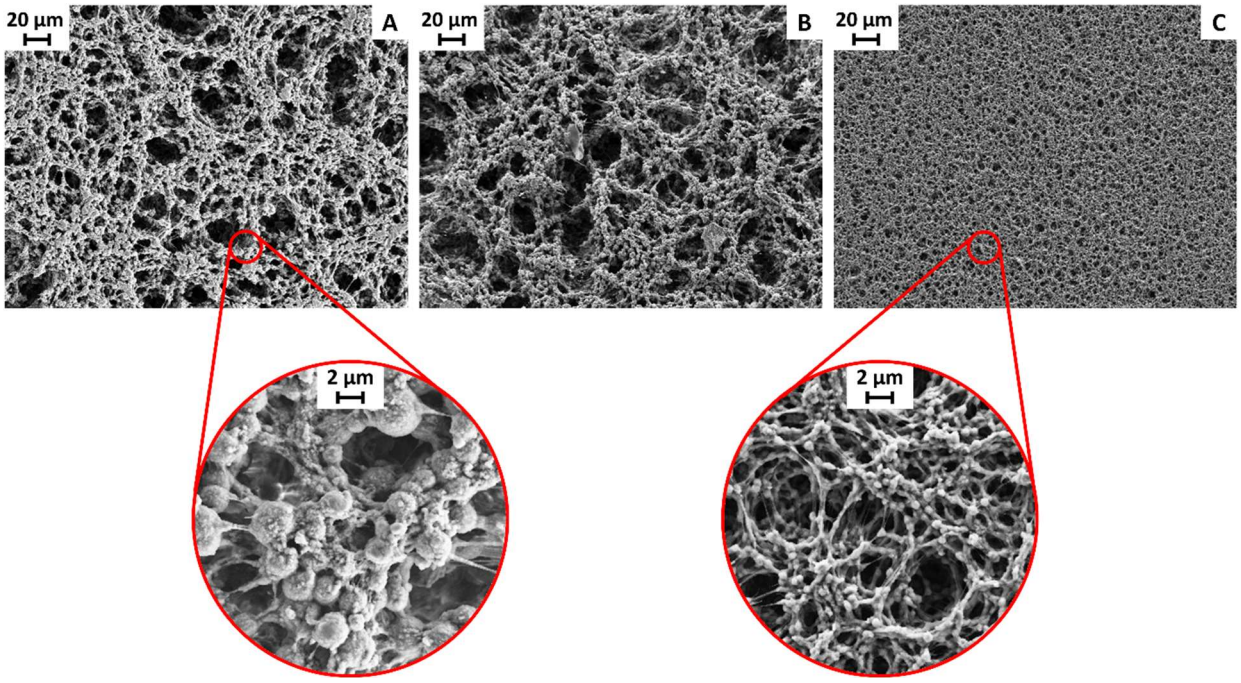

Figure 2.4: FESEM surface images of membranes prepared using ethanol 96% as nonsolvent: (A) 10% PVDF, (B) 12% PVDF and (C) 14% PVDF dope solutions.

The membranes showed a structure characterized by interconnected semi crystalline polymer globules and fibrils [17]. However, for the membranes prepared with 10% and 12% of PVDF, a large spherulite size is obtained (see the enlargement) and, simultaneously, larger lateral crystals of PVDF are formed. Crystallization is a slow process including formation of nuclei and growth of crystals. A high chain mobility, caused by a lower number of entanglements at lower polymer concentrations (refer to Figure 2.2), promote the growth of the crystals during the solid-liquid demixing. These structures show also great voids in the polymer net creating wide pores (even more than 100 µm in breadth and length). Increasing the polymer concentration in the dope solution up to 14% (the critical concentration), led to a much more interconnected network with smaller crystalline structures and smaller pores. This can be attributed to the fact that the rate of PVDF crystallization is reduced by the entanglement of the chains and by the enhancement of the solution viscosity (see again Figure 2.2).

Since the PVDF 14% membrane exhibited favourable characteristics, new dope solutions a little more concentrated (14.5% and 15%) were prepared and new membranes were formed and tested. The evolution of the crystallization process follows the increment in polymer concentration. This

is the key factor that affects the growth of the spherulitic nuclei. The increased concentration enhances the solution viscosity, so although more nuclei could be created, the restrained chain mobility hinders their growth into larger spherulitic globules. A great number of small spherulites was instead obtained, arranged in a well-interconnected polymer structure (Figure 2.5). This morphology can be attributed to a crystallisation-dominated precipitation, i.e. crystallisation preceded liquid–liquid demixing during membrane formation process due to the use of ethanol as nonsolvent. By varying the composition of the coagulating bath, a wide range of possible morphologies can be expected (Section 2.2.2).

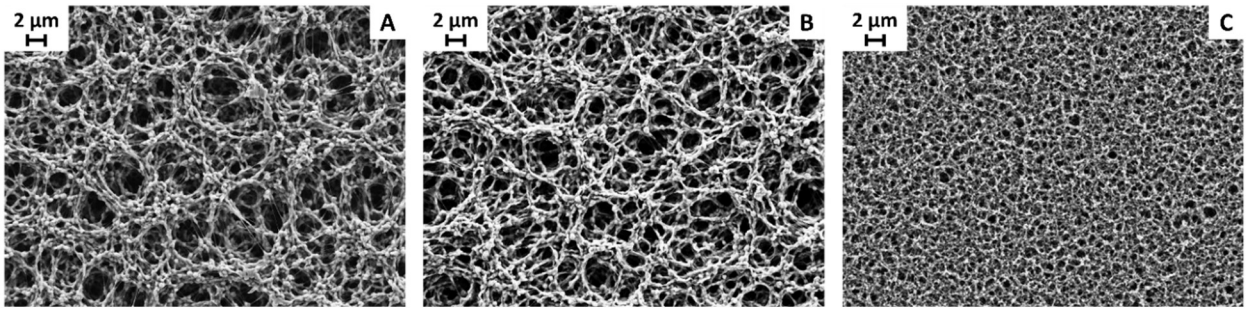

Figure 2.5: FESEM surface images of membranes prepared using ethanol 96% as nonsolvent: (A) 14% PVDF; (B) 14.5% PVDF and (C) 15% PVDF solutions.

The structures of the last membranes were similar but, as the polymer concentration increases beyond 14.5% PVDF, the dimensions of the semi crystalline interconnected particles reduce abruptly creating a denser, less porous network (Figure 2.5C). As already emphasized, moving from 14.5 to 15% PVDF in the dope solution, a high enhancement in the viscosity (about 5500 cP) is observed. This exacerbates the just outlined interrelated phenomena.

The characterizations performed on all the membranes prepared with 96% ethanol as nonsolvent, such as LEP_w and total porosity as well as the mean pore size measured by LLDP, confirmed the difference between the lower concentration membranes and the PVDF 15% one. These results are reported in Table 2.3.

Table 2.3: Properties of the membranes prepared using ethanol 96% as nonsolvent.

Polymer concentration [%w/w]	LEP_w [bar]	R_{mean} [µm]	ε [%]	E [N/mm^2]
10	0.1±0.1	-	-	-
12	0.3±0.1	-	-	-
14	1.0±0.3	0.54±0.08	72	1792±154
14.5	1.5±0.2	0.49±0.02	76	1518±127
15	7.0±0.5	0.03±0.01	62	1503±114

Using low PVDF concentrations in the dope solutions (10 and 12%), even if an interconnected membrane is created, the associated pores are extremely wide. Thus, the liquid entry pressure drops to values below 0.5 bar, preventing the use of these two membranes for successful MD tests. The membranes prepared with 14% and 14.5% PVDF showed more promising properties; moreover, only little differences were registered both in terms of LEP_w – increasing from 1.0 bar to 1.5 bar – and for what concerns the mean pore size that remains around 0.5 μm; also, the overall porosity of the two membranes is similar. Even if the LEP_w values are below the one usually suggested for MD applications [18], they were enough to perform the VMD tests in the lab scale plant (Section 2.2.3).

Finally, the membrane prepared from the most concentrated solution (15% PVDF) showed totally different results, owing to the different morphology, characterized by the denser network observed during the FESEM observations.

In addition, the total porosity of this membrane was quite lower than the one of the others. This fact suggests that the differences in the membrane structure are not only localized on the surface but also in the lower layers that appear to have less void volume. Finally, the elastic modulus was also measured to estimate the mechanical resistance of the membranes. The values are reported in Table 2.3 and show that the mechanical properties of all the tested membranes are mainly determined by the non-woven support (see Paragraph 2.1.1). Nevertheless, the effect of the dope solution concentration on the elastic modulus of the membranes is also detectable; in fact, at lower polymer concentrations the viscosity of the solution is lower and the solution can easily impregnate the non-woven. As the dope concentration increases, the penetration into the support network is hindered and the elastic modulus of the membrane decreases.

2.2.2 Effect of coagulating bath composition

As seen during the preliminary assessments performed with both water and 96% ethanol as nonsolvents, the composition of the coagulating bath has a major impact on the morphology and on the properties of the membrane. Then, the effect of different concentrations of ethanol in the nonsolvent bath was explored: in particular 25, 50 and 75% ethanol solutions were selected for the membranes prepared from 14 to 15% PVDF solutions. Since the behaviour is similar for all the three polymer concentrations, only the results obtained with the most promising 14.5% PVDF membranes are showed. Figure 2.6 reports the FESEM images of the active surface and the cross section of the 14.5% PVDF membranes prepared with different ethanol concentration in the coagulation bath coupled with the relative water drop profiles.

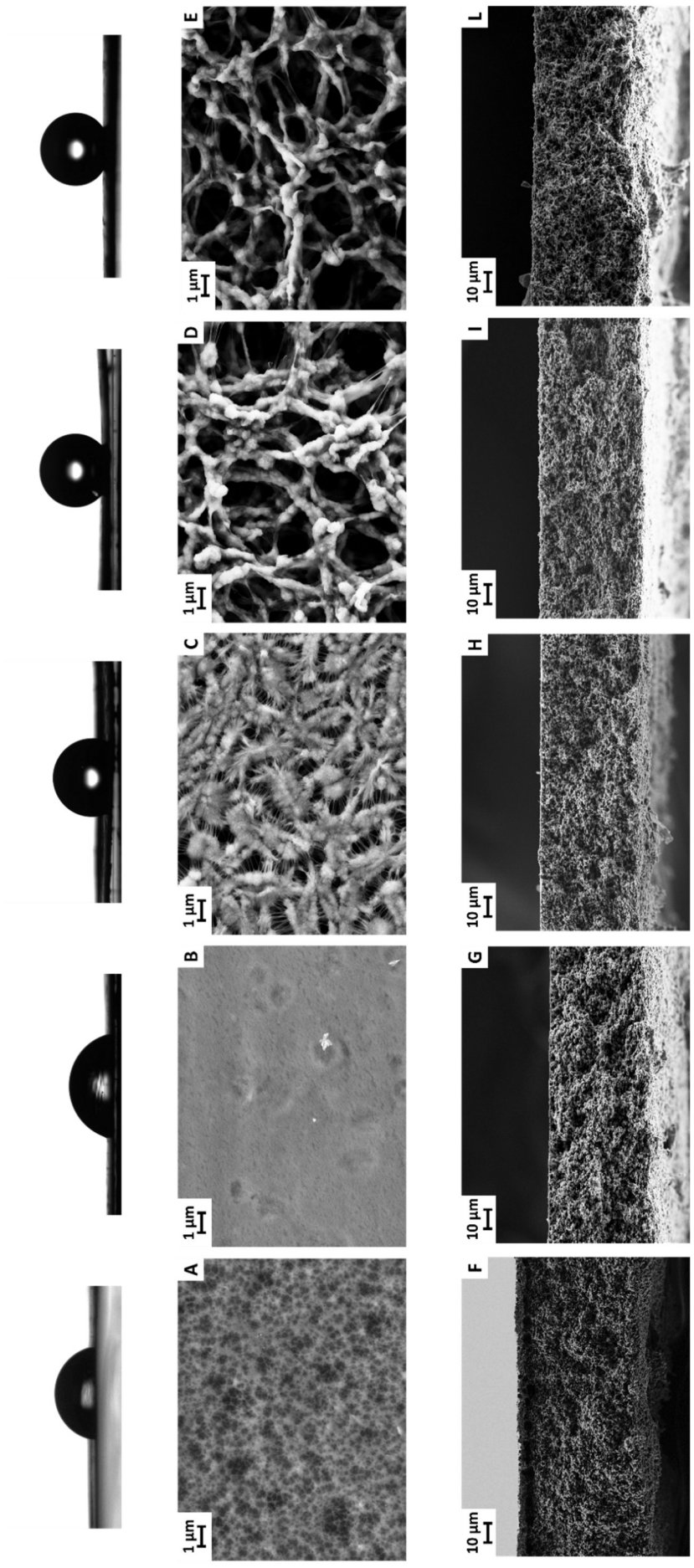

Figure 2.6: Water drop profile (top) and FESEM micrographs of the surface (middle) and the cross section (bottom) of 14.5% PVDF membranes coagulated in different nonsolvent baths. (A;F) H_2O;(B;G) EtOH 25%, (C;H) EtOH 50%, (D;I) EtOH 75% and (E;L) EtOH 96%.

Although the phase diagram was not directly determined in this work, a qualitative interpretation of Figure 2.6 can be easily provided on the basis of various studies available in the literature [3,4,6,17]. Two well-known facts should be taken into account: 1) the kinetics plays a very important role during the membrane formation; 2) crystallization is a slow process compared to liquid–liquid demixing.

For the membrane showed in Figure 2.6A, the typical globular morphology associated with a crystallization-dominated process was not observable in the active top layer. After immersion, being water a harsh nonsolvent, the solvent/nonsolvent interdiffusion was fast and the binodal gap was rapidly reached. Therefore, liquid-liquid demixing in this case prevailed, leading to a cellular morphology where the pores, grown from the polymer-lean phase, are embedded in a solid polymeric matrix, originated from the polymer-rich phase.

The introduction of ethanol in the coagulation bath lowered the nonsolvent strength and then the liquid phase separation was no longer instantaneous. In the sample of Figure 2.6B (EtOH 25%), on the top surface an initial formation of many nuclei probably occurred due to the presence of a degree of supersaturation for PVDF crystallization. The solvent/nonsolvent interdiffusion however was still fast and the nuclei did not have time to grow, so leading to a nearly smooth surface. Reaching a concentration of 50% in ethanol in the coagulation bath (Figure 2.6C) a more developed crystalline structure was observable, as it is likely that the crystallization line and the binodal line became more separated.

Finally, in the cases of Figure 2.6D and Figure 2.6E (EtOH 75% and 96% respectively), crystallization occurred undoubtedly prior to liquid–liquid demixing and the precipitation process was crystallization-dominated. In this situation, the distance between the crystallization and the binodal lines increased further so that all crystalline particles were allowed to grow and coalesce to form a bicontinuous structure.

Accordingly with Figure 2.6, Table 2.4 reports the water contact angles measured on the active (top) surface for the 14.5% PVDF membranes prepared with different coagulating bath compositions. The associated standard deviations are reported too.

Table 2.4: Water contact angle measured on the top surface of 14.5% PVDF membrane for different coagulation bath compositions.

H_2O [°]	EtOH 25% [°]	EtOH 50% [°]	EtOH 75% [°]	EtOH 96% [°]
84±2	78±4	116±4	144±8	150±1

The membrane prepared by immersion in the EtOH 25% bath had a quite smooth surface and showed the lowest contact angle. The different surface roughness plays indeed a key role in the hydrophobicity grade of the membranes as highlighted by the contact angle measurements.

When studying rough hydrophobic surfaces it is usual to invoke the Cassie Baxter equation [19], which in its most general formulation evaluates the contact angle of a drop placed on a flat composite micro-heterogeneous surface:

$$\cos\theta_{CB} = \sum_i \phi_i cos\theta_i \qquad 2.2$$

Where ϕ_i is the surface fraction occupied by phase i. The cosine of the final contact angle ($cos\,\theta_{CB}$) is the weighted average of the cosines of the different contact angles θ_i on the pure phases.

In the particular case of a rough (micro- or nano-structured) surface, the water droplet rests on a "composite" flat surface made of solid with trapped air pockets. The particular form of equation 2.2 then becomes:

$$\cos\theta_{CB} = \phi_s(cos\theta + 1) - 1 \qquad 2.3$$

where ϕ_s is the surface fraction occupied by the solid and θ is the intrinsic contact angle of the solid without voids. It is apparent that if the air surface fraction under the drop increases, θ_{CB} also increases.

For the membrane under investigation, the evolution of the active surface texture as a function of ethanol concentration, showed in Figure 2.6, was very impressive on this regard. The area fraction of the solid increased moving from water to EtOH 25% and accordingly θ_{CB} decreased, whereas ϕ_s decreased more and more from EtOH 50% to EtOH 96%, and the Cassie-Baxter equation predicts an enhancement of the apparent contact angle. As a matter of fact, as reported in Table 2.4, the membranes prepared with less than 50% of ethanol in the coagulating bath, with a denser surface layer, showed a hydrophilic behaviour with contact angle values similar to literature data for plain PVDF films (83.6° [20]). On the contrary, when ethanol was the main component of the nonsolvent mixture, the membranes became hydrophobic, and in the last formulations the membrane contact angles entered the superhydrophobic region.

The effect of adding ethanol in the coagulation bath was further clarified by analysing the FESEM images of the membrane cross sections reported in Figure 2.6 (G-L) and in Figure 2.7. The membrane precipitated from water showed an asymmetric structure (see Figure 2.6F and Figure 2.8A). Three different regions can be roughly identified. On the top surface there was the thin layer discussed above (Figure 2.6A). Underneath the top layer there was a region presenting pear shaped macrovoids typically associated with instantaneous liquid-liquid demixing. The lower part of the

membrane cross-section showed a different morphology formed by loose-packed globules. This happened because the precipitated top layer became a barrier that hindered a further solvent-nonsolvent exchange and, in the bottom layer, the polymer solution could undergo the slower liquid-solid demixing (crystallization).

By adding ethanol to the coagulation bath, the solvent-nonsolvent exchange rate dropped and the membrane formation took longer time, creating a more symmetric structure where macrovoids gradually disappeared. The grade of symmetry of the membrane section depended on the amount of ethanol in the nonsolvent bath, as highlighted in Figure 2.6. The membrane prepared with just 25% ethanol in the coagulating bath (Figure 2.6G and Figure 2.7B), still had a dense top film; however, in the underlying region the macrovoids were suppressed due to the reduced mass exchange rate. When the ethanol concentration was raised up to 50% (Figure 2.6H and Figure 2.7C) a thin top layer was barely distinguishable. Finally, when ethanol became the main constituent of the nonsolvent bath, the top layer disappeared, creating a totally symmetric membrane (Figure 2.6 I and L). The polymeric structure was well interconnected, and spherulites of small dimensions were detectable. Noticeably, these membranes did not possess the so-called "particulate" morphology [3,4], where the linkage points between the polymer globules can be too limited and lead to unsatisfactory mechanical strength.

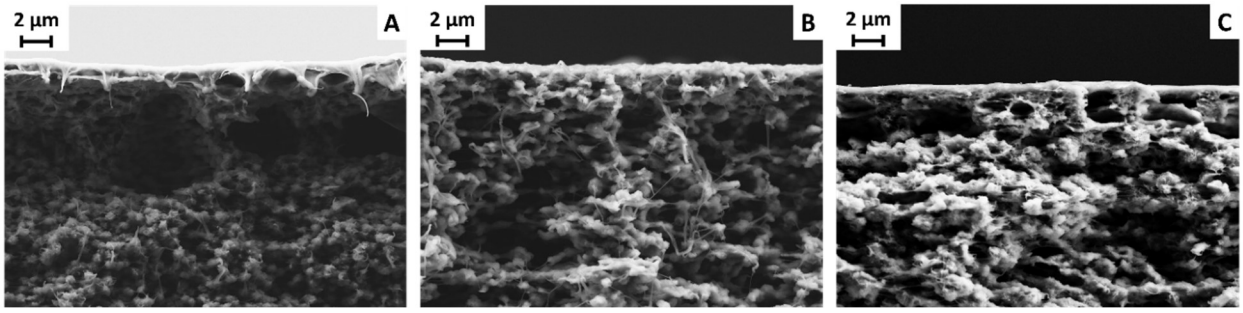

Figure 2.7: Detail of the active surface of 14.5 PVDF membranes prepared with (A) H_2O, (B) EtOH 25%, (C) EtOH 50%.

The effect of the top layer was also elucidated by LEP_W and LLDP measurements on the 14.5% PVDF membranes. The results are collected in Table 2.5 together with the values of the overall porosity. In fact, the membrane prepared in 25% ethanol in the coagulating bath presented an almost dense top layer and it was impossible to detect active pores on the surface in the LLDP test conditions.

Table 2.5: Properties of the 14.5% PVDF membranes prepared with different nonsolvent solution composition.

Ethanol concentration [%v/v]	LEP_w [bar]	R_{mean} [µm]	ε [%]
25	-	-	69
50	1.8±0.1	0.19±0.04	77
75	1.4±0.2	0.51±0.03	76
96	1.5±0.1	0.49±0.02	76

Moreover, using 50% ethanol, the membrane presented a smaller mean pore size – as well as a higher LEP_w – than the ones prepared with higher ethanol concentrations. However, its overall porosity matched the one of the others, confirming that the bulk morphologies were similar while only their surfaces had different properties. Therefore, the overall porosity of these membranes was mainly determined by the initial solution concentration and not by the membrane formation process.

2.2.3 Membrane distillation tests

Based on the results of the characterizations (see Table 2.3, 2.4, 2.5), of the 25 membranes prepared with the conditions reported in Table 2.1, only nine membranes were selected for vacuum membrane distillation. To summarize, membranes from:

- Polymer concentrations lower than 14% were discarded because of wetting phenomena (too low LEP_w values);
- Polymer concentrations higher than 15% were discarded because of too small pores size;
- Ethanol concentrations in the nonsolvent bath lower than 50% were discarded because of poor hydrophobicity (contact angle lower than 90°).

The first VMD tests were performed using pure water as feed in order to evaluate the maximum distillate flux without interference from both concentration polarization and fouling effects due to the presence of solutes. The values of mean distillate flux for the nine membranes at three different feed temperatures (30, 50, 70°C) are reported in Figure 2.8A. Then a solution of NaCl with a concentration of 90 g/L was selected in order to evaluate the separation performances. The results are showed in Figure 2.8B.

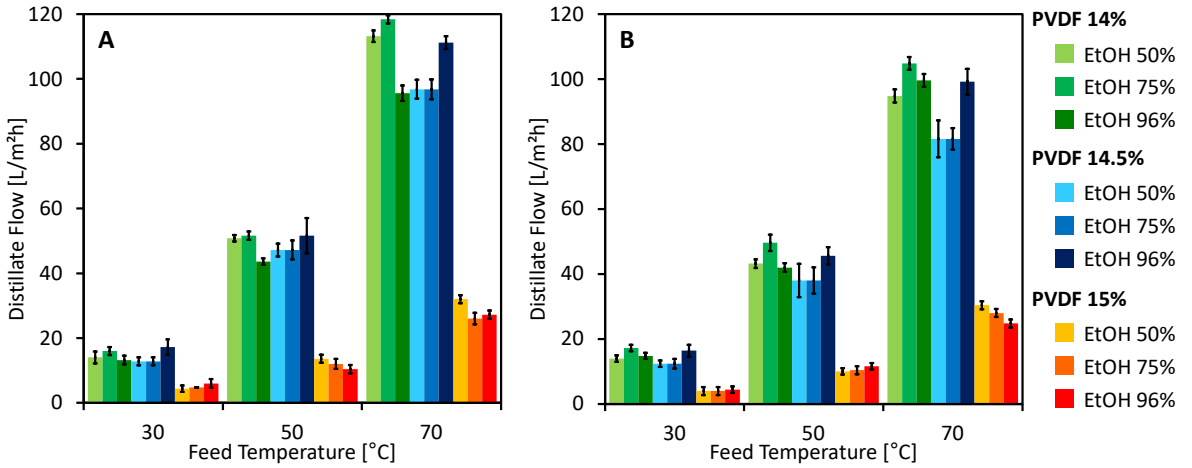

Figure 2.8: Mean distillate fluxes for VMD tests on pure water (A) and 90 g/L sodium chloride solution (B).

The tests run with both pure water and the sodium chloride solution confirmed the differences highlighted in the previous sections between the membranes prepared at lower PVDF concentrations (14% and 14.5%) and the 15% one. In fact, the first ones exhibited similar behaviour in all the test conditions. The membranes prepared with 15% PVDF solution performed again similarly independently from the coagulating bath composition, but compared with the membranes prepared with more diluted polymer solutions, they provided very modest distillate fluxes.

An interesting finding was that the coagulating bath composition, if the ethanol content exceeds 50%, appeared to have a minor influence on the membrane permeability. The bulk characteristics (overall porosity, symmetric structure) were indeed similar as well as the surface characteristics (LEP_w and, in a more limited extent, contact angle).

The same performance trend observed with pure water was also confirmed during the tests carried out with the concentrated sodium chloride solution. The influence of possible concentration polarization phenomena seemed scarce and only a hardly demonstrable presence could be perhaps hypothesized at 70°C. Using the saline feed, it was also possible to determine retention towards the solute. In fact, starting with a feed solution characterized by an electrical conductivity of almost 130000 µS/cm, the permeate conductivity never exceeded 2 µS/cm corresponding to a NaCl concentration lower than 1 ppm (complete salt rejection).

Because of its great distillate flow and higher wetting resistance, the 14,5% PVDF membrane performance was compared with literature data available for a commercial membrane commonly used for MD processes, the Accurel® PP2E (Membrana – Germany), made of polypropylene (PP). The properties of the two membranes are summarized in Table 2.6.

Table 2.6: Accurel® PP2E and PVDF 14.5% EtOH 96% membrane properties. Accurel® data adapted from Mohammadi et al. [21].

	Accurel® PP2E	PVDF 14.5 EtOH 96%
Material	PP	PVDF
Mean Pore Size [µm]	0.2	0.5
Thickness [µm]	163	65+100*
Porosity [%]	75	76
Contact Angle [°]	120	150

*Membrane + support thickness

The performance comparison is showed in Figure 2.9. The operating condition were similar for the two membranes (P_{vac} = 30 mbar, feed: NaCl solution 100 g/L for Accurel® PP2E [21], P_{vac} = 20 mbar, feed: NaCl solution 90 g/L for the 14,5% PVDF membrane), but the PVDF membrane performed significantly better.

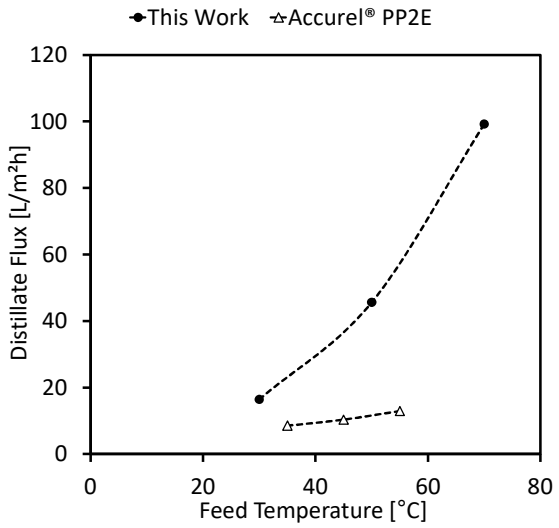

Figure 2.9: Accurel® PP2E and PVDF 14.5% EtOH 96% membrane performance comparison. Accurel® data adapted from [21].

In order to explain these results, a discussion on the influence of the water contact angle on the performances seems noteworthy. Actually, polypropylene as membrane material would seem the better choice, owing its intrinsic hydrophobicity. Contact angles on smooth polymer surfaces are 96.7° for PP [22] and 83.6° for PVDF [20], respectively. Hence, an effect of the surface morphology has to be called into question (note that the membrane porosity is the same in both cases, whereas the mean pore size is different). Figure 10 shows a comparison between the FESEM images of the two cross sections for Accurel® PP2E and 14,5% PVDF, where on the top part to the active layer of the membrane is observable.

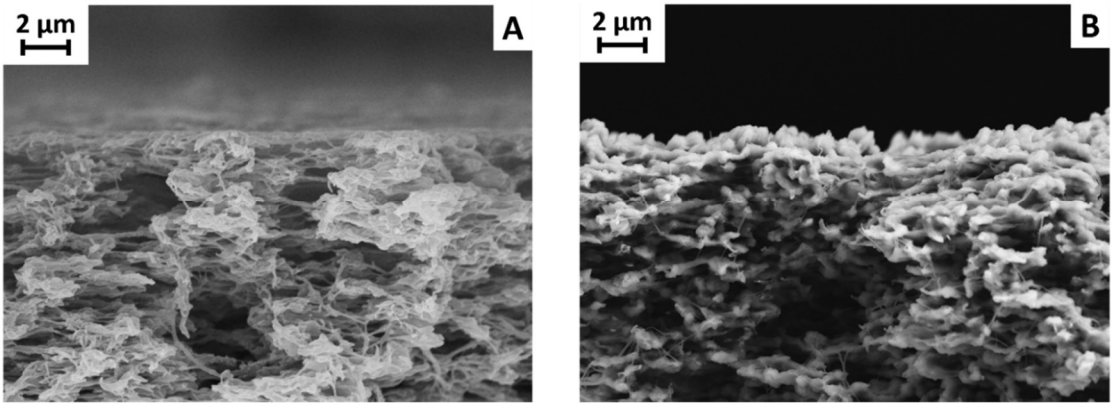

Figure 2.10: FESEM micrographs of Accurel® PP2E (A) and PVDF 14.5% (B) cross sections.

The active surface of Accurel® PP2E is quite flat, whereas the active surface of the 14.5% PVDF membrane is very rough with a spike-like nanostructure, so in equation 2.3 the value for ϕ_s is expected much smaller for the last membrane. In that case, thanks to the irregularities of nanometric scale obtained in this work, the water drop rests on the top layer in the so-called Fakir-state, typical of superhydrophobic surfaces. This very important feature allowed to have higher contact angle and larger pores without wetting phenomena, thus creating a larger surface for water evaporation. In our opinion, this is the most innovative characteristic among the various desirable membrane properties discussed in the text.

2.3 Conclusions

Porous membranes have been prepared by isothermal immersion-precipitation of PVDF/DMF solutions in coagulating baths consisting of water, a harsh nonsolvent, and ethanol, a weaker nonsolvent capable of inducing delayed demixing. The effects of initial polymer concentration and of the nonsolvent composition (relative amount of water and ethanol) on the final membrane morphology and properties were extensively explored. Several characterization tests were carried out, including mean pore size, LEP_w, contact angle measurements and FESEM observations.

The principal factor determining the external and internal membrane structure is the rate of crystallization of PVDF during the membrane formation process. This crucial parameter can direct the process towards a crystallisation-dominated precipitation as well as towards a liquid–liquid demixing-governed transformation. Being aware of this fact, the membrane properties were tuned as desired by exploiting the dope concentration and the nonsolvent composition.

Some of the membranes prepared showed excellent features for MD operation (i.e. very high water contact angle, sufficient LEP_w, large pores, good mechanical strength). Under VMD tests, these

membranes achieved very high fluxes ranging from about 15 L/(m^2 h) at 30°C to 50 L/(m^2 h) at 50°C up to 100 L/(m^2 h) at 70°C. The salt rejection turned out to be essentially complete.

References

[1] D. Zuo, B. Zhu, C. Jian-hua, Y. Xu, Influence of alcohol-based nonsolvents on the formation and morphology of PVDF membranes in phase inversion process, Chinese J. Polym. Sci. 24 (2006) 281–289.

[2] M. Tao, F. Liu, B. Ma, L. Xue, Effect of solvent power on PVDF membrane polymorphism during phase inversion, Desalination. 316 (2013) 137–145. doi:10.1016/j.desal.2013.02.005.

[3] L.P. Cheng, T.H. Young, L. Fang, J.J. Gau, Formation of particulate microporous poly(vinylidene fluoride) membranes by isothermal immersion precipitation from the 1-octanol/dimethylformamide/poly(vinylidene fluoride) system, Polymer (Guildf). 40 (1999) 2395–2403. doi:10.1016/S0032-3861(98)00462-5.

[4] T.H. Young, L.P. Cheng, D.J. Lin, L. Fane, W.Y. Chuang, Mechanisms of PVDF membrane formation by immersion-precipitation in soft (1-octanol) and harsh (water) nonsolvents, Polymer (Guildf). (1999). doi:10.1016/S0032-3861(98)00747-2.

[5] F. Liu, N.A. Hashim, Y. Liu, M.R.M. Abed, K. Li, Progress in the production and modification of PVDF membranes, J. Memb. Sci. 375 (2011) 1–27. doi:10.1016/j.memsci.2011.03.014.

[6] P. Sukitpaneenit, T.S. Chung, Molecular elucidation of morphology and mechanical properties of PVDF hollow fiber membranes from aspects of phase inversion, crystallization and rheology, J. Memb. Sci. 340 (2009) 192–205. doi:10.1016/j.memsci.2009.05.029.

[7] A. Bottino, G. Capannelli, S. Munari, A. Turturro, Solubility parameters of poly(vinylidene fluoride), J. Polym. Sci. Part B Polym. Phys. 26 (1988) 785–794. doi:10.1002/polb.1988.090260405.

[8] A.F.M. Barton, CRC Handbook of Solubility Parameters and Other Cohesion Parameters, Routledge, 2017. doi:10.1201/9781315140575.

[9] A.F.M. Barton, CRC Handbook of Solubility Parameters and Other Cohesion Parameters, Routledge, 2017. doi:10.1201/9781315140575.

[10] M. Haponska, A. Trojanowska, A. Nogalska, R. Jastrzab, T. Gumi, B. Tylkowski, PVDF membrane morphology - Influence of polymer molecularweight and preparation temperature, Polymers (Basel). 9 (2017) 1–14. doi:10.3390/polym9120718.

[11] J.M. Sanz, D. Jardines, A. Bottino, G. Capannelli, A. Hernández, J.I. Calvo, Liquid–liquid porometry for an accurate membrane characterization, Desalination. 200 (2006) 195–197. doi:10.1016/j.desal.2006.03.293.

[12] J.I. Calvo, A. Bottino, G. Capannelli, A. Hernández, Comparison of liquid–liquid displacement porosimetry and scanning electron microscopy image analysis to characterise ultrafiltration track-etched membranes, J. Memb. Sci. 239 (2004) 189–197. doi:10.1016/J.MEMSCI.2004.02.038.

[13] F. Abdulla AlMarzooqi, M. Roil Bilad, H. Ali Arafat, Improving Liquid Entry Pressure of Polyvinylidene Fluoride (PVDF) Membranes by Exploiting the Role of Fabrication Parameters in Vapor-Induced Phase Separation VIPS and Non-Solvent-Induced Phase Separation (NIPS) Processes, Appl. Sci. 7 (2017) 181. doi:10.3390/app7020181.

[14] T.S. Chung, S.K. Teoh, X. Hu, Formation of ultrathin high-performance polyethersulfone hollow-fiber membranes, J. Memb. Sci. 133 (1997) 161–175. doi:10.1016/S0376-7388(97)00101-4.

[15] A. Bottino, G. Camera-Roda, G. Capannelli, S. Munari, The formation of microporous polyvinylidene difluoride membranes by phase separation, J. Memb. Sci. 57 (1991) 1–20. doi:10.1016/S0376-7388(00)81159-X.

[16] A.F. Ismail, L.P. Yean, Review on the development of defect-free and ultrathin-skinned asymmetric membranes for gas separation through manipulation of phase inversion and rheological factors, J. Appl. Polym. Sci. 88 (2003) 442–451. doi:10.1002/app.11744.

[17] D.J. Lin, K. Beltsios, C.L. Chang, L.P. Cheng, Fine structure and formation mechanism of particulate phase-inversion poly(vinylidene fluoride) membranes, J. Polym. Sci. Part B Polym. Phys. 41 (2003) 1578–1588. doi:10.1002/polb.10513.

[18] L. Eykens, K. De Sitter, C. Dotremont, L. Pinoy, B. Van Der Bruggen, How to Optimize the Membrane Properties for Membrane Distillation: A Review, Ind. Eng. Chem. Res. 55 (2016) 9333–9343. doi:10.1021/acs.iecr.6b02226.

[19] G. Whyman, E. Bormashenko, T. Stein, The rigorous derivation of Young, Cassie-Baxter and Wenzel equations and the analysis of the contact angle hysteresis phenomenon, Chem. Phys. Lett. 450 (2008) 355–359. doi:10.1016/j.cplett.2007.11.033.

[20] L. Yan, Y. Li, C. Xiang, S. Xianda, Effect of nano-sized Al2O3-particle addition on PVDF ultrafiltration membrane performance, J. Memb. Sci. 276 (2006) 162–167. doi:10.1016/j.memsci.2005.09.044.

[21] T. Mohammadi, M.A. Safavi, Application of Taguchi method in optimization of desalination by vacuum membrane distillation, Desalination. 249 (2009) 83–89. doi:10.1016/j.desal.2009.01.017.

[22] P.F. Rios, H. Dodiuk, S. Kenig, S. McCarthy, A. Dotan, The effect of polymer surface on

the wetting and adhesion of liquid systems, J. Adhes. Sci. Technol. 21 (2007) 227–241. doi:10.1163/156856107780684567.

Chapter 3

3 Influence of pore forming agents

One of the major parameters that can be tuned to obtain the needed characteristics of the membrane is the polymer solution composition. Using the selected polymer, it is possible to modify the solution properties in different ways, like changing the polymer molecular weight and concentration [1–3], adding additives like pore forming agents, nanoparticles, nonsolvent [4–6]. In particular, the pore forming agents can be inorganic salts (e.g. LiCl, $BaCl_2$) [1,7] or low molecular weight polymers that can be dissolved in water, like polyethylene glycol (PEG) [1,8,9] and polyvinyl pyrrolidone (PVP) [7,10].

The use of pore forming agents allows the improvement of the membrane porosity and effective active surface for vapour transport, increasing by consequence the distillate flux during MD operation.

Kong and Li [7] verified that adding LiCl and PVP to the PVDF solution led to higher porosity membranes but also to a decrease of their hydrophobicity. These results were confirmed by Tang et al. [1] who verified that an increase of the LiCl concentration in the dope solution results in a more porous sponge-like structure of membrane. Moreover, they investigated the effect of PEG-400 as oligomeric pore forming agent. The great affinity of PEG with water leads to fast phase separation and favours the formation of macrovoids. These effects led to an enhancement of the DCMD permeate flux from 1 up to almost 9 kg/m^{2}h (C_f = 9% NaCl, T_f = 65°C, T_p = 20°C).

Similar results were obtained by Li et al. [9] who confirmed the formation of big macrovoids and denser skin layer when PEG-400 was added to the solution, and by Huo et al. [8] who also registered an increase of the porosity from 68.7% up to 79.7% and an enhancement of the contact angle from 86° to 105° adding both LiCl and PEG-1500 to the PVDF dope solution. Again, the introduction of pore forming agents increased dramatically the DCMD performance from almost 10 kg/m^{2}h to 41 kg/m^{2}h treating a 3.5% NaCl solution (at T_f = 80°C and T_p = 20°C). The performance stability was also investigated confirming that treating the NaCl solution for 200 h, only minor flux and rejection reduction happened.

Simone et al. [10] investigated the effect of PVP as pore forming agent highlighting that the effect on the membrane structure highly depends on its concentration: at low concentrations, the addition of PVP favours the formation of macrovoids increasing the total porosity but also affecting the mechanical properties of the membranes. Further addition of PVP instead, creates a sponge structure with a small decrease of porosity but better mechanical strength. The change of the porosity was then confirmed during the VMD tests by the distillation flux that was increased from

4.3 kg/m^{2}h when no PVP was used, to 17.9 kg/m^{2}h when 9% of PVP was added; while further increase up to 15% resulted in a distillate flux decline to 15.3 kg/m^{2}h.

The aim of this part of the PhD work, carried out in the laboratories of the Research Group "Membranes and Renewable Energies" associated to the Department of Structure of Matter, Thermal Physics and Electronics of the Complutense University of Madrid, was focused on the preparation of unsupported flat PVDF membranes. The effect of the dope solution composition as well as the influence of different pore forming agents on the morphology and MD performance of the membranes was investigated.

Moreover, it was found necessary to develop a different drying technique in order to supply the needed resistance to shrinkage that in supported membranes is guaranteed by the nonwoven support.

3.1 Materials and Methods

3.1.1 Unsupported flat sheet membranes preparation

Unsupported flat sheet membranes were prepared under similar conditions as the supported ones. In order to improve the overall porosity, lithium chloride and two polyethylene glycols (Sigma Aldrich – USA) were added to the dope solutions to act as pore forming agents. The tested compositions are reported in Table 3.1.

Table 3.1: Dope solutions composition for unsupported flat sheet and hollow fibre membranes.

Polymer concentration [wt%]	Solvent concentration [wt%]	Additive concentration [wt%]	Coagulation bath [wt%]
PVDF 12-14	DMF 76-83	PEG-400: 5-10 PEG-6000: 5-10 LiCl: 5-10	H_2O: 100 EtOH/H_2O: 50/50

The difference between PEG-400 and PEG-6000 was the mean molecular weight, being 400 and 6000 Da respectively.

Thin films (400 μm) of the solutions were casted on a flat glass using an automatic film applicator (Elcometer 4340) and immersed in the coagulation bath. After 24 hours they were washed with deionized water and dried at room temperature. In order to maintain the membrane shape and prevent shrinkage phenomena during the drying process, some films were attached to a metal plate with adhesive tape.

3.1.2 Characterization

Generally, the same techniques used for supported flat sheet membranes were exploited for both unsupported flat sheet and hollow fibre membranes. Moreover, some additional investigations were performed in the laboratory of the Complutense University of Madrid. In particular, mean pore size and pore size distributions were measured using an automatic gas-liquid displacement porometer (GLDP, POROLUX 100, Porometer). First, a sample of the membrane was impregnated with a wetting liquid (POREFIL, Porometer, surface tension: 16 mN/m) and poured into the sample holder. The wet curve was then obtained by measuring the transmembrane air flow rate at increasing applied pressures. Once the wetting liquid was completely removed from the membrane, the dry curve was obtained following the same procedure. The mean pore size was determined using both data sets by the computer software.

3.1.3 Performance evaluation

The distillation tests were carried out with the direct contact membrane distillation (DCMD) configuration. This mode, schematized in Figure 3.1, was selected because it requires for the membrane a lower mechanical strength compared with VMD.

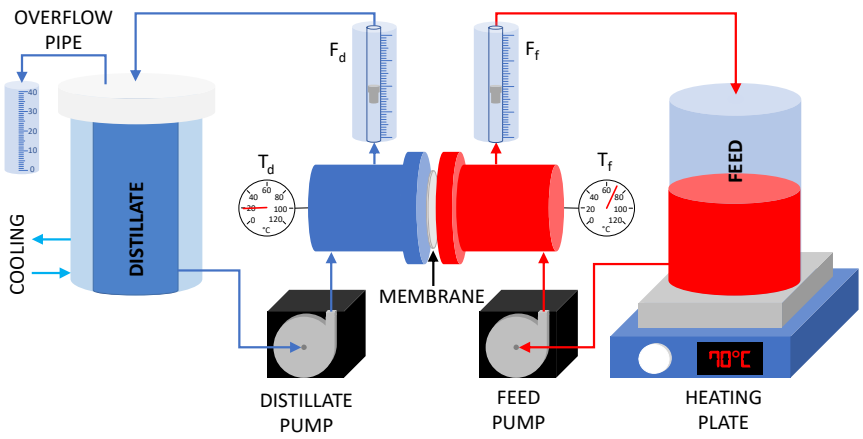

Figure 3.1: DCMD setup; F_d: distillate recirculation flux, F_f: Feed recirculation flux, T_d: distillate temperature, T_f: feed temperature.

The feed solution (2 litres) was heated with a heating plate and sent to the membrane cell at a constant flowrate of 40 L/h using a gear pump. The cold stream was contained in a closed tank equipped with an overflow pipe and kept at 20°C using and external jacket. Using a second gear pump the cold stream was sent to the membrane cell at 40 L/h. The hot and the cold circuit lines were designed to be equivalent in order to obtain equal pressures at the two sides of the membrane

and the recirculation fluxes were measured using two rotameters. Since the distillate tank was sealed and completely filled, the water passing through the membrane was forced through the overflow pipe and collected in an external sample holder. The flux was measured by weighing the liquid at fixed time intervals. The test conditions are summarized in Table 3.2.

Table 3.2: DCMD tests conditions.

Tested Feeds	Deionized water NaCl solution 90 g/L
Feed temperatures	30°C 50°C 70°C
Distillate temperature	20°C
Feed flowrate	40 L/h
Distillate flowrate	40 L/h
Membrane area	7 cm^2

3.2 Results

3.2.1 Effect of drying method and nonsolvent

Various flat sheet membranes have been prepared. However, the first tests highlighted a severe shrinkage during the drying process, in particular when pore forming additives were put in the dope solution. Figure 3.2 shows the evolution of the membrane geometry after two drying methods that were tested.

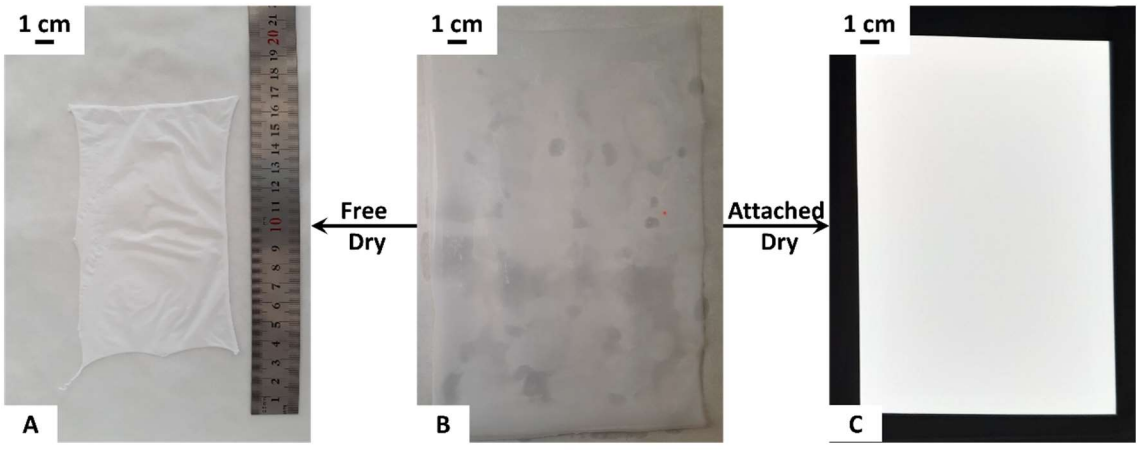

Figure 3.2: Wet membrane (B). Freely dried (A) and attached dried (C).

When the membrane was left drying freely in air at room temperature for 24 hours (A), a severe reduction of its size was observed, with a decrease of the surface area of almost 40%. The FE-SEM analysis (showed in Figure 3.3) highlighted a complete collapse of the porous structure that resulted in the formation of an almost dense, not permeable film.

In order to try maintaining the membrane size, it was decided to block the wet membrane on a metallic plate (Figure 3.2C) using a normal adhesive tape. This procedure has proved valid to preserve the membrane shape without creating defects and also to maintain the porous structure.
The membrane morphology was also deeply influenced by the coagulation bath composition as showed in Table 3.3 and in Figure 3.3

Table 3.3: Properties of membranes prepared with 14% PVDF, 81% DMF and 5% PEG-6000.

Sample	CB	Drying method	Thickness [µm]	Contact angle [°]	Pore size [nm]	Porosity [%]	LEP_w [bar]
FS02	H_2O	Free	160 ± 2	85	-	71 ± 1	>5
FS15	H_2O	Attached	90 ± 1	81	-	73 ± 1	> 5
FS16	EtOH 50%	Free	70 ± 1	105	-	40 ± 3	> 5
FS12	EtOH 50%	Attached	70 ± 1	103	63	67 ± 1	3.4

When pure water was used (FS02 and FS15, Figure 3.3 A and B respectively), thicker and smother films were created. These membranes exhibited low contact angles – almost equal to the dense PVDF – and the porometry measurements did not detect any active pore. In fact, the surface layer of both membranes, reported in Figure 3.3 A2 and B2, appeared almost flat and with no visible pores. The cross-section FE-SEM observations showed wide macrovoids under the surface skin of the membranes. These structures are normally obtained when the phase separation happen at high rates and their formation is enhanced when using a strong nonsolvent like water [11].

Using ethanol solutions as coagulation bath was found to be a key factor to obtain highly hydrophobic and porous films during the preparation of supported flat sheet membranes (Chapter 2). FS16 membrane was prepared using a 50% ethanol solution as coagulant, the cross-section and surface FE-SEM images are reported in Figure 3.3 C1 and C2, respectively. The weaker nonsolvent suppressed the formation of macrovoids and a symmetric structure was obtained. Moreover, the surface appeared rougher and the contact angle was slightly increased up to 105°. However, the lack of a support resulted in the collapse of the porous structure and the porometry tests did not detect any active pore.

Finally, the FS12 membrane (Figure 3.3 D) was prepared exploiting both the weak coagulant and the attached drying. In comparison with the FS16, the contact angle was slightly lowered but the total porosity increased from 40% to 67%. The cross-section FE-SEM images confirmed the

successful preservation of the porous structure while the surface images showed the presence of pores in the skin layer.

The role of the two needed preparation conditions affected two distinct phenomena: the membrane precipitation and the preservation of the porous structure. In fact, pure water acted as a strong nonsolvent and induced a fast demixing creating an almost dense superficial layer as confirmed by the low contact angle. In this phase, the addition of ethanol to the coagulation bath reduced the nonsolvent strength allowing the polymer chains to rearrange in crystalline domains and creating a more porous structure.

However, without the presence of a support material the membrane morphology was deeply modified during the drying process. Leaving the membrane to freely dry in air, the porous structure obtained using ethanol solution as nonsolvent completely collapsed and the final membrane resulted completely dense. Attaching the wet membrane to a rigid support using adhesive tape was enough to preserve the pores during the drying process.

.

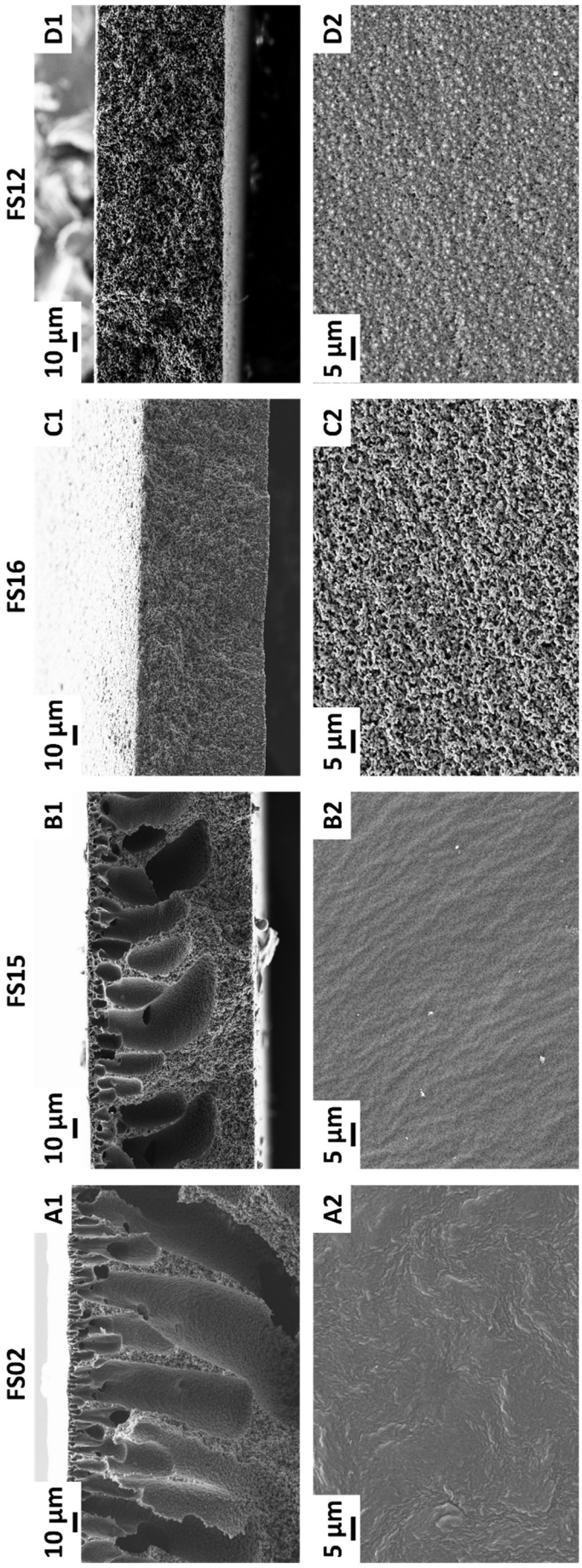

Figure 3.3: FE-SEM images (1 cross section and 2 surface) of membranes prepared using A, B water and C, D EtOH 50% as coagulation bath. And effect of drying technique: A, C free dry and B, D attached dry.

3.2.2 Effect of pore forming agent type

When additives are included into the polymeric solution two different effects take place.
Firstly, hydrophilic pore formers have a thermodynamic effect: in fact, acting as nonsolvents they reduce the stability of the dope solution and enhance the liquid-liquid phase separation rate. This effect increases the precipitation rate and favours the formation of macrovoids under the surface of the membrane [5].
Secondly, the addition of pore forming agents can induce a kinetic effect by increasing the viscosity of the polymeric solution. Higher viscosities hinder the mobility of the molecules slowing the exchange between solvent and nonsolvent. The phase separation is then delayed and more symmetric membranes are formed [12].
The predominance of one effect over the other is influenced by various parameters such as the concentration of the additive [13] or its molecular weight [14,15].
Three different types of pore forming agents were tested: lithium chloride, PEG-400 and PEG 6000. In order to compare the effects of these additives, the membranes were prepared using a dope solution containing 12% of PVDF in DMF and precipitated in EtOH 50%. Table 3.4 reports the main properties of the membranes with the best structure and characteristics for each pore forming agent while Figure 3.4 shows the cross section and surface FE-SEM images.

Table 3.4: Properties of the membranes prepared with 12% PVDF dissolved in DMF and precipitated in EtOH 50%

Sample	Additive [w%]	Thickness [μm]	Contact angle [°]	Pore size [nm]	Porosity [%]
FS11	PEG 6000 5%	60	102	97	72 ± 3
FS14	PEG 400 10%	55	104	157	70 ± 1
FS20	LiCl 5%	80	100	58	70 ± 1

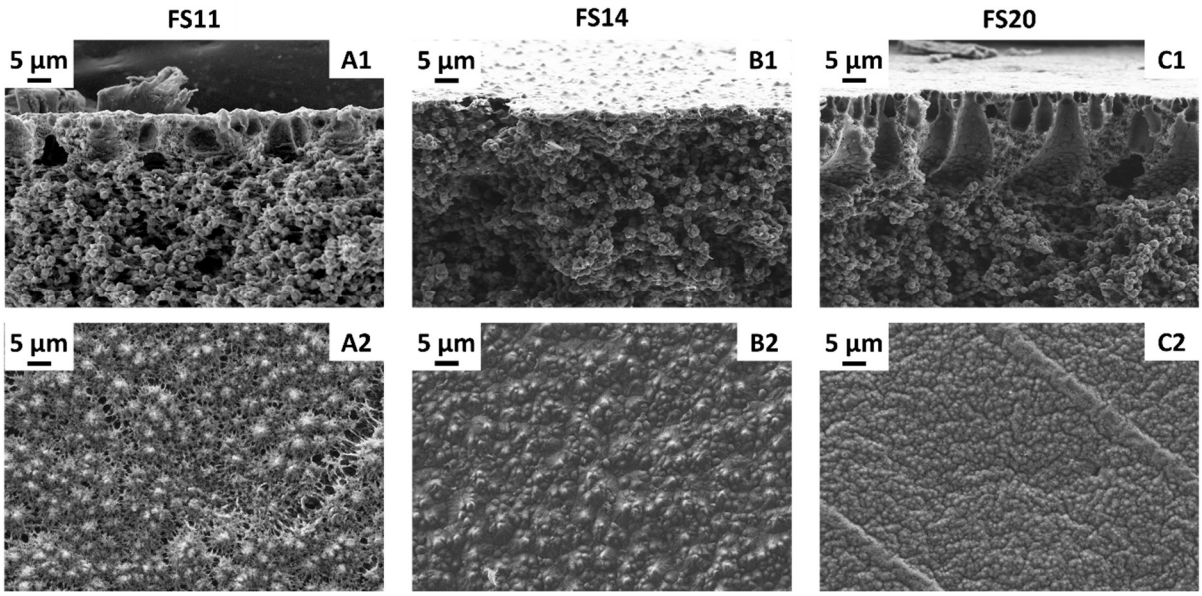

Figure 3.4: FE-SEM images (1 cross section and 2 surface) of membranes prepared with different additives: A) PEG-6000 5%; B) PEG-400 10%; C) LiCl 5%.

The membrane prepared using PEG-6000 as pore forming agent (FS11, Figure 3.4A) showed a cross section structure similar to the one obtained without using pore forming agents. Under the top surface, a small portion of the cross section – almost 10 µm – was characterized by fingerlike cavities while the rest of the membrane was formed by uniform polymer spherulites interconnected. Using a lower molecular weight PEG (FS14, Figure 3.4B), the membrane structure became even more symmetric. Just below a thin surface skin, the cross section was characterized by a uniform distribution of spherulites without any macrovoid dominated layer. This effect can be ascribed to the higher additive concentration used: in fact larger amounts of pore formers increase the dope solution viscosity and the kinetic effect overcomes the thermodynamic one [12]. The porometric analysis carried out using a GLDP apparatus showed an increase of the mean pore size of the membrane when low molecular weight PEG was used as pore forming agent. Similar results were found also by Pei at al. [16], who ascribed the change of the mean pore size to a kinetic effect induced by the different diffusion rates of the additives during the phase inversion process. After the formation of the top layer, smaller molecules can diffuse more easily from the bulk of the dope solution to the coagulation bath while larger ones need more time. This effect allows the formation of a denser surface, characterized by smaller pores, when higher molecular weight pore forming agents are used [17].

Using LiCl, the membrane structure was deeply modified. The fingerlike cavities became bigger than that observed with PEG additives and reached lengths up to 20 µm through the cross section. Li^+ ion is highly solvated by DMF [18] and can interact with electron donor groups of PVDF destabilizing the dope solution and facilitating the phase separation [5]. These interactions

increased the importance of the thermodynamic effect during the phase separation favouring the precipitation process. Fontananova et al. [12] found that LiCl acts differently on the basis of its concentration in the dope solution: at low concentrations the thermodynamic effect is dominant while when higher amounts are added, the increase of the solution viscosity is predominant and the kinetic effect drive the separation process.

3.2.3 Effect of pore forming agent concentration

In order to evaluate the effect of the pore forming agent concentration, four dope solutions with different amounts of PEG-6000 were prepared: the main characteristics registered for the final membranes are reported in Table 3.5. All the four membranes were prepared with 14% PVDF dissolved in DMF, a 50% ethanol solution was used as non-solvent and the membranes were attached dried. A similar approach was applied using LiCl as pore forming agent but the dope solutions with more than 7% of additive were unstable and completely gelled when cooled to room temperature.

Table 3.5: Properties of the membranes prepared with 14% PVDF dissolved in DMF and precipitated in EtOH 50%

Sample	Additive [w%]	Thickness [μm]	Contact angle [°]	Pore size [nm]	Porosity [%]	LEP_w [bar]
FS10	-	55	110	110	60 ± 1	>5
FS12	PEG-6000 5%	70	103	63	67 ± 1	3.4
FS22	PEG-6000 7%	145	76	63	72 ± 1	2.1
FS23	PEG-6000 10%	145	75	61	72 ± 1	1.7

The effect of the PEG concentration was more complicated and was controlled by the interplay of thermodynamic and kinetic effects during the phase separation. The membrane prepared without ~~of~~ pore forming additive was characterized by a similar structure compared with the one made with 5% PEG (Figure 3.5 A and B, respectively). Both the samples showed a symmetric cross section constituted by interconnected PVDF spherulites. However, the crystallization of the polymer happened under different conditions and led to spherulites of different dimensions. In fact, while for the FS10 (Figure 3.5 A) the mean size of the crystallites was 1.7 μm, while it dropped to 0.6 μm for the FS12 membrane. The presence of the hydrophilic additive increased the phase separation rate ad reduced the time available for the spherulite growth during the solid-liquid

phase separation, therefore the FS12 morphology was characterized by a larger number of small spherulites.

Further increase of the PEG content inside the dope solution up to 7%, drastically modified the membrane structure (Figure 3.5 C and D). The higher instability of the polymeric solution induced by the presence of PEG, caused a fast precipitation of the top surface of the casted film. This effect resulted in the formation of a fingerlike macrovoids section under the superficial skin of almost 20 μm of depth. The almost dense surface layer lowered the solvent-nonsolvent exchange rate for the underlying portion of the dope solution. In these conditions, the PVDF chains had more time to arrange themselves in ordered structures and the spherulites grew up to 3 μm of diameter. Moreover, the water contact angle dropped from almost 100° to values around 75°, turning the membrane from hydrophobic to hydrophilic and, by consequence, not suitable for MD operation. Increasing the PEG from 7% to 10% had only minor effects on the membrane characteristics.

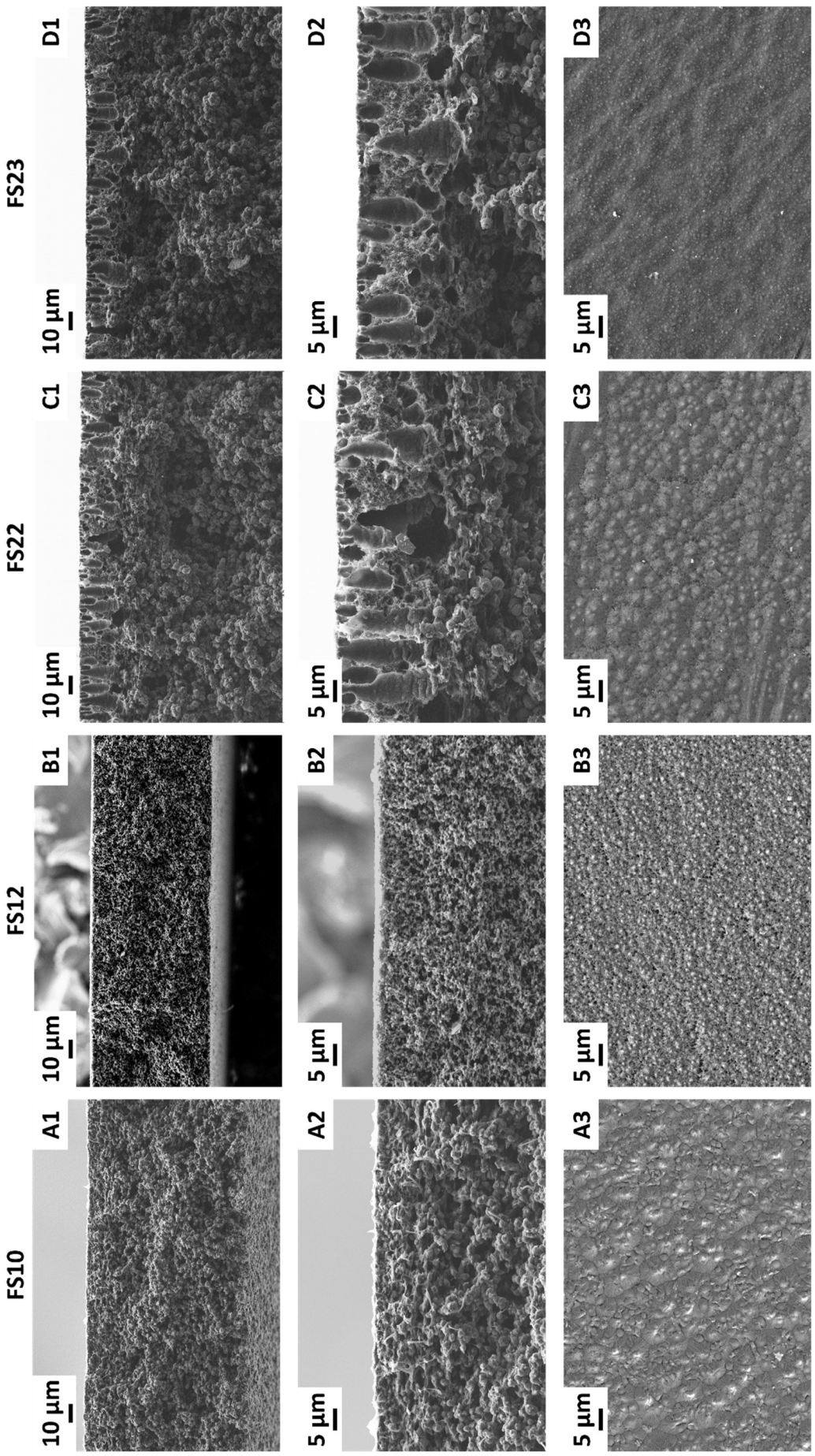

Figure 3.5: FE-SEM images (1,2 cross section and 3 surface) of membranes prepared with different amounts of PEG-6000: A) 0%; B) 5%; C) 7%; D) 10%.

3.2.4 Distillation performance

During the research activity a total of 25 flat sheet membranes were prepared. Among these, all the samples obtained using water as nonsolvent had a dense skin on the surface that prevented their use in MD plants. Similarly, all the membranes freely dried were discharged for the same reason. Finally, out of all the samples prepared using both techniques, four were tested in the DCMD setup schematized in Figure 3.1.

The DCMD tests were performed using both distilled water (Figure 3.6) and a 90 g/L NaCl solution (Figure 3.7) as feed, heated at 50°C, 60°C and 70°C while the cold distillate was kept at 20°C.

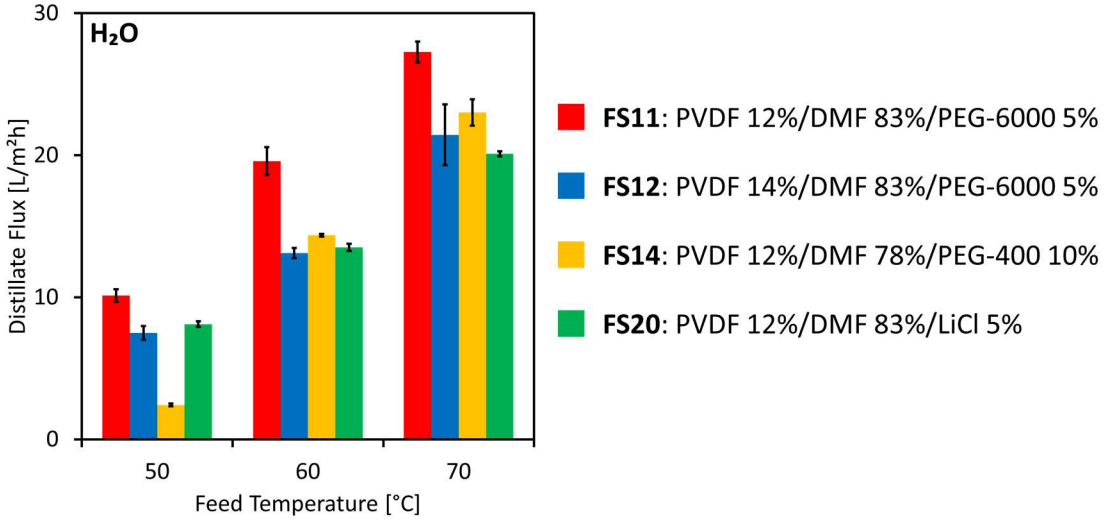

Figure 3.6: Distillate flux during DCMD tests using distilled water as feed.

The FS11 membrane, prepared with a dope solution containing 12% of PVDF and 5% of PEG-6000 as pore forming agent, delivered the highest flux during the DCMD tests with pure water. The increase of the PVDF content up to 14% (FS12) generated a 25%-30% decrease of the distillate flux at all the tested feed temperatures. The higher polymer amount in the dope solution resulted, as previously reported in Table 3.4 (FS11) and in Table 3.5 (FS12), in a decrease of both the pore size and the total porosity of the membrane, causing the registered diminution of the distillate flow during MD tests.

The FS14 membrane was prepared with a larger amount of PEG-400 and had a symmetric cross-section and the lowest thickness among the tested membranes. These characteristics resulted in high distillate fluxes during the DCMD tests.

The tests performed using NaCl as feed allowed to evaluate the salt rejection of the prepared membranes; the distillate flux and salt rejection are reported in Figure 3.7 A and B, respectively.

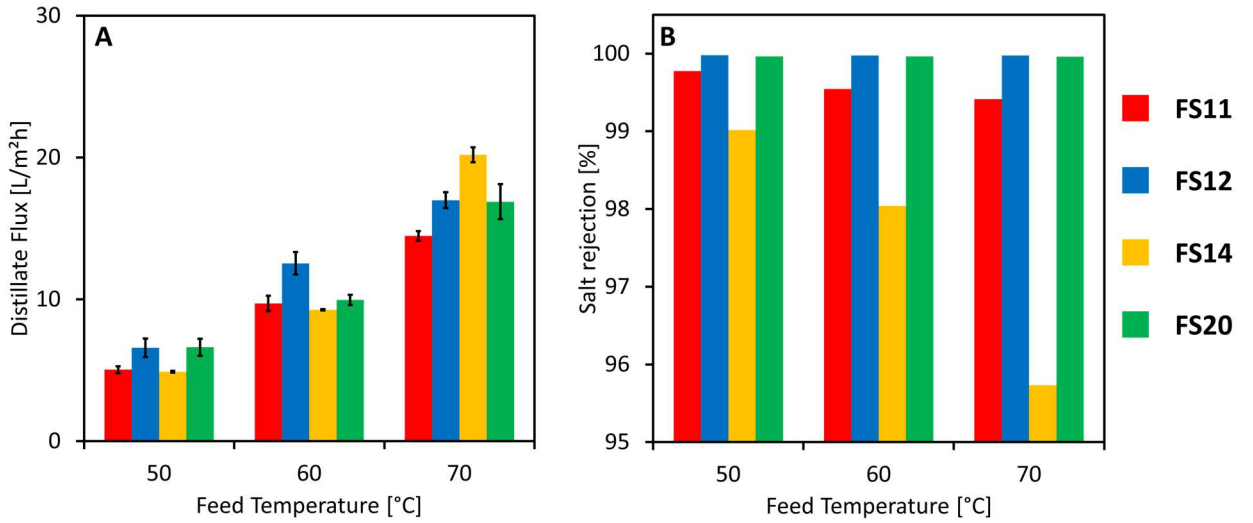

Figure 3.7: DCMD results using a 90 g/L solution as feed. A) distillate flux and B) salt rejection.

During these tests, the FS11 membrane was affected by the greatest flux decline compared with the results obtained treating pure water. This behaviour can be related to a partial flooding of the larger pores of the membrane and a subsequent precipitation of NaCl inside the pore structure. This phenomenon led to a decrease of the effective surface area available for vapour transport, reducing by consequence the distillate flow and the separation ability of the membrane.

During the test with the FS14 membrane using the NaCl solution as feed, an even greater salt rejection decrease was registered.

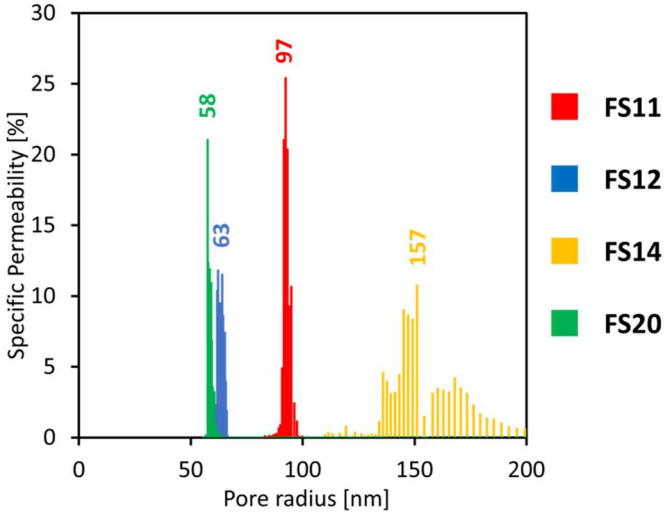

Figure 3.8: Pore radius distribution of membranes prepared in different conditions.

This behaviour could be explained taking into account the results of the porometric analysis reported in Figure 3.8. FS14 had the largest mean pore size and also the wider pore distribution was among the tested membranes. In these conditions, a sensible percentage of large pores was

available for flooding phenomena and allowed the direct passage of the liquid feed through the membrane. Therefore, the overall transmembrane flux was increased but the salt rejection was lowered even more than wat was registered for the FS11 membrane. After prolonged DCMD test – not reported in Figure 3.7 – the salt rejection dropped to 85%.

FS12 membrane had a symmetric structure across its whole section, characterized by interconnected PVDF spherulites, similar to the one obtained with the supported membranes described in Chapter 2. The DCMD test carried out using the NaCl solution as feed confirmed the good stability of this structure and the great separation abilities of such membrane. Despite having a completely different morphology, characterized by fingerlike cavities underneath the surface, the FS20 membrane had pore size and thickness similar to the FS12 and during the DCMD tests with the 90 g/L NaCl solution the two membranes showed comparable distillate fluxes as well as an almost complete and constant salt rejection.

3.3 Conclusions

Unsupported flat sheet membranes were prepared using various additives as pore forming agents in order to tune their structure. In particular, the effect of the additive type and concentration into the dope solution was investigated. Moreover, the severe shrinkage problem observed during the drying process was fixed by blocking the wet membrane, preventing the total collapse of the porous structure.

Similarly to what was found during the preparation of supported PVDF membranes (Chapter 2), the use of a weak coagulation bath was mandatory to create a porous structure on the membrane surface.

The addition of pore forming agents allowed to create membranes with higher overall porosity and smaller pore size. In particular, using PEG-6000 as pore forming agent, membranes with adequate structure and characteristics for MD applications were produced. The concentration of the additive plays a significant role on the membrane structure as a result of a complex interplay of thermodynamic and kinetic effects.

Two different categories of pore forming agents were tested: inorganic (LiCl) and polymeric (PEG-400 and PEG-6000). With every tested concentration, LiCl increased the precipitation rate of the dope solution creating a fingerlike layer under the surface skin of the membrane. Otherwise, using polyethylene glycols both symmetric globular membranes and asymmetric ones were obtained by tuning the additive and PVDF concentrations.

The MD tests were performed by means of DCMD operation mode, treating both pure water and a 90 g/L NaCl solution at 50°C, 60°C and 70°C. The membranes with larger pores provided the higher fluxes when deionized water was used but during the tests with the NaCl solution suffered different grades of flooding that reduced both the distillate flux and the salt rejection.

However, by finely tuning the dope solution composition, it was possible to obtain membranes able to deliver good distillate fluxes and total salt rejection even during the treatment of a concentrated NaCl solution.

References

[1] Y. Tang, N. Li, A. Liu, S. Ding, C. Yi, H. Liu, Effect of spinning conditions on the structure and performance of hydrophobic PVDF hollow fiber membranes for membrane distillation, Desalination. 287 (2012) 326–339. doi:10.1016/j.desal.2011.11.045.

[2] H. Karkhanechi, S. Rajabzadeh, E. Di Nicolò, H. Usuda, A.R. Shaikh, H. Matsuyama, Preparation and characterization of ECTFE hollow fiber membranes via thermally induced phase separation (TIPS), Polymer (Guildf). 97 (2016) 515–524. doi:10.1016/j.polymer.2016.05.067.

[3] B. Wu, K. Li, W.K. Teo, Preparation and characterization of poly(vinylidene fluoride) hollow fiber membranes for vacuum membrane distillation, J. Appl. Polym. Sci. 106 (2007) 1482–1495. doi:10.1002/app.26624.

[4] R. Naim, A.F. Ismail, A. Mansourizadeh, Effect of non-solvent additives on the structure and performance of PVDF hollow fiber membrane contactor for CO 2 stripping, J. Memb. Sci. 423–424 (2012) 503–513. doi:10.1016/j.memsci.2012.08.052.

[5] A. Bottino, G. Capannelli, S. Munari, A. Turturro, High performance ultrafiltration membranes cast from LiCl doped solutions, Desalination. 68 (1988) 167–177. doi:10.1016/0011-9164(88)80052-3.

[6] F. Liu, N.A. Hashim, Y. Liu, M.R.M. Abed, K. Li, Progress in the production and modification of PVDF membranes, J. Memb. Sci. 375 (2011) 1–27. doi:10.1016/j.memsci.2011.03.014.

[7] J. Kong, K. Li, Preparation of PVDF hollow-fiber membranes via immersion precipitation, J. Appl. Polym. Sci. 81 (2001) 1643–1653. doi:10.1002/app.1595.

[8] D. Hou, J. Wang, D. Qu, Z. Luan, X. Ren, Fabrication and characterization of hydrophobic PVDF hollow fiber membranes for desalination through direct contact membrane distillation, Sep. Purif. Technol. 69 (2009) 78–86. doi:10.1016/j.seppur.2009.06.026.

[9] Y. Li, C. Jin, Y. Peng, Q. An, Z. Chen, J. Zhang, L. Ge, S. Wang, Fabrication of PVDF hollow fiber membranes via integrated phase separation for membrane distillation, J. Taiwan Inst. Chem. Eng. 95 (2019) 487–494. doi:10.1016/j.jtice.2018.08.036.

[10] S. Simone, A. Figoli, A. Criscuoli, M.C. Carnevale, A. Rosselli, E. Drioli, Preparation of hollow fibre membranes from PVDF/PVP blends and their application in VMD, J. Memb. Sci. 364 (2010) 219–232. doi:10.1016/j.memsci.2010.08.013.

[11] C.A. Smolders, A.J. Reuvers, R.M. Boom, I.M. Wienk, Microstructures in phase-inversion membranes. Part 1. Formation of macrovoids, J. Memb. Sci. 73 (1992) 259–275.

doi:10.1016/0376-7388(92)80134-6.

[12] E. Fontananova, J.C. Jansen, A. Cristiano, E. Curcio, E. Drioli, Effect of additives in the casting solution on the formation of PVDF membranes, Desalination. 192 (2006) 190–197. doi:10.1016/j.desal.2005.09.021.

[13] T. Malik, H. Razzaq, S. Razzaque, H. Nawaz, A. Siddiqa, M. Siddiq, S. Qaisar, Design and synthesis of polymeric membranes using water-soluble pore formers: an overview, Polym. Bull. 76 (2019) 4879–4901. doi:10.1007/s00289-018-2616-3.

[14] S. Wongchitphimon, R. Wang, R. Jiraratananon, L. Shi, C.H. Loh, Effect of polyethylene glycol (PEG) as an additive on the fabrication of polyvinylidene fluoride-co-hexafluropropylene (PVDF-HFP) asymmetric microporous hollow fiber membranes, J. Memb. Sci. 369 (2011) 329–338. doi:10.1016/j.memsci.2010.12.008.

[15] B. Chakrabarty, A.K. Ghoshal, M.K. Purkait, Effect of molecular weight of PEG on membrane morphology and transport properties, J. Memb. Sci. 309 (2008) 209–221. doi:10.1016/j.memsci.2007.10.027.

[16] L. Pei, W. Zhao, L. Zhang, Preparation and characterization of porous poly(vinylidene fluoride) membranes for dehumidification with poly(ethylene glycol) as an additive, J. Appl. Polym. Sci. 118 (2010) 2696–2703. doi:10.1002/app.32628.

[17] B. Jung, J.K. Yoon, B. Kim, H.-W. Rhee, Effect of molecular weight of polymeric additives on formation, permeation properties and hypochlorite treatment of asymmetric polyacrylonitrile membranes, J. Memb. Sci. 243 (2004) 45–57. doi:10.1016/j.memsci.2004.06.011.

[18] J.N. Butler, J.C. Synnott, Thermodynamics of Lithium Chloride in Dimethylformamide, J. Am. Chem. Soc. 92 (1970) 2602–2607. doi:10.1021/ja00712a002.

Chapter 4

4 Importance of the support material

Membranes for the MD process exist mainly in two basic configurations: hollow fibres and flat sheet. The first ones have the advantage of allowing high packing density and being self-supported; on the other hand, their wall thickness is usually higher than flat sheet membranes one and their distillate flux is generally lower. Instead, flat sheet membranes must be supported on an adequate material to reach the mechanical properties required for their use in MD plants [1]. However, the support material, usually a non-woven sheet, can add a supplementary mass transport resistance that can decrease the productivity of this kind of membranes. The presence of the non-woven support also plays a role in governing the porous structure of the membrane [2]. In fact, during the membrane preparation via phase separation, the polymer solution faces different grades of shrinkage depending on the precipitation conditions. In extreme cases, the shrinkage can be severe enough to lead to an almost complete collapse of the porous structure, deteriorating the membrane performance [3–5]. The adhesion between the polymer film and the support during the phase inversion process hinders the shrinkage and allows to maintain the pore dimensions [6,7]. The effectiveness of the support in preventing the polymer shrinkage depends on different characteristics of the non-woven, like its mechanical properties and porosity, as well as on the membrane production methodology (e.g. polymer solution viscosity, casting thickness, time between the film casting and the immersion in the coagulation bath, precipitation rate) [2]. By contrast, the choice of an inadequate support can also lead to the formation of defects and by consequence to a deterioration of the separation ability of the membrane [2,5].
In this work, PVDF membranes were prepared by the nonsolvent induced phase separation (NIPS) technique on six different non-woven tissues and three thin nets. The effect of the support structure on the membrane morphology was deeply investigated by FE-SEM images, while the influence on their performance was evaluated in a lab scale vacuum membrane distillation setup measuring the distillate flow with both pure water and a 90 g/L NaCl solution.

4.1 Materials and Methods

4.1.1 Membrane preparation

The membranes were prepared by non-solvent induced phase separation using a dope solution obtained dissolving a commercial PVDF (Solef 6020 – Solvay Speciality Polymers, Italy) in N,N-dimethylformamide (DMF – Carlo Erba, Italy).

Based on a previous work (Chapter 2) [8], ethanol was chosen as non-solvent in order to obtain a very rough membrane surface that increases the hydrophobic character, enhancing the wetting resistance of the membrane.

Two different kind of support were investigated: six non-woven tissues and three nets.

The selected non-woven were all produced by Freudenberg Filtration Technologies (Germany) and displayed noticeable differences both in terms of porosity and morphology as well as a relevant difference in thickness. The nets tested were actually designed to be used as permeate spacer inside industrial spiral wound reverse osmosis modules and were characterized by very different structures.

To prepare the membranes, the supports – both non-woven and nets – were put on a flat glass and impregnated with DMF in order to improve the membrane adhesion to the support itself. The lowest possible amount of solvent was used for each support and any excess was removed using absorbent paper before casting the polymer solution. In order to compare the final membrane properties, independently from the thickness of the support material, different spacers were used to obtain membranes with a similar casted solution thickness, as showed in Figure 4.1.

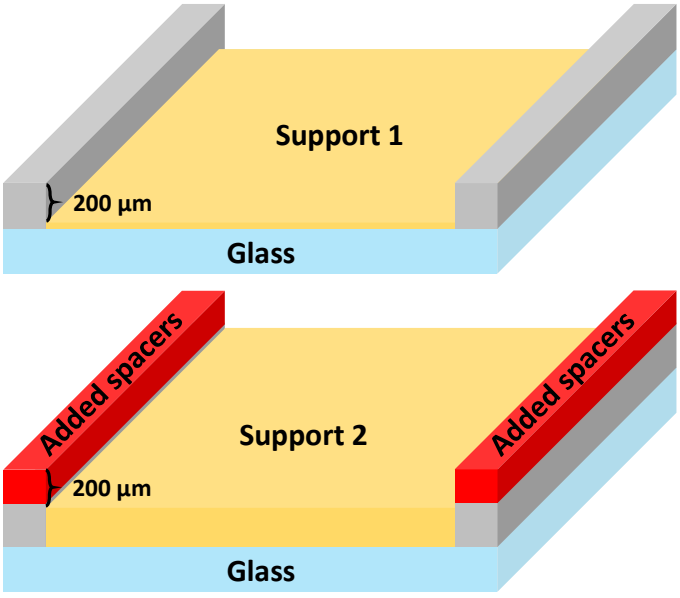

Figure 4.1: Scheme of the method exploited to obtain similar dope solution thickness on supports with different depths.

Immediately after the dope solution casting, the glass was immersed at constant speed and angle in the ethanol bath (EtOH 96% – VWR International) by using a motorized sled.

4.1.2 Membrane characterization

The main characteristics of the pristine supports and of the final membranes were tested with various techniques. The support morphology was investigated using both digital microscopy (Dino-lite digital microscope) and field emission scanning electron microscopy (FE-SEM Zeiss SUPRA 40 VP). The selective surface, as well as the cross section were observed at different magnifications, ranging from 100X to 15000X. The images were recorded collecting secondary electrons (SE) using both a common detector and an in-lens detector and the acceleration voltage was set at 5 kV in order to prevent beam induced modifications of the sample. The preparation of the specimens was slightly different for the membrane surface samples and for the cross-section ones. For the surface observation, a small piece of the membrane was attached to a stub with a double-sided conductive adhesive tape and coated with a very thin carbon film using an Edwards BOC EXC 120 sputter coater in order to render the sample electrically conductive. Instead, for the cross-section examination the sample preparation was more complex. In fact, before mounting the sample on the stub and the coating process, the membrane cross section had to be brought to light without causing any structure deformation. To this end, a portion of the membrane was immersed in liquid nitrogen for thirty minutes and then cut using a sharp scalpel, so exposing two internal almost flat zones. This phase is particularly critical for the membranes casted on the nets, as the support offers a higher resistance to slit. The cut samples were then mounted vertically on a stub and coated like the membrane surface ones.

Since the chemical composition of the three nets was unknown, FT-IR analyses were performed using a Bruker Vertex 70 FT-IR spectrometer in ATR (Attenuated Total Reflectance) mode.

The mass transport resistance of the supports was estimated by measuring their gas permeation using nitrogen. The sample was put in a small cell (20 mm^2) and nitrogen was fed to one side while the other was connected to a gas flowmeter at atmospheric pressure; by measuring the trans membrane pressure drop at different gas flux the support gas permeability was calculated.

Since the support plays a major role in defining the membrane mechanical properties, both the supports and the prepared membranes were tested using a tensometer (INSTRON 5565) evaluating their elastic modulus. The samples were stretched at a constant speed of 2 mm/min and the applied strength was measured. While the non-woven present a quite isotropic structure, the nets were greatly anisotropic. Therefore, they were tested in two orthogonal directions, namely parallel (//) and perpendicular (⊥) based on the membrane casting direction. The elastic modulus of the pristine supports and of the different membranes was calculated as the slope of the stress-strain curve during the first stage (elastic behaviour).

The water contact angle was measured using a digital tensiometer (Biolin Scientific Attension Theta) in order to estimate the hydrophobicity of the membrane surface. The instrument is equipped with a syringe that automatically creates a 3 μL drop which is then deposited on the membrane surface. The integrated camera subsequently records a 10 seconds video at 15 frame per second: therefore, for each drop 150 contact angle data are recorded and a minimum of three drops per sample was analysed.

Liquid entry pressure of water (LEP_w) was evaluated using an in-house built apparatus. The water contained in a steel tank was pressurized using compressed air and fed to a cell that contained the membrane. The pressure was increased step-by-step using a pressure regulator and monitored with a differential digital manometer. For each membrane, at least 3 different samples were analysed.

The total porosity of the membranes (ε%) was measured gravimetrically. The procedure was slightly different for the membranes casted on non-woven supports and those prepared with the nets.

In the first case, the membrane was easily separated from the non-woven, which is impossible for the nets. Instead, when using the nets as support, three samples of each membrane and of each net were cut using a die cutter in order to obtain geometrically equal samples. All the membrane samples were dried under vacuum and then weighed on an analytical balance; they were then impregnated with 1-octanol and weighed again. Several measurements were performed until the samples reached a constant weight. The total porosity for the non-woven membranes was calculated using the Equation 2.1.

To calculate the porosity of the membranes casted on the nets, the support contribution to the total volume must be taken into account; therefore, Equation 2.1 must be modified as follows:

$$\varepsilon\% = \frac{V_{empty}}{V_{tot}} \cdot 100 = \frac{\frac{m_{oc}}{\rho_{oc}}}{\frac{m_{pol}}{\rho_{pol}} + \frac{m_{oc}}{\rho_{oc}} + \frac{m_s}{\rho_s}} \cdot 100 = \frac{\frac{(m_w - m_d)}{\rho_{oc}}}{\frac{(m_d - m_s)}{\rho_{pol}} + \frac{(m_w - m_d)}{\rho_{oc}} + \frac{m_s}{\rho_s}} \cdot 100 \qquad 4.1$$

Where m_w and m_d are the masses of impregnated and dry membrane, respectively, ρ_{oc} is the 1-octanol density (0.83 g/cm^3) and ρ_{pol} is the density of PVDF (1.8 g/cm^3) at 25°C, while m_s and ρ_s are the mass and the density at 25°C (1.4 g/cm^3 for PET and 0.92 g/cm^3 for PP) of the dry supports.

4.2 Results

4.2.1 Support characterization

The aim of using a support to prepare a PVDF membrane is to increase its mechanical properties in order to withstand the operation conditions in the distillation plant. However, the support must not enhance the resistance to vapor transfer. The non-woven supports were differentiated by the material (polyethylene terephthalate, PET or a mix of polypropylene, PP and polyethylene, PE) as well as by their thickness and fibre diameter. The three nets had different structures and thickness. However, their material was unknown. Therefore, FT-IR analyses were carried out in order to determine it. The spectra registered are reported in Figure 4.2.

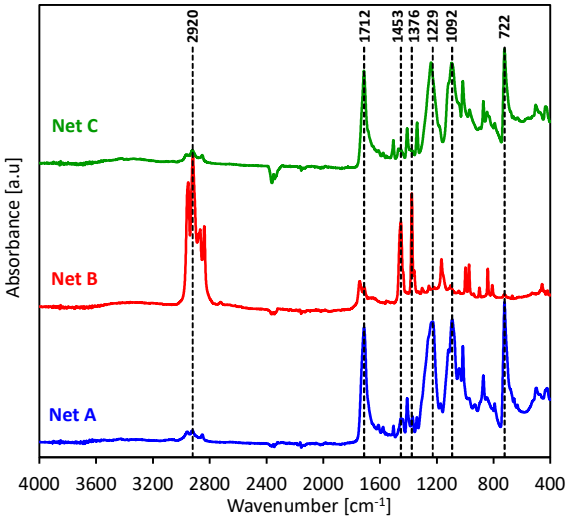

Figure 4.2: FT-IR spectra of nets A (bottom), B (centre) and C (top).

Nets A and C appeared to be made of the same material. Comparing the spectra with literature data, four main peaks related to polyethylene terephthalate were identified. In particular it is possible to distinguish at 722 cm^{-1} the aromatic C–H vibrations, the two peaks at 1092 and 1229 cm^{-1} corresponding to the asymmetric C–C–O and the O–C–C stretching, and the C=O stretching at 1712 cm^{-1} [9].

Instead, net B spectrum was characterized by a broad band around 2920 cm^{-1} that is related to the C–H bond stretching as well as by two peaks at 1453 and 1376 cm^{-1} due to CH_2 and CH_3 deformation that are typical of polypropylene [10]. These results were in concordance with the optical microscopy analysis (Figure 4.3); in fact, net A and C were transparent while net B was white, suggesting that the two polymers had different crystallinity degrees. Literature data report

a degree of crystallinity of 30-35% for PET [11] while for PP the values range between 50 and 65% [12].

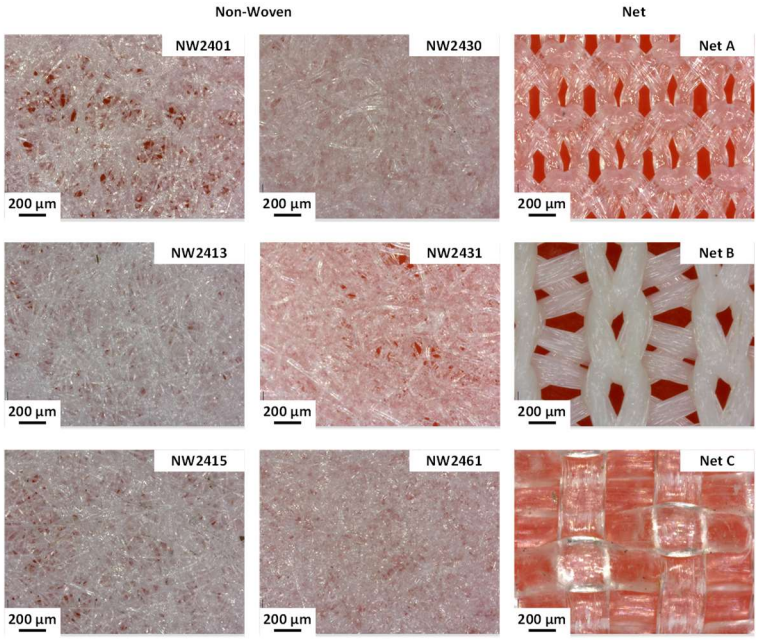

Figure 4.3: Digital microscope images of the tested supports.

The optical microscope observations allowed to determine the structure of the tested supports. The six non-woven were characterized by a similar structure composed by a random distribution of polymer filaments, of different size for each support. By the images in Figure 4.3, the NW2430 and NW2431 were characterized by thicker filaments (almost 25 µm in comparison of 15 µm of the others). Since the aim of supports is to enhance the membrane mechanical properties without hindering the mass transport, their mechanical properties as well as the nitrogen permeability were tested. The data collected are reported in Table 4.1.

Table 4.1: Support elastic modulus and nitrogen permeability.

Support	Material	Thickness [µm]	Elastic modulus [N/mm²]	N_2 Permeability [cm²/s]
NW2401	PET	100 ± 4	1251 ± 141	271
NW2413	PET	179 ± 4	936 ± 135	239
NW2415	PET	219 ± 6	617 ± 68	225
NW2430	PP/PE	202 ± 5	720 ± 32	101
NW2431	PP/PE	141 ± 7	535 ± 44	116
NW2461	PP/PE	191 ± 3	647 ± 24	139
Net A	PET	210 ± 1	⊥ 134 ± 22 // 1362 ± 58	ND*
Net B	PP	293 ± 1	⊥ 771 ± 43 // 853 ± 10	ND*
Net C	PET	515 ± 5	⊥ 553 ± 51 // 998 ± 105	ND*

* The value was higher than the measuring setup upper limit.

The random orientation of the fibres in the non-woven supports granted an isotropic behaviour when tested for elastic modulus evaluation while the nets presented great differences. The symbols ⊥ and // represent the values registered testing the nets perpendicularly and in parallel with the membrane casting direction.

The nitrogen permeabilities of the various non-wovens were quite similar and ranged between 101 and 279 cm^2/s depending on their morphology (thickness and free volume) while the three nets reached far higher values. Indeed, because of a more open structure, they did not offer any resistance to the gas flow during the measuring tests. Therefore, it was not possible to precisely measure their permeability with the equipment available in the laboratory.

4.2.2 Membrane morphology

Membrane morphology was investigated exploiting mainly FE-SEM observation of both selective surface and cross section. Because of the great difference between non-woven supports and nets, great differences were registered for these two sets of membranes. Figure 4.4 shows the cross section of two membranes prepared on non-woven supports (2413 and 2461).

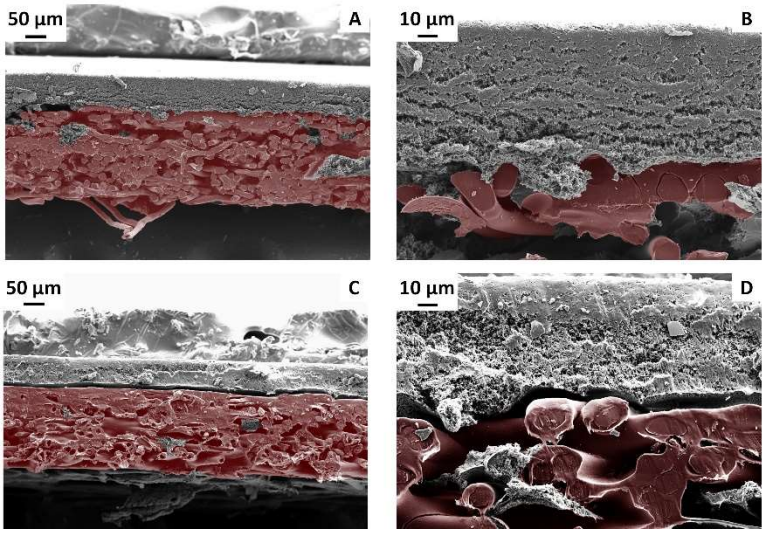

Figure 4.4: Non-woven membrane cross section (support is highlighted in red).

The membrane structure above the support appears to be similar for all the membranes prepared with non-wovens which presented a porous and homogeneous PVDF layer. However, some differences could be seen at the interface between the PVDF and the non-woven. When using NW2413 (Figure 4.4 A and B), the PVDF showed a good adhesion with the support, even after

the cross section was cut. Instead, the membrane prepared using NW2461 (Figure 4.4 C and D) reported an almost complete delamination after the cross section cut.

The different materials composing the support could explain the different behaviours detected for the two membranes showed in Figure 4.4. In fact, NW2413 was made by PET, while NW2461 was composed of PE/PP fibres. The different adhesion between PVDF and the support can be explained by means of polymer-polymer interactions. Table 4.2 reports the Hansen solubility parameters (HSP) for PE, PP, PET and PVDF.

Table 4.2: PP, PET and PVDF Hansen solubility parameters.

Polymer	δ_d [$MPa^{½}$]	δ_p [$MPa^{½}$]	δ_h [$MPa^{½}$]	δ_{TOT} [$MPa^{½}$]
PE [13]	14.8	-3.9	1.8	15.4
PP [14]	16.1	0	0	16.1
PET [14]	16.8	10.4	11	22.6
PVDF [15]	17.2	12.5	9.2	23.2

The fully aliphatic repetition unit of the PP and PE reflects in almost null – or even negative – values for the polar (δ_p) and the hydrogen bonding (δ_h) components of the HSP. Instead, the PET and PVDF repetition units are characterized by more polar groups that increase the interactions between the polymer chains.

These chemical differences of the support material can explain the different morphologies registered for the membranes prepared, since the low interactions between PP/PE and PVDF resulted in a limited adhesion between the support and the dope solution during the membrane casting.

The morphology of the membranes prepared using the nets appeared quite different compared to the ones casted on the non-woven supports as reported in Figure 4.5.

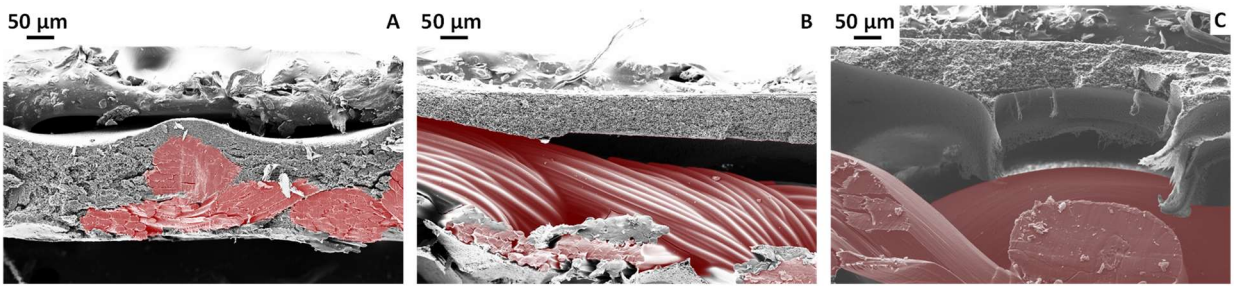

Figure 4.5: FE-SEM cross section images of membranes prepared using net supports (highlighted in red).

The dope solution invaded in all the three cases the nets but in different extent, based on their structure (highlighted in red).

The thinner net (A) made of PET was completely surrounded by the polymer solution and the membrane was characterized by a full integration of the net and the PVDF layer. Net B was also totally flooded but the different material (PP) led to a lower adhesion of the PVDF on the net fibres and the connection between the support and the PVDF layer was mainly granted by the mechanical entanglement of the two materials. Net C finally had a much denser structure and the dope solution was able to only partially invade the net structure, creating however some mechanical binding between the net structure and the final PVDF layer.

Table 4.3 reports the PVDF layer thickness measured from the cross-section FE-SEM images.

Table 4.3: PVDF layer thickness.

Support	Polymer thickness [µm]	
NW2401	70 ± 15	
NW2413	47 ± 4	
NW2415	56 ± 3	
NW2430	54 ± 13	
NW2431	53 ± 7	
NW2461	78 ± 20	
Net A	31 ± 2	126 ± 16
Net B	73 ± 9	142 ± 7
Net C	69 ± 11	143 ± 9

The particular structure of the membrane prepared using the nets resulted in two different polymer thicknesses: a thinner layer on the crests of the net, and a thicker one in correspondence of the net holes. This also caused a different morphology of the membranes in the two zones, as shown in Figure 4.5 and highlighted in Figure 4.6 for the net A membrane.

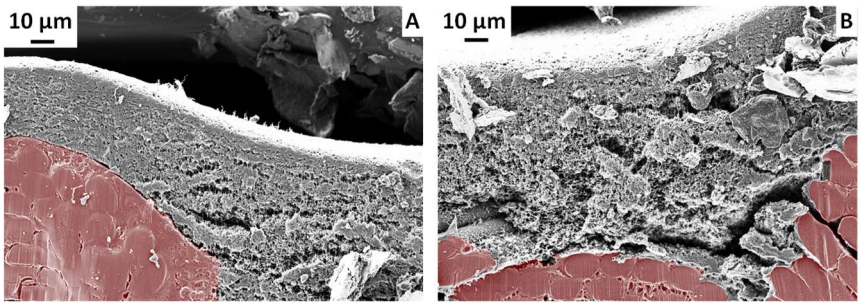

Figure 4.6: Magnification of the two zones (A: crest and B: hole) observed for net A membrane (support is highlighted in red).

On the top of the net crest, the PVDF layer is more much thinner than in the zone corresponding to the net holes. Moreover, by the images reported in Figure 4.6, the two zones appeared to be characterized by different porosities: denser on the net crest and more porous in the holes. It has been found that, during membrane preparation using NIPS process, the dope solution thickness has effects on the macrovoid formation and, by consequence, on the membrane porosity [16–18]. The same effect is visible, in different extent, in the other two net membranes.

4.2.3 Membrane performances

The different membrane structures resulted in different characteristics and performances during MD operation. One of the key parameters to be controlled to exploit porous membranes in VMD process is the LEP_w; the values registered for all the prepared membranes are reported in Table 4.4 together with the measured porosity.

Table 4.4: Liquid entry pressure and overall porosity of the membranes prepared.

Support	LEPw [bar]	Porosity [%]
NW2401	1.6 ± 0.3	72 ± 4
NW2413	1.9 ± 0.2	70 ± 3
NW2415	1.7 ± 0.3	68 ± 6
NW2430	1.9 ± 0.1	71 ± 5
NW2431	1.8 ± 0.3	67 ± 5
NW2461	1.7 ± 0.3	65 ± 7
Net A	4.4 ± 0.5	34 ± 5
Net B	5.2 ± 0.4	60 ± 2
Net C	5.6 ± 0.6	37 ± 2

The LEP_w values depends on the maximum pore size of the membrane. Highest values are registered when the membranes have smaller maximum pore size. The data reported in Table 4.4 confirm the substantial difference between the membranes prepared on the non-woven supports and those made using the nets. Like the FE-SEM images suggested, the great similarities among the non-wovens, responsible for the almost equal membrane structure, had the same effect on the LEP_w values that range between 1.6 and 1.9 bar in accordance with data registered in previous works (Chapter2) [8]. The nets show LEP_w values definitely higher. The difference between the non-woven and net membranes can be explained analysing the surfaces of two samples reported in Figure 4.7.

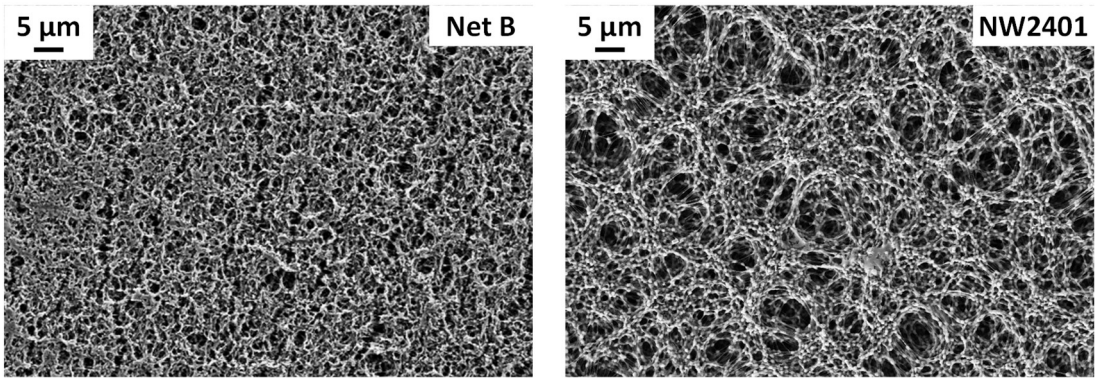

Figure 4.7: FE-SEM images of surface of Net B and NW2401 membranes.

The net membranes were characterized by a denser surface with smaller pores. It is well known that unsupported membranes are characterized by smaller pores in respect with supported ones. This phenomenon is related to the shrinkage that unsupported membranes encounter when dried. The support was found to prevent the PVDF layer shrinkage, leading to more porous and more permeable membranes [2,3].

The net supports offer looser attaching points to the polymer solution in respect to the non-wovens and, in particular, in the spaces between the net fibres a portion of the solution acts like it was unsupported. Therefore, during the drying phase, these portions of membrane had more freedom to shrink ad the final structure was characterized by smaller pores for all the net membranes.

These results are confirmed by the porosity measurements performed on the membranes and reported in Table 4.4. In fact, the non-woven membranes present higher values, ranging around 70%, while the nets were characterized by lower porosity. Moreover, the net structure appears to have an influence on the membrane structure as Net A and Net C membranes showed a significantly lower porosity in respect with the Net B.

The VMD performance of all the nine membranes was tested in the setup schematized in Chapter 2 using as feed both deionized water and a 90 g/L NaCl solution heated at 30, 50 and 70°C; Figure 4.8 reports the mean distillate fluxes registered treating deionized water.

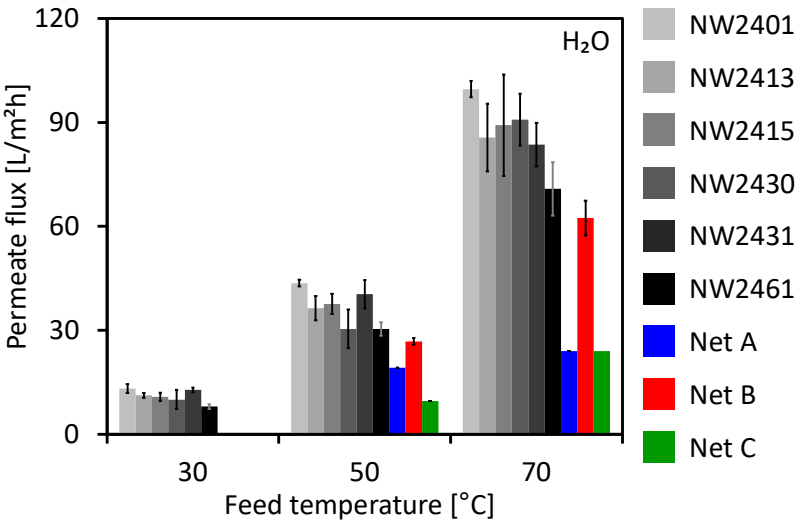

Figure 4.8: Mean VMD flux using H_2O as feed at 30, 50 and 70°C.

The membranes prepared using the nets delivered lower performance compared to the ones deposited on the non-wovens and at 30°C it was impossible to collect any permeate in one-hour tests for all the net membranes

The generally lower permeability of the net membranes can be related to their lower porosity and their different structure in the two zones (crest and hole) described above, as illustrated for each membrane in Figure 4.9.

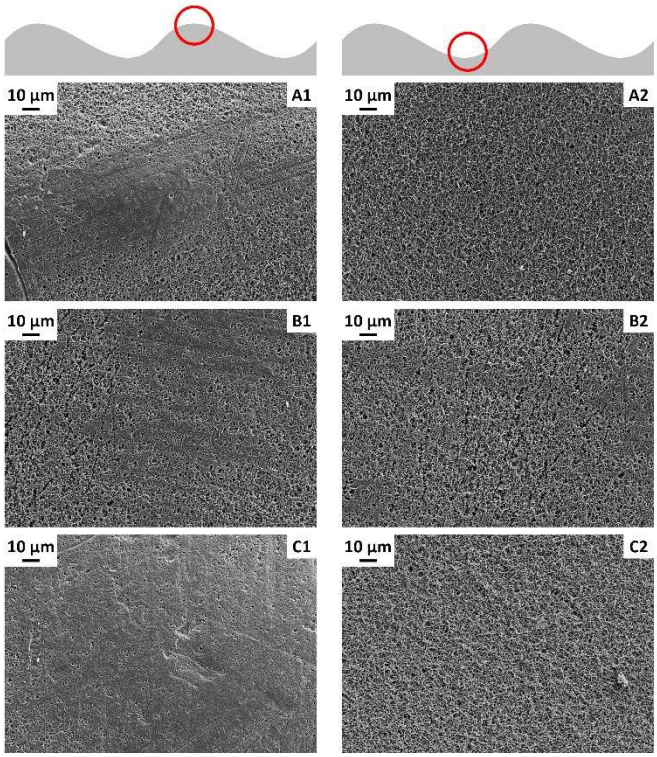

Figure 4.9: FE-SEM images of the highest (1) and lowest (2) point of net membranes. A: Net A, B: Net B and C: Net C.

As reported in Figure 4.9 all the three net membranes had different surface structure in the highest point (where a thinner polymer layer was formed) and inside the net holes. In fact, as highlighted for Net A membrane in Figure 4.6, the zones above the crests of the net were characterized by a lower porosity than the zones relying in the net holes. Moreover, these last parts of the membranes solidified like unsupported membranes which results in a greater polymer shrinkage than on the non-woven support.

All these factors can justify the large difference of the porosity between the non-woven membranes and the net ones and, by consequence, the difference in the VMD performance.

A great difference was also registered for net B membrane that consistently delivered better flux compared to net A and B membranes. The higher roughness of the fibres (diameter roughly equal to 20 µm) that compose the Net B, showed in Figure 4.5B, offered a larger surface for physical adhesion between the dope solution and the support structure. During the membrane solidification these interactions reduced the shrinkage. Therefore, Net B membrane had a larger porosity that can be attributed also to the smaller pore size differences between the crest and hole zones in comparison with the other two net membranes.

The membranes were then tested using a concentrated NaCl solutions as feed, in order to measure their separation performance, in term of salt rejection.

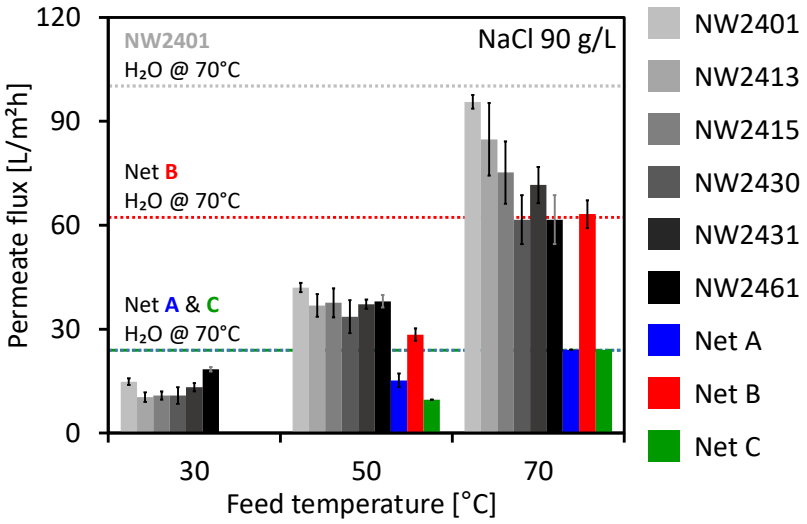

Figure 4.10: Mean VMD flux using NaCl 90 g/L solution as feed at 30, 50 and 70°C. The dotted lines represent the fluxes of Net A and C (green-blue), of net B (red) and NW2401 (grey) registered with water at 70°C.

Figure 4.10 reports the mean distillate flux registered during the VMD tests treating a 90 g/L solution as feed at 30, 50 and 70°C. The rejection values are not reported since every membrane provided an almost complete salt retention and the permeate conductivity never exceeded 2µS/cm.

As expected, the mean flux decreased in respect with the test with pure water because of the presence of NaCl in the feed solution and, because of polarization phenomena. The latter are enhanced at higher feed temperatures when the driving forces of the process are maximized and the transmembrane flux is improved [19]. However, this effect was less evident for the net membranes. This difference could be explained by their surface morphology, reported in Figure 4.11.

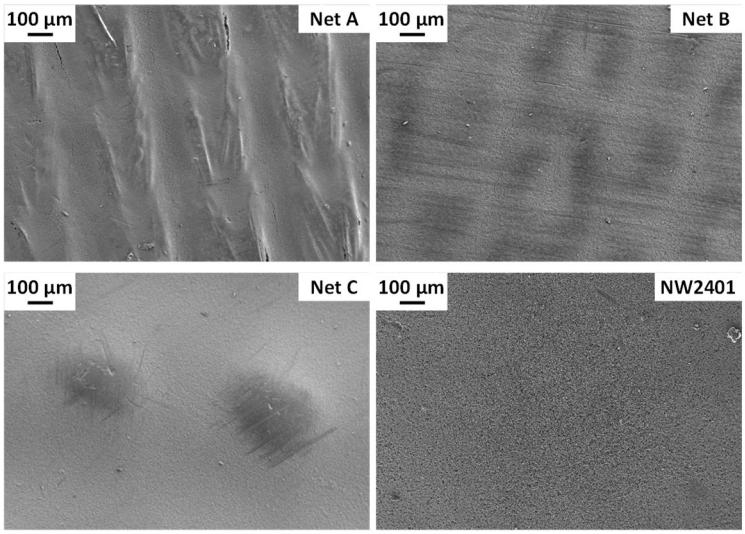

Figure 4.11: FE-SEM images of membrane surfaces.

All non-woven membranes had similar superficial morphologies (Figure 4.11 reports only NW2401 membrane as an example) characterized by a flat structure composed by cavities and polymer.

Differently from the non-wovens, the nets created a pattern that can modify the fluid dynamics on the membrane surface. The increased roughness of the net membranes can induce a turbulent flow on the feed channel reducing the boundary layer close to the membrane surface; this modification can lower the polarization effects that decrease the local driving forces of the process, enhancing the membrane performance [20].

4.3 Conclusions

The effect of the support morphology and composition on VMD membrane performance has been investigated. In particular, six different non-woven and three nets were used to prepare PVDF membranes via non-solvent induced phase separation technique.

The membranes prepared on the nets had deeply different structures. The less attachment of the dope solution to the support fibres during the phase separation process induced a higher shrinkage than the one observed on non-woven membranes. This phenomenon resulted in a decrease of the maximum pore size of the net membranes and in an increase of the liquid entry pressure. Moreover, the thin layer of polymer solution casted on the top of the crests of the net structure generated almost dense zones. These two effects combined resulted in a lower porosity of the net membranes compared to the non-woven ones.

The vacuum membrane distillation tests highlighted higher distillate fluxes for the membranes prepared with non-wovens in accordance with the porosity values measured.

During the membrane distillation tests using a concentrated NaCl solution (90g/L), the membranes prepared using on the nets delivered fluxes similar to that observed treating pure water. It is believed that this behaviour can be related to the improved turbulence induced by the net structure on the feed channel, decreasing the polarization effects.

Instead, the membranes prepared on the six non-wovens showed similar morphologies. The homogeneous random distribution of the fibres on the whole surface of the support provided more adhesion points for the polymer solution, preventing the shrinkage phenomenon and creating a more regular structure of the membranes.

These similar morphologies resulted in comparable performance during the distillation tests, treating both pure water and a 90 g/L NaCl solution for all the membranes casted on nonwovens.

References

[1] L. Eykens, K. De Sitter, C. Dotremont, L. Pinoy, B. Van der Bruggen, Membrane synthesis for membrane distillation: A review, Sep. Purif. Technol. 182 (2017) 36–51. doi:10.1016/j.seppur.2017.03.035.

[2] M.R. Bilad, E. Guillen-Burrieza, M.O. Mavukkandy, F.A. Al Marzooqi, H.A. Arafat, Shrinkage, defect and membrane distillation performance of composite PVDF membranes, Desalination. 376 (2015) 62–72. doi:10.1016/j.desal.2015.08.015.

[3] M. Khayet, T. Matsuura, Preparation and Characterization of Polyvinylidene Fluoride Membranes for Membrane Distillation, Ind. Eng. Chem. Res. 40 (2001) 5710–5718. doi:10.1021/ie010553y.

[4] D. Hou, H. Fan, Q. Jiang, J. Wang, X. Zhang, Preparation and characterization of PVDF flat-sheet membranes for direct contact membrane distillation, Sep. Purif. Technol. 135 (2014) 211–222. doi:10.1016/j.seppur.2014.08.023.

[5] Y. Yang, D. Rana, T. Matsuura, S. Zheng, C.Q. Lan, Criteria for the selection of a support material to fabricate coated membranes for a life support device, RSC Adv. 4 (2014) 38711–38717. doi:10.1039/C4RA04638B.

[6] A. Bottino, G. Capannelli, A. Comite, M. Oliveri, Development of novel membranes with controlled porosity from fluorinated polymer, Filtration. 4 (2004) 130–135.

[7] M. Haponska, A. Trojanowska, A. Nogalska, R. Jastrzab, T. Gumi, B. Tylkowski, PVDF membrane morphology - Influence of polymer molecularweight and preparation temperature, Polymers (Basel). 9 (2017) 1–14. doi:10.3390/polym9120718.

[8] M. Pagliero, A. Bottino, A. Comite, C. Costa, Novel hydrophobic PVDF membranes prepared by nonsolvent induced phase separation for membrane distillation, J. Memb. Sci. 596 (2020) 117575. doi:10.1016/j.memsci.2019.117575.

[9] I.N. Strain, Q. Wu, A.M. Pourrahimi, M.S. Hedenqvist, R.T. Olsson, R.L. Andersson, Electrospinning of recycled PET to generate tough mesomorphic fibre membranes for smoke filtration, J. Mater. Chem. A. 3 (2015) 1632–1640. doi:10.1039/C4TA06191H.

[10] A. Rjeb, L. Tajounte, M.C. El Idrissi, S. Letarte, A. Adnot, D. Roy, Y. Claire, A. Périchaud, J. Kaloustian, IR spectroscopy study of polypropylene natural aging, J. Appl. Polym. Sci. 77 (2000) 1742–1748. doi:10.1002/1097-4628(20000822)77:8<1742::AID-APP11>3.0.CO;2-T.

[11] L.A. Baldenegro-Perez, D. Navarro-Rodriguez, F.J. Medellin-Rodriguez, B. Hsiao, C.A. Avila-Orta, I. Sics, Molecular weight and crystallization temperature effects on

poly(ethylene terephthalate) (PET) homopolymers, an isothermal crystallization analysis, Polymers (Basel). 6 (2014) 583–600. doi:10.3390/polym6020583.

[12] T. Parenteau, G. Ausias, Y. Grohens, P. Pilvin, Structure, mechanical properties and modelling of polypropylene for different degrees of crystallinity, Polymer (Guildf). 53 (2012) 5873–5884. doi:10.1016/j.polymer.2012.09.053.

[13] J. Camacho, E. Díez, I. Díaz, G. Ovejero, Hansen solubility parameter: from polyethylene and poly(vinyl acetate) homopolymers to ethylene-vinyl acetate copolymers, Polym. Int. 66 (2017) 1013–1020. doi:10.1002/pi.5351.

[14] R. Auras, B. Harte, S. Selke, Sorption of ethyl acetate and d-limonene in poly(lactide) polymers, J. Sci. Food Agric. 86 (2006) 648–656. doi:10.1002/jsfa.2391.

[15] A. Bottino, G. Capannelli, S. Munari, A. Turturro, Solubility parameters of poly(vinylidene fluoride), J. Polym. Sci. Part B Polym. Phys. 26 (1988) 785–794. doi:10.1002/polb.1988.090260405.

[16] N. Vogrin, Č. Stropnik, V. Musil, M. Brumen, The wet phase separation: The effect of cast solution thickness on the appearance of macrovoids in the membrane forming ternary cellulose acetate/acetone/water system, J. Memb. Sci. 207 (2002) 139–141. doi:10.1016/S0376-7388(02)00119-9.

[17] D. Li, T.S. Chung, J. Ren, R. Wang, Thickness Dependence of Macrovoid Evolution in Wet Phase-Inversion Asymmetric Membranes, Ind. Eng. Chem. Res. 43 (2004) 1553–1556. doi:10.1021/ie034264g.

[18] A. Conesa, T. Gumí, C. Palet, Membrane thickness and preparation temperature as key parameters for controlling the macrovoid structure of chiral activated membranes (CAM), J. Memb. Sci. 287 (2007) 29–40. doi:10.1016/j.memsci.2006.10.006.

[19] L. Martínez-Díez, M.. Vázquez-González, Temperature and concentration polarization in membrane distillation of aqueous salt solutions, J. Memb. Sci. 156 (1999) 265–273. doi:10.1016/S0376-7388(98)00349-4.

[20] H. Roth, M. Alders, T. Luelf, S. Emonds, S.I. Mueller, M. Tepper, M. Wessling, Chemistry in a spinneret — Sinusoidal-shaped composite hollow fiber membranes, J. Memb. Sci. 585 (2019) 115–125. doi:10.1016/j.memsci.2019.05.029.

Chapter 5

5 Functionalization of ceramic membranes

Hydrophobic polymers are today the most studied and applied materials for developing MD membranes [1–3]. Although in most of the applications the feed temperature is lower compared to the traditional distillation processes, in some cases it might be required a temperature of the feed close to its boiling point or even higher for pressurized feeds [4]. However, with polymeric membranes the maximum temperature of the feed stream is limited by the physical properties of the material itself. The high temperature sensitivity typical of the polymeric membranes results in a reduction of their working life.

The development of hydrophobic ceramic membranes can extend the possible applications of MD to cases in which the operating conditions (e.g. temperature and pressure) prevent the use of polymeric membranes [5]. It has been pointed out that increasing the feed temperature allows to reach higher vapour flux through the membrane and higher thermal efficiency of the process [6,7]. Moreover a higher thermal stability allows the use of more severe cleaning conditions in order to recover permeability losses due to fouling phenomena [8] and in order to warrant a sterile environment in food industry.

Ceramic membranes are mainly prepared by sintering metal oxides such as alumina, zirconia and titania [9–11] and silicon based materials (e.g. SiAlON and yttrium silicate) [12,13]. However ceramic membranes are, by nature, intrinsically hydrophilic because of the presence of surface hydroxyl groups. Many techniques have been used to switch the membrane behaviour towards hydrophobicity such as grafting of alkylsilanes (AS) or fluoroalkylsilanes (FAS), [14–19] plasma modifications [20,21] and carbon derived materials deposition (e.g. carbon nanotubes) [22]. The main aim of these surface modifications is to increase the contact angle and thus the liquid entry pressure (LEP_w).

On the other hand, these treatments could affect the morphology of the pristine membranes since the grafted molecules can polymerize and create a thin layer that reduces the pore size or even closes some pores lowering the membrane porosity [15–17,23].

Even if the use of FAS allows to obtain membranes with great performances and high contact angles, in the last years concerns about their environmental sustainability increased and one of the most used fluoroalkylsilane (1H,1H,2H,2H-Perfluorooctyltriethoxysilane) has already been banned [24] in some country because of lung damage in mice [25].

In this work commercial tubular ceramic membranes made of alumina with different pore sizes were functionalized with methyltrichlorosilane (MTS) and the effect of this treatment on membrane morphology was evaluated. MTS was selected as an interesting candidate because it is

a far less harmful reagent than FAS and it has a very short hydrophobic chain, so it is expected to cause minimal alterations in pore size and geometry. The hydrophobicity of the treated membranes was also carefully assessed.

After the functionalization and characterization steps the performance in vacuum membrane distillation process was investigated in a lab plant by feeding either pure water or a high concentrated sodium chloride solution.

5.1 Materials and Methods

The characteristics of the tubular membranes used in this work are summarized in Table 5.1.

Table 5.1: Main characteristics (nominal values) of the tubular membranes employed in this work.

Commercial name	IKTS70	IKTS200	PP V8/2HF
Material	Al_2O_3	Al_2O_3	polypropylene
Supplier	Inocermic GmbH*	Inocermic GmbH*	Membrana GmbH
Pore size of selective layer [nm]	70	200	200
Internal diameter [mm]	7	7	5.5
External diameter [mm]	10	10	8.5
Selective inner layer	Al_2O_3	Al_2O_3	polypropylene

*now Fraunhofer IKTS, Germany

The inherently hydrophobic polypropylene membrane Accurel® PP V8/2HF, having internal and external diameter similar to the IKTS ceramic membranes and suitable pore size, was selected as a benchmark for performance comparison.

Ceramic membranes are usually characterized by a layered structure where, upon a highly porous support, various thinner layers of particles are deposed. Every successive layer is composed by smaller particles and has a lower pore size.

5.1.1 Functionalization

The ceramic membranes were treated with methyltrichlorosilane (MTS) in order to reduce the presence of surface hydroxyl groups by the grafting a hydrophobic substituent (see Figure 5.1A) [14,26].

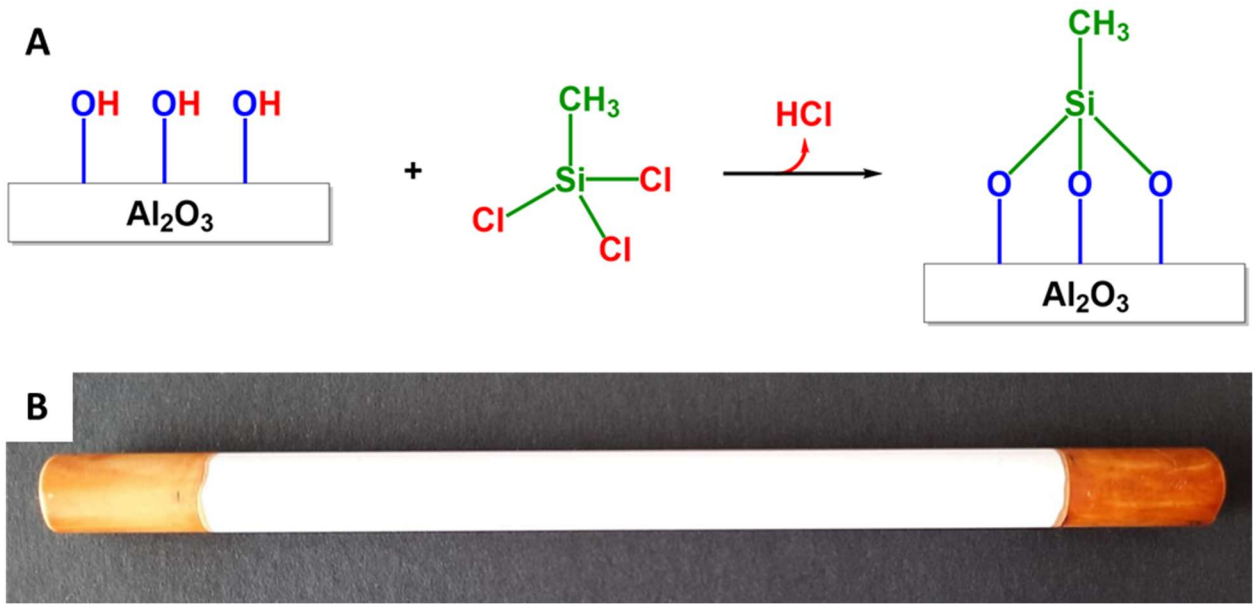

Figure 5.1: A) functionalization reaction scheme and B) ceramic membrane sample.

First of all, the ceramic tubes were cut in samples 15 cm long. In order to create an impermeable zone able to seal the gaskets needed for the characterizations, the two extremities were impregnated with an epoxy resin and non-porous surfaces were created for an extent of about 1.5 cm (Figure 5.1B).

The samples were dried at 100°C in an oven to remove every trace of humidity. Water can promote hydrolysis and condensation of the silanizing agent resulting in a bridging oxygen that links two silicon atoms. This mechanism could lead to the development of a final semicontinuous film with a consequent porosity drop. After been cooled down to room temperature, each sample was kept immersed for 24 hours in 30 mL of a solution of methyltrichlorosilane in ethyl acetate of predetermined concentration. The solution components were both supplied by Sigma-Aldrich. The immersion time was set after verifying that a more prolonged time did not produce further functionalization.

The functionalized samples were then withdrawn, washed with pure ethyl acetate and dried. Based on the concentration of the reactive solution two grades of functionalization were achieved. The two categories of related samples were identified by F1 (from 3.5% v/v MTS solution) and F2

(from 7.0% v/v MTS solution) tags. Higher concentrations of MTS were also tested, but the results are not included here because no improvement in the membrane performance was obtained.
For the Accurel® PP V8/2HF membrane the only modification consisted in coating the ends with a thick layer of epoxy resin to reach the external diameter necessary for housing in the VMD module.
In Table 5.2 the characteristics of the hydrophobized membranes selected for the tests are collected.

Table 5.2: Characteristics of the modified selected samples.

Sample name	Original membrane	Functionalization type	MTS concentration [% v/v]	Length [cm]	Surface [cm²]
70F1	IKTS70	F1	3.5	10.8	24
70F2	IKTS70	F2	7	11.8	26
200F1	IKTS200	F1	3.5	11.9	26
200F2	IKTS200	F2	7	9.2	20
200PP	PPV8/2HF	-	-	11.8	20

5.1.2 Characterization

Some small samples (2 cm long) of each membrane were prepared simultaneously together with the 15 cm long ones in order to investigate the morphology of the modified membranes and to evaluate the effect of the grafting reaction on the membrane surface. These small samples were then cut into smaller pieces to perform different analyses such as electron microscopy observations together with EDX analysis, FT-IR spectra, contact angle evaluation.
FE-SEM observations were carried out using a field emission scanning electron microscope ZEISS SUPRA 40VP. These analyses require specimen preparation. To this end the samples were properly broken and then covered with a carbon nanofilm in order to make them conductive.
On the basis of the results obtained from the EDX probe during FE-SEM observation, supported by the IR spectra previously registered on the same samples, it was possible to estimate the degree of functionalization. FT-IR analyses were performed on the internal (selective) surface of the treated membranes using a Bruker Vertex 70 FT-IR spectrometer in DRIFTS (Diffuse Reflectance for Infrared Fourier Transform Spectroscopy) mode. For every membrane, FE-SEM and FT-IR analyses were repeated in different locations.

The hydrophobic character of the membranes was evaluated by contact angle measurements using a Biolin Scientific Attension Theta optical tensiometer that automatically generated a 3µL water drop. After deposition of the drop on the membrane surface, the instrument camera recorded 15 photographs per second for a time of 10 seconds. For each sample, at least three different spots were analysed. For all the treated membranes, the contact angle remained constant for more than 10 seconds and no absorption in the porous structure took place. The reported data represent the mean value of all the 450 measurements.

In addition, contact angle measurements were also used to evaluate the thermal stability of the MTS-based layer. Some 200F1 samples were annealed for 1 hour in an oven at different temperatures (up to 600°C). Once cooled, the contact angle was measured for each sample.

The mean pore size of the selective layer for every membrane was estimated from gas permeation (GP) data in order to evaluate the effect of functionalization on the membrane morphology. Nitrogen permeation rates were determined using the system showed in Figure 5.2. Using a mass flow controller, a known flowrate of gas was sent inside the lumen of the membrane, located in a proper vessel, and forced to pass across the membrane walls. The inlet and trans-membrane pressures were measured using two digital manometers with adequate sensibilities. The trans-membrane gas flowrate was then measured at vessel exit connector, using a bubble flow meter.

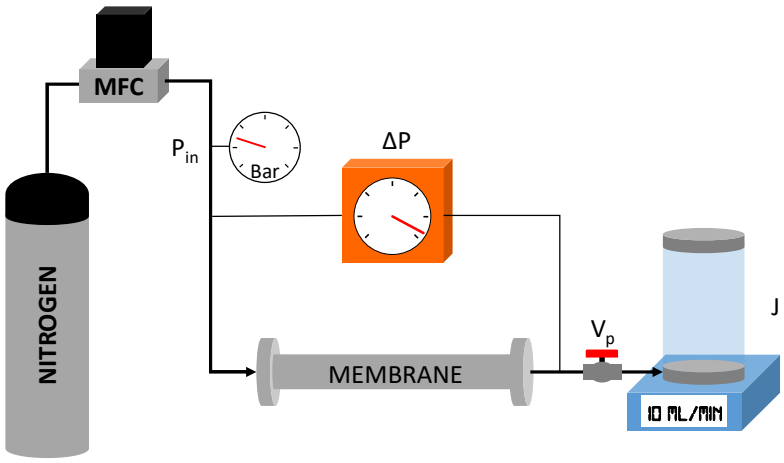

Figure 5.2: Experimental setup for gas permeation measurement. MFC: mass flow controller, Pin: inlet pressure gauge, ΔP: transmembrane pressure transducer, V_p: backpressure valve, J: bubble flow meter.

The mean pore size was estimated following the approach proposed by Beuscher and Gooding [27]. In particular, if only the Poiseuille and the Knudsen mechanism are assumed, the gas permeability K [cm^2/s] through the membrane depends on the average pressure across the membrane and on specific geometric properties of the porous structure. For single gas permeation,

the following equation shows that *K* can be obtained by the sum of two contributions: the first term accounts for viscous flow and the second term for Knudsen diffusion:

$$K = \frac{NRT}{\Delta P/\delta} = \frac{B_0}{\mu} \cdot P_{av} + \frac{4}{3} K_0 v_M \qquad 5.1$$

where *N* is the molar flux across the membrane [mol/cm^2 s]; *R* is the gas constant [J/K mol]; *T* is the temperature [K]; δ is the membrane thickness [cm]; ΔP is the pressure drop across the membrane [Pa]; $P_{av} = 1/2\left(P_{feed} + P_{permeate}\right)$ is the mean pressure across the membrane [Pa]; μ is the dynamic viscosity of the gas [g/cm s] and v_M is the mean molecular speed of the gas [cm/s]. The parameters B_0 and K_0 are defined as follows:

$$B_0 = \frac{\varepsilon}{\tau^2} \frac{r^2}{k_0} \qquad 5.2$$

$$K_0 = \frac{\varepsilon}{\tau^2} \frac{\beta r}{k_l} \qquad 5.3$$

where *r* is the mean pore size; ε is the porosity; τ *is the* tortuosity; k_0 and k_1/β are shape factors. *K* may be plotted against P_{av} to obtain B_0 and K_0 from the slope and intercept of a straight line. Finally, setting $\beta k_0/k_1 = 2$, [27] *r* can be evaluated by the ratio:

$$r = \frac{2B_0}{K_0} \qquad 5.4$$

the membrane porosity (ε%) was measured gravimetrically. A small sample of the membrane was put in an oven at 100°C until it reached a constant weight and was subsequently impregnated with 1-octanol. Weighting again the sample, the total porosity was calculated using the following equation:

$$\varepsilon\% = \frac{V_{empty}}{V_{tot}} \cdot 100 = \frac{\frac{(m_w - m_d)}{\rho_{oc}}}{\frac{m_d}{\rho_{Al}} + \frac{(m_w - m_d)}{\rho_{oc}}} \cdot 100 \qquad 5.5$$

where V_{empty} is the total pore volume, V_{tot} is the total volume of the sample, m_w and m_d are the masses of impregnated and dry membrane, respectively, ρ_{oc} is the 1-octanol density (0.83 g/cm^3) and ρ_{Al} is the density of alumina (3.99 g/cm^3) at 25°C. The procedure was repeated three times for each sample.

Gas liquid displacement porometry (GLDP) is a technique that allows evaluating both the mean pore size and the pore size distribution, which are two main parameters in membrane applications. The membrane was wetted with a suitable liquid and then a gas pressure was applied to the feed side in order to progressively replace the liquid in the pores with the gas (refer to Jakobs and Koros

[28]). The correlation between the pore size and the applied pressure is given by the Laplace equation:

$$r_i = \frac{2 \cdot \gamma_l}{P_i} cos\vartheta \qquad 5.6$$

where γ_l is the liquid surface tension at the working temperature, θ is the liquid-membrane contact angle, r_i is the pore size and P_i is the applied pressure.

Since the tested membranes had small pores, a low surface tension gas-liquid system had to be chosen. The membranes were soaked in a commercial fully fluorinated liquid (3M fluorinert® FC-77) and the gas used was air. At ambient temperature the surface tension of this system is 13 mN/m and the contact angle is supposed to be 0.

5.1.3 Performance evaluation

The performances of the membranes in MD application were tested adapting the vacuum membrane distillation setup used for flat sheet membranes, as schematized in Figure 5.3:

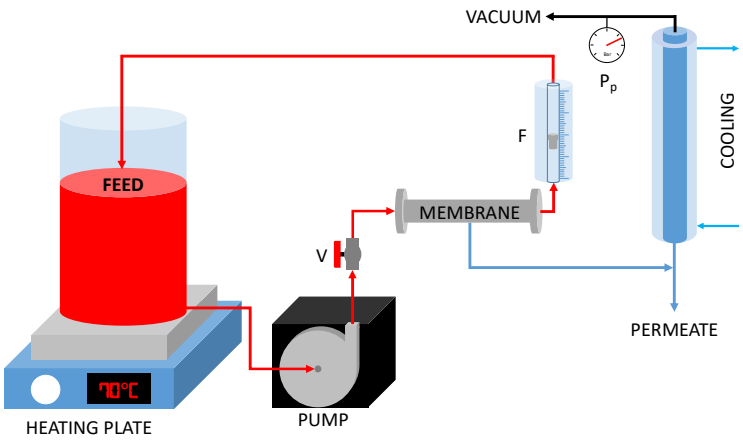

Figure 5.3: VMD experimental setup. F: concentrate flowmeter, V: feed valve, P_p: vacuum meter.

The tubular membrane was housed in a cylindrical glass vessel and mounted in the experimental setup using silicone rubber pipes. Since all the tested membranes had the selective layer on the inner side, the liquid was sent into the membrane lumen and vacuum was applied to the membrane outer surface.

A glass tank containing 2 L of feed was put on a heating plate and connected to a centrifugal pump. Using a flow meter, the feed flux was monitored and a constant feed velocity (1.4 m/s) inside the membrane cell was set using a valve. In order to maintain constant the feed concentration, the concentrate stream was continuously recirculated to the feed tank and the condensed permeate was added again to the tank after every flux measurement (10 minutes).

In VMD the driving force is produced by applying vacuum at the permeate side of the membrane. A water pump was used to reach the desired vacuum grade and a digital vacuum-meter was used to monitor the pressure at the permeate side (20 mbar). Since the applied vacuum pressure is lower than the equilibrium vapour pressure, no condensation occurs into the membrane module. The stream of vapour extracted from the module was condensed downstream with glass condensers connected to a refrigerator set at 0.1 °C. The permeate flow through the membrane was evaluated by measuring the liquid permeate volume collected in a fixed time interval (10 minutes).

Since NaCl was the only solute possibly present in the treated solution, it was possible to directly relate its concentration with the electrical conductivity of the solution, therefore, the separation efficiency of the membranes was determined by measuring the electrical conductivity σ of the permeate and calculating the salt rejection *R%* with the expression:

$$R\% = \frac{\sigma_f - \sigma_d}{\sigma_f} \cdot 100 \qquad 5.7$$

where σ_f and σ_d are the electrical conductivity [µS/cm] of the feed and the distillate, respectively. For each membrane sample two feeds (deionized water and NaCl solution 90 g/L), and three feed temperatures (50, 70 and 90°C) were tested, while feed concentration and velocity, membrane active surface (20 – 26 cm^2) and vacuum grade (20 mbar) were kept constant.

5.2 Results and Discussion

5.2.1 Untreated membrane structure

Membranes with pore sizes ranging from 10 to l000 nm can be used in MD [29]. The permeate flux increases with the increase in pore size, however larger pores can foster membrane wettability. The molar permeate flux *N* is related to the membrane structural parameters by the simplified expression [30]:

$$N \propto \frac{2r^{\alpha}\varepsilon}{\tau\delta} \qquad 5.8$$

where *r* is the average pore size ($\alpha = 0$ for pure diffusion, $\alpha = 1$ for Knudsen diffusion, $\alpha = 2$ for viscous flux); ε is the membrane porosity; τ is the membrane tortuosity and δ is the membrane thickness. Knowledge of these critical parameters is essential to explain or predict the membrane performance. In this work particular attention was paid to possible plugging or size reduction phenomena in pore lumen after the silanizing treatment.

The porosity ε is generally considered as the most important morphological parameter in MD. Indeed, if the common approximation $\tau \approx 1/\varepsilon$ [31] is adopted, equation 5.8 becomes:

$$N \propto \frac{2r^{\alpha}\varepsilon^{2}}{\delta} \qquad 5.9$$

and the molar flux depends quadratically on the porosity. The measured values for the ceramic membranes tested are reported in Table 5.3. The differences are small since the main contribute to ε derives from the supports, which should be very similar.

In tubular ceramic membranes, the majority of the flow resistance, proportional to the transport path length, $\tau\delta$, and decreasing with r and ε, is located in the separation layer. These membranes usually have an asymmetric structure composed of stacked layers of different pore size. In general, the macro-porous support is a few millimetres in thickness and has a pore size in the range 1–10 μm, the intermediate layer has a thickness in the range of 10–100 μm and pore size of 50–500 nm and the top layer has a smaller thickness and pore size [32].

In this work, the tubular ceramic membranes were all based on an alumina macro-porous support. The layered structure was investigated by FE-SEM observations of the membrane cross section in different zones. The IKTS70 membrane (Figure 5.4A) was constituted of an alumina macroporous tube (thickness of 1.5 mm, not entirely visible in the micrograph) supporting, on the inner side, two less porous layers, each about 20 μm thick, containing finer alumina particles. The IKTS200 membrane (Figure 5.4B) was composed of the macroporous alumina tube supporting again two different inner layers (each nearly 40 μm thick) with decreasing porosity and pore size.

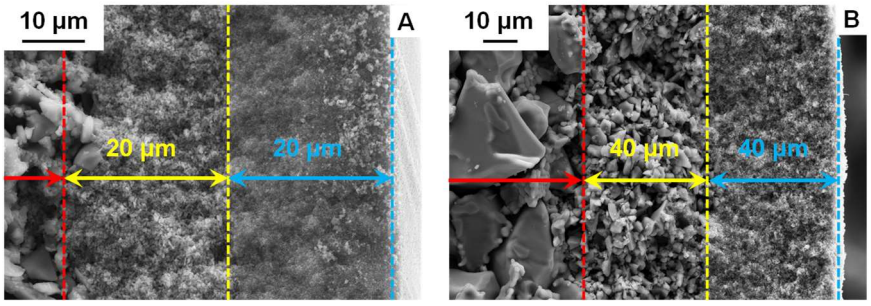

Figure 5.4: FE-SEM images of the layered structure of the IKTS70 (A) and IKTS200 (B) membranes.

In short, the two membranes have an identical macroporous support 1.5 mm thick, and all the differences reside exclusively in the internal very thin layers, varying in thickness, particle and pore size. The overall thickness of the two inner layer is 40 μm for the IKTS70 and 80 μm for the IKTS200.

Table 5.3 collects the different values (with the associated standard deviation) for the mean particle diameter in the two thinner internal layers of the membranes. These values were obtained by counting 200 particles in each layer on micrographs at high magnification. The IKTS200 membrane showed a remarkable degree of polydispersity even in the selective layer.

Table 5.3: Mean particle diameter (dp) in the intermediate and selective layers and total porosity for the IKTS70 and IKTS200 membranes.

Membrane	Layer	Particle size [nm]	Porosity [%]
IKTS70	Intermediate	334±64	29.3±0.6
	Selective	109±35	
IKTS200	Intermediate	2072±955	31.1±0.7
	Selective	318±150	

The mean pore size was assessed with gas permeation measurements using nitrogen in the gas permeation apparatus described in Section 2.2. Adopting the model proposed by Beuscher and Gooding [27] the calculated values were 66±10 nm and 190±43 nm for IKTS70 and IKTS200 respectively. For every membrane type, each measurement was repeated 10 times on different samples, and the SD is reported in addition to the mean pore size value. The measured values are in satisfactory agreement with the data reported by the manufacturer.

Some conjecture can be made on the relationship between pore size and particle size following simple geometrical models [33]. Ideal three-dimensional close-packings of equal spheres of radius *R* can form hexagonal or cubic close packed structures, where each sphere is surrounded by 12 spheres and the empty space (i.e. porosity) is 26%. There are two kinds of voids: tetrahedral or octahedral voids. The radius of a sphere that would just fit into a void is given by 0.225 R in the first case and by 0.414 R in the second case.

The real case under consideration is obviously more complex. The packing will be not so regular and undoubtedly it will be looser, so a greater multiplication factor for *R* can be expected. Moreover, if the particles are nonspherical and if a certain degree of polydispersity is appreciable the identification of "pore size" becomes a very complex issue. A random packing of uniform spheres results in different values of porosity depending on the looseness and organization of the spheres. Porosities from 0.30 to 0.35 are common [34]. Based on the measured values of the porosity (Table 5.3), the membranes considered seem fall within this category. From the data presented in Table 5.3 it is reasonable to suppose that for the IKTS200 membrane the main resistance to the permeate flux is offered by the selective layer. In this case the following very raw empirical relation between mean particle size d_p and mean pore size *r* can be inferred:

$$2r \approx 0.6\, d_p \qquad 5.10$$

It turns out that equation 5.10 holds for the selective layer of IKTS70 membrane too, i.e. for both membranes $2r/d_p \approx 0.6$.

Finally, an important evidence has to be mentioned. All the ceramic membranes examined displayed a certain degree of defectiveness, as shown in Figure 5.5 for an IKTS70 sample (selective layer).

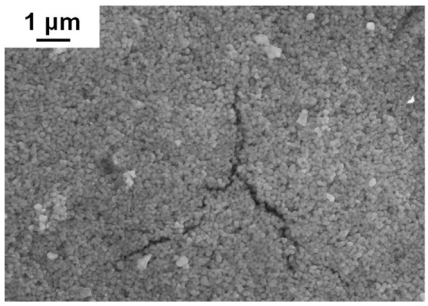

Figure 5.5: FE-SEM image of a chink on the selective layer of an IKTS70 membrane.

The presence of even a single defect can cause a disastrous decline of the membrane performance, so production of defect-free ceramic membranes is a very critical issue.

With regard to the polypropylene membrane Accurel® PP V8/2HF used as a benchmark, it had a thickness of 1500 µm, a nominal pore size of 200 nm, and a measured porosity of 74±0.7%. A FE-SEM micrograph showing the morphology is reported in Figure 5.6.

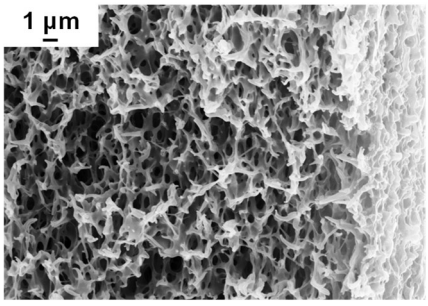

Figure 5.6: FE-SEM images of the cross-section (not entirely visible) of the Accurel® PP V8/2HF membrane.

5.2.2 Effects of functionalization

The success of the MTS grafting reaction was verified by using both FT-IR and EDX spectroscopy. FT-IR spectra carried out on the selective surface of the various membranes confirmed the presence of Si-CH_3 groups after treatment as shown in Figure 5.7 (IKTS70) and in Figure 5.8 (IKTS200). Here U relates to the unfunctionalized membrane, F1 and F2 distinguish the two

treatments with 3.5% v/v MTS and 7.0% v/v MTS respectively. The spectra have been stacked, therefore the peak intensity is in arbitrary units (a. u.).

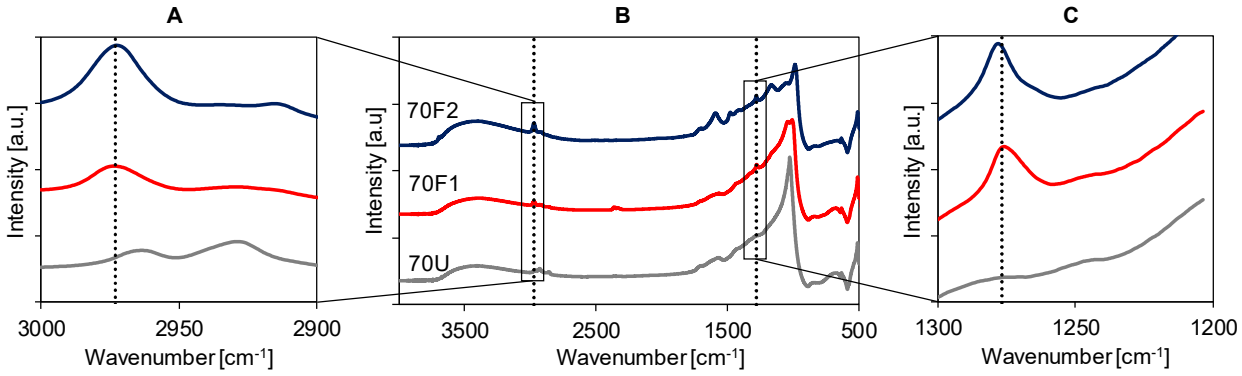

Figure 5.7: FT-IR spectra of untreated (70U), and treated (70F1 and 70F2) IKTS70 membrane, performed on the alumina selective layer.

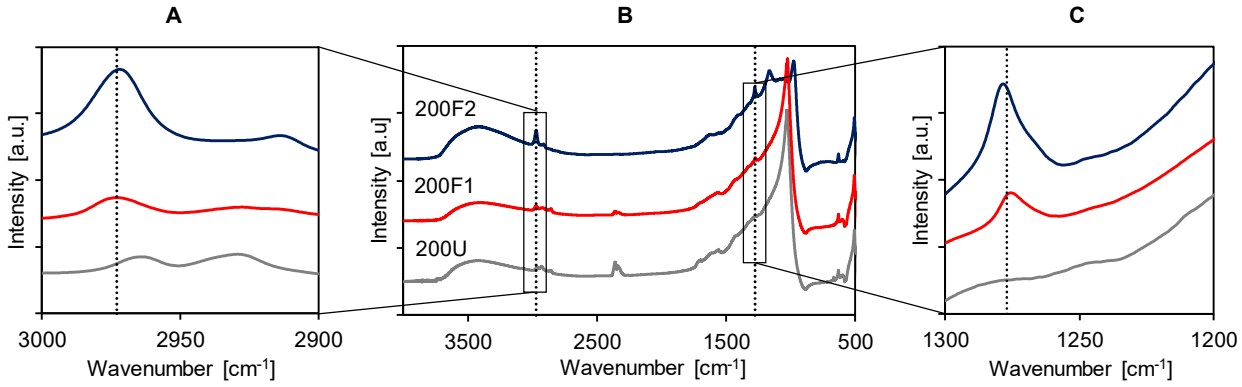

Figure 5.8: FT-IR spectra of untreated (200U), and treated (200F1 and 200F2) IKTS200 membrane, performed on the alumina selective layer.

On the spectra of the treated samples the peak at around 2975 cm^{-1}related to the C-H stretching is distinguishable and its intensity increases from the F1 to the F2 samples as it can be better perceived in Figure 5.7A and 5.8A. Moreover, at around 1275 cm^{-1}, on the spectra of the samples treated with methyltrichlorosilane a small peak appeared (enlarged in Figure 5.7C and 5.8C) related to the Si–C band of the methylsilane [26]. In literature, vibrations of the Al-O and Si-O bonds are also reported in the range 950–1150 cm^{-1} [35,36] but owing multiple overlaps it is difficult to perform the exact assignations.

The EDX spectroscopy provided a more quantitative evaluation of the amount and the distribution of MTS on the membrane selective surface. Table 5.4 reports the concentration of silicon on the different samples. For each membrane ten spot were explored and the mean value is reported together with the standard deviation.

Table 5.4: Silicon atomic percentage in the selective layer of the functionalized membranes.

Sample	Si [atomic%]
70F1	5.0±0.3
70F2	7.6±0.5
200F1	0.3±0.1
200F2	0.7±0.2

The amount of silicon found on the selective layer of the treated membranes increases as the functionalizing solution concentration increases, moving from F1 to F2 samples. The effect of the size of the particles present in the selective layer seems also detectable. In fact, the membranes with smaller pore size are characterized by smaller particles in the selective layer (see Table 5.3) and then by a higher specific area available for MTS grafting.

These data provide a raw assessment of the amount of silicon deposited on the surface but give no information about its distribution. EDX mapping of silicon was then performed on different areas of the selective layer for all the membranes. Figure 5.9 shows, as a representative result, the Si map of the 70F2 sample.

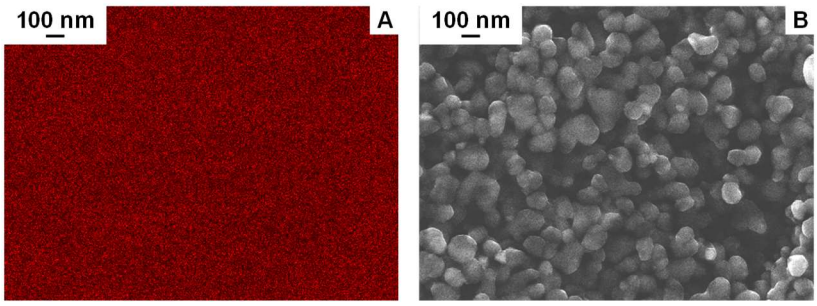

Figure 5.9: EDS silicon map on the 70F2 (A) membrane selective layer. B shows the related morphology.

In all cases the silicon distribution was uniform on all the surface and should assure a good grade of hydrophobicity.

In addition to EDX microanalyses, FE-SEM morphological observations were performed on the internal selective layer of every sample in order to investigate possible effects of the MTS grafting on morphology and pore size. In Figure 5.10 the three samples of IKTS70 and IKTS200 membranes before and after functionalization are shown.

As the MTS concentration in the reaction solution increased (left to right in Figure 5.10) the silanization degree also increased, as demonstrated in Figure 5.7 and 5.8 and in Table 5.4 above. However, using the secondary electron signal, it was not possible to reveal any evident difference

in the membrane morphology related to the grafting reaction. Indeed, the thickness of the silicon-based hydrophobic layer should be at least three orders of magnitude lower than the particle size, so it turns to be non-detectable even at high magnification.

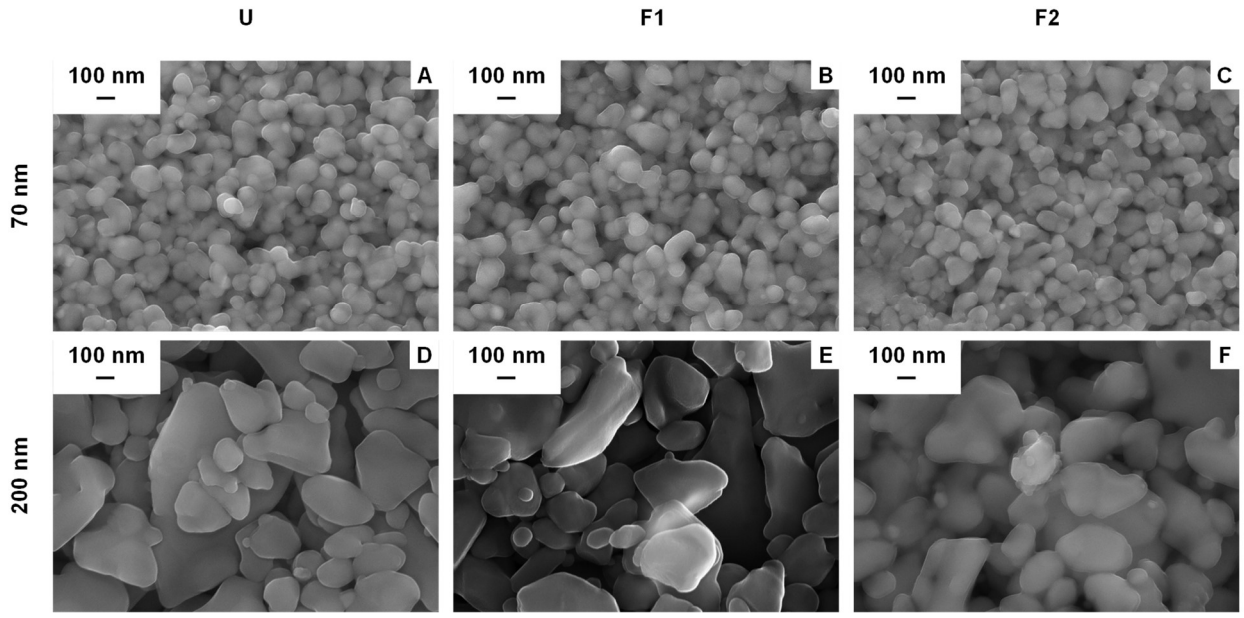

Figure 5.10: FE-SEM images of the selective surface of untreated (U), F1 and F2 samples for every type of ceramic membrane.

The effect of MTS on pore size was further investigated with gas permeation (GP) measurements using nitrogen in the apparatus described in Paragraph 5.1.2.

The mean pore sizes obtained using the model proposed by Beuscher and Gooding [27] are summarized in Table 5.5. For every sample, each measurement was repeated 10 times on different membranes, and the SD is reported in addition to the mean pore size value.

Table 5.5: Calculated mean pore size using GP measurements with Nitrogen

Sample	Mean pore size GP [nm]
70U	66±10
70F1	69±22
70F2	70±19
200U	190±43
200F1	180±86
200F2	188±72

The pore size values obtained using nitrogen as permeating gas fit well with the nominal values and demonstrate that the effect of MTS on the pore size is negligible, as expected and desired.

The GLDP measurements allowed to evaluate the pore size distribution of the treated membranes. The results are reported in Figure 5.11.

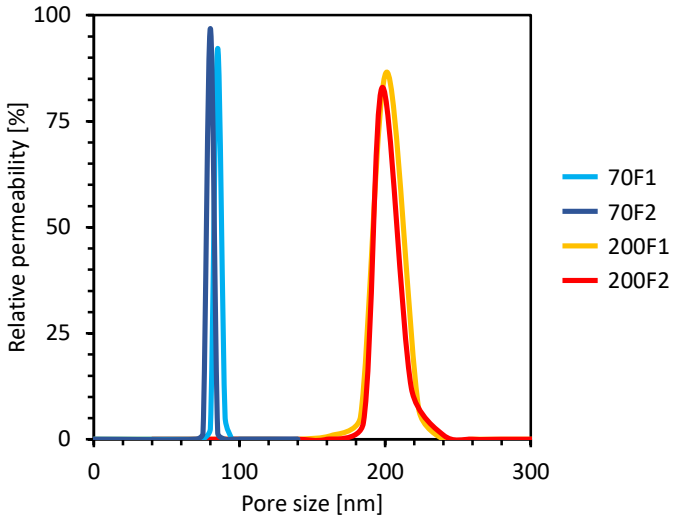

Figure 5.11: Pore size distribution of the functionalized membranes.

The tested membranes were characterized by a narrow pore size distribution, and these results are in good accordance with the mean pore size calculated on the basis of the GP measurements. In fact, the treatment with the MTS had only a minimal impact on the pore size distribution as well as on the mean pore size of the membranes.

The switch from a hydrophilic to a hydrophobic behaviour of the membrane due to the grafting reaction can be easily revealed by contact angle measurements.

The untreated membranes were fully hydrophilic and the water drops were rapidly absorbed by the porous material. Instead, after the treatment, it was possible to measure a stable contact angle both on the internal and external surfaces. The results are reported in Table 5.6.

Table 5.6: Measured contact angle and LEP_w of the functionalized membranes.

Sample	Internal contact angle [°]	External contact angle [°]	LEP_w [bar]
70F1	114 ± 1	126 ± 4	0.7
70F2	128 ± 3	113 ± 5	1.7
200F1	120 ± 4	109 ± 4	1.5
200F2	145 ± 1	122 ± 2	2.1

The data show that the treatment with methyltrichlorosilane turned to hydrophobic for all the samples and that the contact angles raised up to 145° (200F2 sample). Moreover, the F2 samples exhibit higher contact angles then the corresponding F1. Accordingly with these data, also the

water entry pressure was improved by increasing the functionalizing agent concentration and reached values that allowed to exploit these membranes for distillation process.

The thermal stability of the silanizing treatment was investigated using contact angle measurement after thermal annealing of some samples at high temperatures for 1 hour. The data were collected after cooling at ambient temperature. The results for eight samples of 200F1 membrane specifically prepared are reported in Figure 5.12.

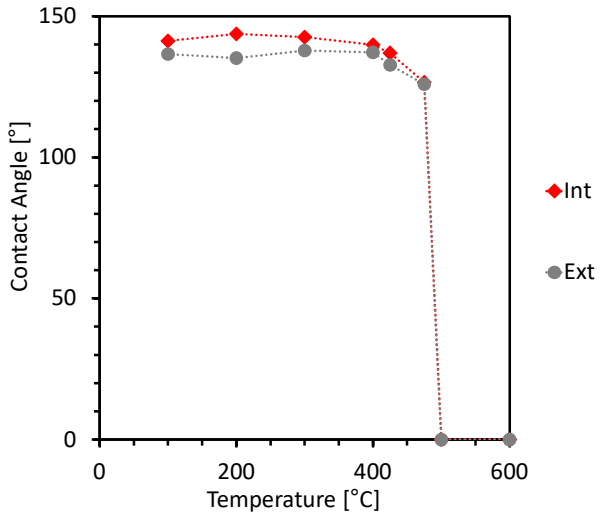

Figure 5.12: Contact angle of thermally treated samples of 200F1.

Both the internal and the external mean contact angles remained almost unchanged until 400°C, then the values started to decrease and suddenly dropped to zero at 500°C. This latter temperature is in accordance with the methyltrichlorosilane auto ignition temperature (490°C) found in the international chemical safety card of the compound. It is clear that the silanizing agent was completely destroyed at these severe conditions.

The high thermal stability of the hydrophobic treatment suggests the applicability of these membranes in membrane contactor-based processes where high temperatures (and possibly high operating pressures) might be important.

5.2.3 Performance investigation

Two different feeds were tested in order to evaluate the performance of the membranes in a vacuum membrane distillation process: deionized water and a NaCl 90 g/L solution.
The results are reported in Figure 5.13 and Figure 5.14 respectively.

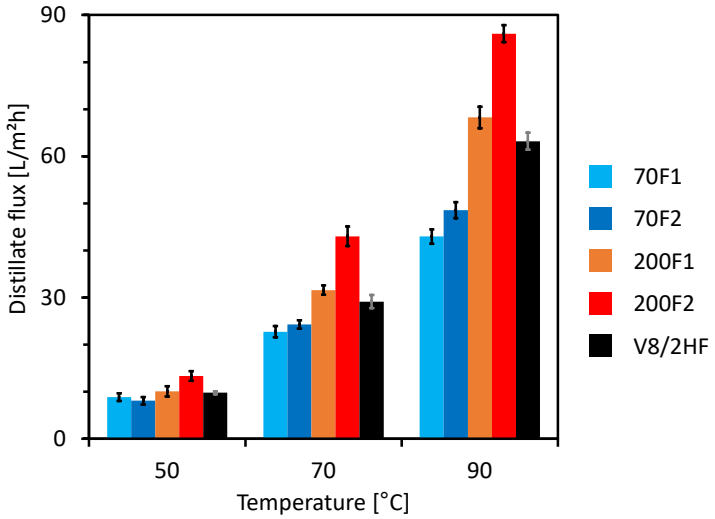

Figure 5.13: Mean distillate flux obtained with the prepared membranes using deionized water as feed at 50, 70 and 90°C.

It is well known that in all MD configurations there is an exponential increase of the water flux with the increase of the feed temperature. This is due to the exponential increase of the water vapor pressure in the feed, which increases the driving force of the process [29].
Figure 5.13 shows the mean distillate flux registered during the tests with deionized water as feed of the plant. In this case, owing to the absence of the solute which affects the mass transfer process, relationships between the water flux and the membrane morphology can be explored.
The Knudsen number $Kn = \lambda/2r$, where λ is the mean free path of a water molecule, was in all the conditions examined >> 1, therefore the main contribute to the flux comes from the Knudsen diffusion. This assumption is in agreement not only with the traditional models assuming independent cylindrical pores but also with a more complex membrane representation including interconnections between pores and using Monte Carlo (MC) simulation model [37] and equation 5.8 becomes

$$N \propto \frac{2r\varepsilon^2}{l} \propto \frac{d_p\varepsilon^2}{l} \qquad 5.11$$

Recalling the results reported in Figure 5.4 and in Table 5.3, the resistances offered by the selective and intermediate layers can be roughly estimated and compared with the experimental results. It

is supposed that the macroporous support makes a negligible contribution to the overall resistance. It is also supposed that the proportionality constant between r and d_p (equation 5.10) is the same for the selective and the intermediate layer. Table 5.7 summarizes these assessments.

Table 5.7: Mass transfer resistance in the intermediate and selective layers for the IKTS70 and IKTS200 functionalized membranes.

	70F1		200F1	
	intermediate layer	selective layer	intermediate layer	selective layer
2r [nm]	210±52	69±22	1235±130	180±86
% of resistance	25	75	13	87
70/200 resistance ratio calc.	1.69			
70/200 resistance ratio exp.	1.59 @ 50°C, 1.58 @ 70°C, 1.66 @ 90°C			
	70F2		200F2	
	intermediate layer	selective layer	intermediate layer	selective layer
2r [nm]	190±48	70±19	1308±180	188±72
% of resistance	27	73	13	87
70/200 resistance ratio calc.	1.73			
70/200 resistance ratio exp.	1.65 @ 50°C, 1.69 @ 70°C, 1.77 @ 90°C			

It can be observed that in the IKTS200 functionalized membranes the intermediate layer makes a little contribution to the overall mass transfer resistance, whereas this contribution becomes more pronounced for the 70F1 and 70F2 samples. In any case, the major part of the resistance is located in the selective layer. The IKTS70 functionalized membranes exhibit a greater overall resistance, having smaller pores in the selective and intermediate layer. The calculated ratio 70/200 resistance shows a good fit with the ratio between the fluxes of 200 and 70 samples experimentally measured. From Figure 5.13, the following trends can be extracted on the membrane performance: 200 > 70 and F2 > F1. The maximum flux was reached using the 200F2 sample, which largely overcome that of the benchmark polypropylene membrane, although the latter one is more hydrophobic and more porous.

These results demonstrate in detail that the functionalization procedure proved to be successful but without an influence on the membrane morphology. The membrane resistance remained

unchanged even when the particle and pore sizes were quite small and no sign of pore plugging was detected.

When non-volatile ionic solutes are present, a decrease in the permeate flux is always observed, as these solutes reduce the partial vapor pressure of the feed and consequently reduce the driving force for the VMD process. Furthermore, a contribution from the concentration polarization can also be expected. These effects increase with the salt concentration and can be well appreciated observing the results shown in Figure 5.14, which reports the mean distillate flux measured during the tests with a NaCl solution at high concentration, 90 g/L, as feed.

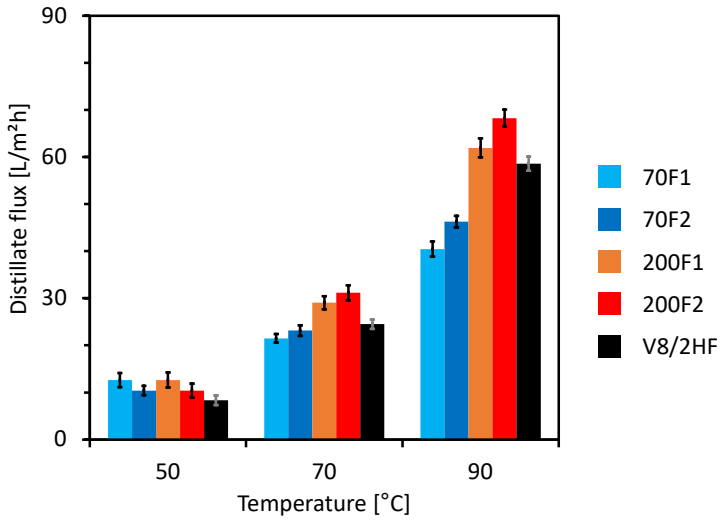

Figure 5.14: Mean distillate flux obtained with the tested membranes using a NaCl 90 g/L solution as feed at 50, 70 and 90°C.

The effect of the feed temperature is again clearly detectable. The trends 200 > 70 and F2 > F1 are maintained but are less evident, especially at lower temperatures. The superiority of the 200F2 sample over all the other membranes, included the polymeric one, is confirmed. This sample displays an excellent performance also when compared with various literature data (see Table 5.8). The separation properties were also evaluated during the NaCl solution tests and were close to the full rejection of salt (*R% > 99.9%*) for all the samples in any operation condition. Table 5.8 reports the results found in literature concerning various modified ceramic membrane used in VMD tests. Solution concentration ranges between 0.5 and 6 w% while in this work a higher concentration (9%) was used

Table 5.8: Performance of various ceramic membranes in VMD tests with NaCl solutions.

Membrane	Geometry	Thickness [μm]	Pore size [μm]	Porosity [%]	LEP_w [bar]	Feed temperature [°C]	Vacuum grade [mbar]	Feed solution [NaCl w%]	Distillate flux [L/m^2h]	Ref.
Silicon nitride	Hollow fiber	500	0.74	50	3.4	70	20	2 4	25 22	[39]
Silicon nitride	Hollow fiber	200-400	0.74	40-60	3.2	70	20	0.5 2 4 6	9.6 8.8 7.9 6.3	[40]
SiAlON	Hollow fiber	250	0.8	48	3.1	70	20	2 4	8.8 7.9	[12]
Alumina - FAS	Hollow fibre	200	0.7	43	1.5	70	40	4	30	[41]
Alumina	Flat Sheet	2400	0.4	31	1.1	70	30	3.5	29	[23]
Alumina - FAS	Hollow fibre	250	0.22	55	2.5	70	30	3.5	60	[42]
Alumina - C16	Tubular	2000	0.15	36	2.5	70	50	3	30	[14]
70F1 70F2 200F1 200F2	Tubular	1500	0.07 0.07 0.2 0.2	29 29 31 31	0.7 1.7 1.5 2.1	70	20	9	21.5 23.1 29.1 31.2	This work

The membranes tested in this work are generally characterized by smaller pores compared to those found in literature. As a matter of fact, data for ceramic membranes with pore size below 0.15µm were not found in VMD applications. Moreover, the porosity of the IKTS membranes is in general lower if compared with the other values reported in Table 5.8. In spite of these seeming unfavourable characteristics the 200F2 membrane reached outstanding performances, as seen in Figure 5.15 where different membranes treating a 4% NaCl solution at 70°C are compared. A dedicated test at this feed concentration was expressly carried out with the 200F2 sample.

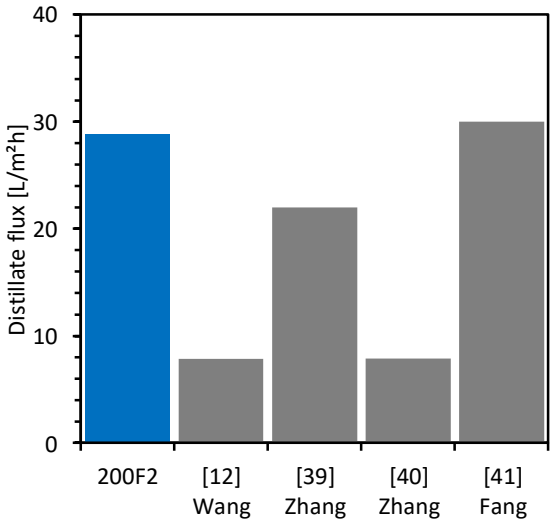

Figure 5.15: Mean permeate fluxes of the 200F2 membrane in comparison with data found in literature for NaCl 4% solution treatment at 70°C.

In conclusion, the prepared membranes seem to be applicable for the treatment of highly concentrated aqueous solutions of salts. In general, the effect of salt crystallization in desalination by VMD should be modest and reversible. It was demonstrated that this phenomenon only occurs on the membrane surface and that the crystals are easily removed by washing with water [38].

5.3 Conclusions

Hydrophobic ceramic membranes were obtained by functionalization with methyltrichlorosilane of commercial alumina tubular porous supports. These membranes showed a high thermal stability of the hydrophobic character even after heat treatments up to 400°C and this result is interesting since it can extend the application of MD to high temperature processes.

Spectroscopic analysis (FT-IR and EDS) showed that the precursor reacted with the hydroxyl groups of the alumina both on the surface of the membrane and throughout the cross section; moreover, the functionalization grade was higher for a higher concentration of MTS in the reacting solution.

Contact angle and water entry pressure values were highly enhanced by increasing the functionalization grade.

FE-SEM morphological observations and related data treatment proved that the mean pore size in the selective and intermediate layers is not affected by the grafting of the silanizing agent. This result was also confirmed by gas permeation tests.

Finally, the membrane performance was assessed in a VMD laboratory plant with both deionized water and a concentrated sodium chloride solution as feeds. The distillate flux increased with pore size and functionalization degree and reached the maximum value for the sample 200F2 (mean pore size in the selective layer = 200 nm, selective layer thickness 40 μm, total thickness = 1.5 mm, porosity % = 31, higher functionalization degree). Moreover, this sample presented an excellent performance in comparison with other ceramic hydrophobized membranes present in the literature.

References

[1] S. Adnan, M. Hoang, H. Wang, Z. Xie, Commercial PTFE membranes for membrane distillation application: Effect of microstructure and support material, Desalination. 284 (2012) 297–308. doi:10.1016/j.desal.2011.09.015.

[2] M. Pagliero, A. Bottino, A. Comite, C. Costa, Novel hydrophobic PVDF membranes prepared by nonsolvent induced phase separation for membrane distillation, J. Memb. Sci. 596 (2020) 117575. doi:10.1016/j.memsci.2019.117575.

[3] K.Y. Wang, T.S. Chung, M. Gryta, Hydrophobic PVDF hollow fiber membranes with narrow pore size distribution and ultra-thin skin for the fresh water production through membrane distillation, Chem. Eng. Sci. 63 (2008) 2587–2594. doi:10.1016/j.ces.2008.02.020.

[4] D. Singh, K.K. Sirkar, High temperature direct contact membrane distillation based desalination using PTFE hollow fibers, Chem. Eng. Sci. 116 (2014) 824–833. doi:10.1016/J.CES.2014.05.042.

[5] Y. Yang, Q. Liu, H. Wang, F. Ding, G. Jin, C. Li, H. Meng, Superhydrophobic modification of ceramic membranes for vacuum membrane distillation, Chinese J. Chem. Eng. 25 (2017) 1395–1401. doi:10.1016/j.cjche.2017.05.003.

[6] A.M. Alklaibi, N. Lior, Membrane-distillation desalination: Status and potential, Desalination. 171 (2004) 111–131. doi:10.1016/j.desal.2004.03.024.

[7] A. Luo, N. Lior, Study of advancement to higher temperature membrane distillation, Desalination. 419 (2017) 88–100. doi:10.1016/j.desal.2017.05.020.

[8] J. Kujawa, S. Cerneaux, S. Koter, W. Kujawski, Highly efficient hydrophobic titania ceramic membranes for water desalination, ACS Appl. Mater. Interfaces. 6 (2014) 14223–14230. doi:10.1021/am5035297.

[9] P. Wang, T.S. Chung, Recent advances in membrane distillation processes: Membrane development, configuration design and application exploring, J. Memb. Sci. 474 (2015) 39–56. doi:10.1016/j.memsci.2014.09.016.

[10] E. Drioli, A. Ali, F. Macedonio, Membrane distillation: Recent developments and perspectives, Desalination. 356 (2015) 56–84. doi:10.1016/j.desal.2014.10.028.

[11] S. Cerneaux, I. Struzyńska, W.M. Kujawski, M. Persin, A. Larbot, Comparison of various membrane distillation methods for desalination using hydrophobic ceramic membranes, J. Memb. Sci. 337 (2009) 55–60. doi:10.1016/j.memsci.2009.03.025.

[12] J.W. Wang, L. Li, J.W. Zhang, X. Xu, C.S. Chen, β-Sialon ceramic hollow fiber membranes

with high strength and low thermal conductivity for membrane distillation, J. Eur. Ceram. Soc. 36 (2016) 59–65. doi:10.1016/j.jeurceramsoc.2015.09.027.

[13] M.Y. Yang, J.W. Wang, L. Li, B. Bin Dong, X. Xin, S. Agathopoulos, Fabrication of low thermal conductivity yttrium silicate ceramic flat membrane for membrane distillation, J. Eur. Ceram. Soc. 39 (2018) 442–448. doi:10.1016/j.jeurceramsoc.2018.09.028.

[14] X. Chen, X. Gao, K. Fu, M. Qiu, F. Xiong, D. Ding, Z. Cui, Z. Wang, Y. Fan, E. Drioli, Tubular hydrophobic ceramic membrane with asymmetric structure for water desalination via vacuum membrane distillation process, Desalination. 443 (2018) 212–220. doi:10.1016/j.desal.2018.05.027.

[15] Z.D. Hendren, J. Brant, M.R. Wiesner, Surface modification of nanostructured ceramic membranes for direct contact membrane distillation, J. Memb. Sci. 331 (2009) 1–10. doi:10.1016/J.MEMSCI.2008.11.038.

[16] S.K. Hubadillah, M.H.D. Othman, T. Matsuura, M.A. Rahman, J. Jaafar, A.F. Ismail, S.Z.M. Amin, Green silica-based ceramic hollow fiber membrane for seawater desalination via direct contact membrane distillation, Sep. Purif. Technol. 205 (2018) 22–31. doi:10.1016/j.seppur.2018.04.089.

[17] J. Kujawa, S. Al-Gharabli, W. Kujawski, K. Knozowska, Molecular Grafting of Fluorinated and Nonfluorinated Alkylsiloxanes on Various Ceramic Membrane Surfaces for the Removal of Volatile Organic Compounds Applying Vacuum Membrane Distillation, ACS Appl. Mater. Interfaces. 9 (2017) 6571–6590. doi:10.1021/acsami.6b14835.

[18] L. García-Fernández, B. Wang, M.C. García-Payo, K. Li, M. Khayet, Morphological design of alumina hollow fiber membranes for desalination by air gap membrane distillation, Desalination. 420 (2017) 226–240. doi:10.1016/j.desal.2017.07.021.

[19] A. Larbot, L. Gazagnes, S. Krajewski, M. Bukowska, W. Kujawski, Water desalination using ceramic membrane distillation, Desalination. 168 (2004) 367–372. doi:10.1016/j.desal.2004.07.021.

[20] W. Kujawski, J. Kujawa, E. Wierzbowska, S. Cerneaux, M. Bryjak, J. Kujawski, Influence of hydrophobization conditions and ceramic membranes pore size on their properties in vacuum membrane distillation of water-organic solvent mixtures, J. Memb. Sci. 499 (2016) 442–451. doi:10.1016/j.memsci.2015.10.067.

[21] J. Kujawa, S. Cerneaux, W. Kujawski, K. Knozowska, Hydrophobic Ceramic Membranes for Water Desalination, Appl. Sci. 7 (2017) 402. doi:10.3390/app7040402.

[22] Y. Dong, L. Ma, C.Y. Tang, F. Yang, X. Quan, D. Jassby, M.J. Zaworotko, M.D. Guiver,

Stable Superhydrophobic Ceramic-Based Carbon Nanotube Composite Desalination Membranes, Nano Lett. 18 (2018) 5514–5521. doi:10.1021/acs.nanolett.8b01907.

[23] C.-Y. Huang, C. Ko, L. Chen, C. Huang, Y. Liao, A simple coating method to prepare superhydrophobic layers on ceramic alumina for vacuum membrane distillation, Sep. Purif. Technol. 198 (2018) 79–86. doi:10.1016/J.SEPPUR.2016.12.037.

[24] The Danish Environmental Protection Agency, Surveys of PFOS, PFOA and other perfluoroalkyl and polyfluoroalkyl substances, The Danish Environmental Protection Agency, Copenhagen, 2013.

[25] A.W. Nørgaard, S.T. Larsen, M. Hammer, S.S. Poulsen, K.A. Jensen, G.D. Nielsen, P. Wolkoff, Lung damage in mice after inhalation of nanofilm spray products: The role of perfluorination and free hydroxyl groups, Toxicol. Sci. 116 (2010) 216–224. doi:10.1093/toxsci/kfq094.

[26] S. Alami-Younssi, C. Kiefer, A. Larbot, M. Persin, J. Sarrazin, Grafting γ alumina microporous membranes by organosilanes: Characterisation by pervaporation, J. Memb. Sci. 143 (1998) 27–36. doi:10.1016/S0376-7388(97)00333-5.

[27] C.H. Beuscher, U.; Gooding, Characterization of the porous support layer of composite gas permeation membranes, J. Memb. Sci. 132 (1997) 213–227. doi:10.1016/S0376-7388(97)00071-9.

[28] E. Jakobs, W.J. Koros, Ceramic membrane characterization via the bubble point technique, J. Memb. Sci. 124 (1997) 149–159. doi:10.1016/S0376-7388(96)00203-7.

[29] M.S.S. El-Bourawi, Z. Ding, R. Ma, M. Khayet, A framework for better understanding membrane distillation separation process, Elsevier, 2006. doi:10.1016/j.memsci.2006.08.002.

[30] K.W. Lawson, D.R. Lloyd, Membrane distillation, J. Memb. Sci. 124 (1997) 1–25. doi:10.1016/S0376-7388(96)00236-0.

[31] L. Eykens, K. De Sitter, C. Dotremont, L. Pinoy, B. Van Der Bruggen, How to Optimize the Membrane Properties for Membrane Distillation: A Review, Ind. Eng. Chem. Res. 55 (2016) 9333–9343. doi:10.1021/acs.iecr.6b02226.

[32] A.K. Fard, G. McKay, A. Buekenhoudt, H. Al Sulaiti, F. Motmans, M. Khraisheh, M. Atieh, Inorganic membranes: Preparation and application for water treatment and desalination, Materials (Basel). 11 (2018). doi:10.3390/ma11010074.

[33] L. V Azároff, Introduction to solids, 1st ed., McGraw-Hill, 1960. https://books.google.it/books?id=9j1RAAAAMAAJ.

[34] R.A. Greenkorn, Flow phenomena in porous media : fundamentals and applications in petroleum, water, and food production, Marcel Dekker, New York, 1983.

[35] H. Azour, J. Derouault, P. Lauroua, G. Vezon, Fourier transform infrared spectroscopic characterization of grafting of 3-aminopropyl silanol onto aluminum/alumina substrate, Spectrochim. Acta - Part A Mol. Biomol. Spectrosc. 56 (2000) 1627–1635. doi:10.1016/S1386-1425(00)00216-X.

[36] C.Y. Wang, J.Z. Zheng, Z.X. Shen, Y. Lin, A.T.S. Wee, Elimination of O2plasma damage of low-k methyl silsesquioxane film by As implantation, Thin Solid Films. 397 (2001) 90–94. doi:10.1016/S0040-6090(01)01401-8.

[37] A.O. Imdakm, M. Khayet, T. Matsuura, A Monte Carlo simulation model for vacuum membrane distillation process, J. Memb. Sci. 306 (2007) 341–348. doi:10.1016/J.MEMSCI.2007.09.021.

[38] J.-P. Mericq, S. Laborie, C. Cabassud, Vacuum membrane distillation of seawater reverse osmosis brines, Water Res. 44 (2010) 5260–5273. doi:10.1016/J.WATRES.2010.06.052.

[39] J.W. Zhang, H. Fang, L.Y. Hao, X. Xu, C.S. Chen, Preparation of silicon nitride hollow fibre membrane for desalination, Mater. Lett. 68 (2012) 457–459. doi:10.1016/j.matlet.2011.11.041.

[40] J.-W. Zhang, H. Fang, J.-W. Wang, L.-Y. Hao, X. Xu, C.-S. Chen, Preparation and characterization of silicon nitride hollow fiber membranes for seawater desalination, J. Memb. Sci. 450 (2014) 197–206. doi:10.1016/J.MEMSCI.2013.08.042.

[41] H. Fang, J.F. Gao, H.T. Wang, C.S. Chen, Hydrophobic porous alumina hollow fiber for water desalination via membrane distillation process, J. Memb. Sci. 403–404 (2012) 41–46. doi:10.1016/J.MEMSCI.2012.02.011.

[42] C.-C.C. Ko, C.-H.H. Chen, Y.-R.R. Chen, Y.-H.H. Wu, S.-C.C. Lu, F.-C.C. Hu, C.-L.L. Li, K.-L.L. Tung, Increasing the Performance of Vacuum Membrane Distillation Using Micro-Structured Hydrophobic Aluminum Hollow Fiber Membranes, Appl. Sci. 7 (2017) 357. doi:10.3390/app7040357.

Conclusions

Conclusions

During the three years of PhD research various aspects of the preparation of hydrophobic membranes for distillation application were investigated.

Firstly, the nonsolvent induced phase separation technique was exploited to prepare PVDF flat sheet membranes. The effect of several preparation variables on the membrane structure and MD performance was evaluated. Using a high molecular weight PVDF, it was found that the coagulation bath strength had a major role in defining the membrane characteristics. In fact, when a harsh nonsolvent (e.g. water) was used, the PVDF precipitated almost instantly creating a dense and not permeable layer. Instead, a highly porous and rough surface was obtained by lowering the strength of the coagulation medium through addition of ethanol. Many different samples were prepared and characterized, and many different morphologies were identified by careful FESEM analyses. Finally, a correct balance of polymer concentration and nonsolvent composition allowed to prepare almost superhydrophobic membranes with excellent performance that guaranteed high distillate flux during VMD operation without undesired wetting phenomena.

A further strategy to fine-tune the membrane characteristics, and in particular pore size and porosity, is the use of pore forming agents. Two polyethylene glycols, with different molecular weight, and an inorganic salt were tested. Unsupported membranes were initially prepared. It was found that the addition of pore forming agents, in combination with the absence of a supporting material caused a severe shrinkage of the membrane and collapse of the porous structure. A simple procedure to prevent deterioration of the membrane morphology during the drying process was found and several combinations of preparation conditions were investigated.

Using a polyethylene glycol with and adequate molecular weight and the proper PVDF concentration, flat sheet membranes with the needed characteristics were prepared. Lower molecular weight PEG caused the formation of membranes with a wide pore size distribution that were affected by wetting phenomena during MD operation.

Lithium chloride was found to be a good alternative to polymeric pore forming additives but its concentration in the dope solution is limited by the negative effect on the thermodynamic stability of the solution itself. At low concentrations the thermodynamic effects are dominant while when higher amounts are added the increase of the solution viscosity becomes substantial and the kinetic effects drive the separation process.

Using a high molecular weight PVDF, adoption of a weak coagulation bath was anyway necessary to obtain a porous surface; in fact, when strong nonsolvents were used, even the addition of pore forming agents did not allow to create pores in the top skin.

The noticeable difference between unsupported and nonwoven casted PVDF membranes highlighted the importance of the support material during their preparation via nonsolvent induced phase separation. Various commercial nonwovens tissues, characterized by different thickness, morphology, free volume and material, were used to prepare PVDF membranes and were compared with three polymeric nets also tested as unconventional support material.

The membranes casted on the nonwovens displayed similar morphologies and performance highlighting that, in the tested conditions, the contribution to the support material to the mass transfer resistance was negligible. Instead, the three nets formed membranes with greatly different features. The membrane morphology was deeply influenced. On the top of the net structure~~,~~ the thinner dope solution film generated a less dense zone, while inside the holes of the nets the membrane appeared more porous. However, because of the lower physical interactions between the support and the dope solution, inside the net holes a certain grade of shrinkage during the drying process was registered and the net casted membranes were generally less porous than the nonwoven ones. These morphological differences affected the VMD performance and the membranes prepared on ~~the~~ nonwoven tissues provided higher distillate fluxes. However, thanks to the highest surface roughness induced by the support structure, the net casted membranes suffered a lower flux decrease when a concentrated NaCl solution was used as feed. It is believed that the patterned morphology imparted by the net improved the feed turbulence at the feed side of the membrane lowering the polarization phenomena and increasing, by consequence, the effective driving force.

Finally, completely different membranes – both in terms of material and geometry – were investigated in order to explore a possible extension of MD to more demanding processes. Commercially available tubular membranes made of alumina and designed for microfiltration applications were tested. Ceramic membranes have the advantage of being more resistant to mechanical stress and to harsh chemical and thermal conditions. Moreover, the tubular geometry allows to create modules with higher packing density with consequent savings in an industrial application.

However~~,~~ alumina, as well as other ceramic materials, is inherently hydrophilic and the direct use of the pristine membranes in MD application is impossible. Therefore, a functionalization protocol was developed selecting a suitable silanizing agent able to hydrophobize the selective membrane side by reaction with the surface hydroxyl groups of alumina. The effect of the reaction conditions were investigated on membranes with different pore size. The increase of the reactant concentration resulted in a higher functionalization grade, with improvements of the contact angle

and of the liquid entry pressure of the membranes. In this way, exploiting a simple process it was possible to obtain highly hydrophobic ceramic membranes without affecting the morphology of the pristine support. The thermal stability of the functionalization layer was tested by heating the membranes at high temperatures for one hour: the hydrophobic character was maintained up to 400°C, extending the application of these membranes to high temperature MD processes.
The membranes were tested in a VMD setup following the protocol defined in the beginning of the PhD work. However, in order to verify the high temperature MD performance, the highest feed temperature was increased to 90°C. In general, the distillate flux improved with pore size and with the functionalization degree and reached the maximum value for the sample with the larger pores and the higher silanization grade.
Finally, considering all the different type of membranes studied during the PhD research, it is believed that the ones prepared on the non-woven support using ethanol as coagulation bath showed the most interesting performance (Chapter 2). Moreover, the production of such membranes can be easily brought to the industrial scale since it exploits conventional membrane casting equipment that are already available. However, this step requires machines that can operate with flammable liquids such as ethanol.

Further developments

The PhD work has put some basis for future research activities in the field of hydrophobic membranes preparation. In particular, the study on unsupported flat sheet membranes preparation described in Chapter 3 was the starting point of a new research line to be pursued in collaboration with the Complutense University of Madrid and focused on the preparation of hollow fibre PVDF membranes. The preliminary tests already performed confirmed the shrinkage problems detected for flat sheets as well as the importance of pore forming agents and coagulation media in directing membrane characteristics. Further studies are already ongoing. Moreover, other inorganic fillers, more sustainable than LiCl should be tested.
The prepared membranes were always tested with model solutions and for short operation times. The evaluation of long-term stability as well as the determination of fouling resistance will be key steps needed to validate the membrane performance before developing a possible product suitable for real applications. In this perspective, real feed solutions must be tested.
Secondly, it will be interesting to apply special knowledge acquired during the modification of ceramic membranes to functionalization of inorganic nanoparticles. The so-called mixed matrix membranes – characterized by the presence of inorganic fillers into the polymeric structure – are

gathering growing interest. Fillers on this kind are a promising route for improving the mechanical properties and the hydrophobicity of the membrane maintaining at the same time a lower thickness, which reduces the mass transfer resistance. Moreover, using particles with different characteristics it is possible to depress potential fouling phenomena on the membrane surface.

Hydrophobic mixed matrix membranes could be applied to different processes, for example acting as an interface for CO_2 capture using absorbing solutions, or as air diffusers in biological wastewater treatment plants.

Finally, by adding electro conductive fillers, hydrophobic membranes could be exploited as gas diffusion layers in proton exchange membrane fuel cells for the production of electric power.